

Airborne Geophysics Data Analysis and Interpretation, Canadian Shield, Northeastern Alberta

AER/AGS Special Report 119

Airborne Geophysics Data Analysis and Interpretation, Canadian Shield, Northeastern Alberta

G.P. Lopez, D. McGill and J. McKenzie

Ronacher McKenzie Geoscience Inc.

August 2024

©His Majesty the King in Right of Alberta, 2024
ISBN 978-1-4601-5719-0

The Alberta Energy Regulator / Alberta Geological Survey (AER/AGS), its employees and contractors make no warranty, guarantee, or representation, express or implied, or assume any legal liability regarding the correctness, accuracy, completeness, or reliability of this publication. Any references to proprietary software and/or any use of proprietary data formats do not constitute endorsement by the AER/AGS of any manufacturer's product.

If you use information from this publication in other publications or presentations, please acknowledge the AER/AGS. We recommend the following reference format:

Lopez, G.P., McGill, D. and McKenzie, J. (2024): Airborne geophysics data analysis and interpretation, Canadian Shield, northeastern Alberta; Alberta Energy Regulator / Alberta Geological Survey, AER/AGS Special Report 119, 111 p.

Publications in this series have undergone only limited review and are released essentially as submitted by the author.

Authors address:

G.P. Lopez, D. McGill and J. McKenzie
Ronacher McKenzie Geoscience Inc.
6 – 2140 Regent Street
Sudbury, ON P3E 5S8
Canada

Published August 2024 by:

Alberta Energy Regulator
Alberta Geological Survey
Suite 205
4999 – 98 Avenue NW
Edmonton, AB T6B 2X3
Canada

Tel: 780.638.4491
Email: AGS-Info@aer.ca
Website: ags.aer.ca

Contents

Foreword.....	v
1.0 Summary.....	4
2.0 Introduction.....	6
3.0 Project Location.....	7
4.0 Geological Setting.....	9
5.0 Aeromagnetic Survey Data.....	16
6.0 Methodology and Results.....	37
7.0 Interpretation.....	55
8.0 Conclusions.....	61
9.0 References.....	62
Appendix 1 – Automatic Detection – Fathom Geophysics Report.....	65

Appendices

Appendix A – Interpretation and map products

The appendix is in the accompanying folder entitled ‘Appendix A – Interpretation and Map Products’, located in the download zip file.

Appendix B – Geophysical inversions

The appendix is in the accompanying folder entitled ‘Appendix B – Geophysical Inversions’, located in the download zip file.

Appendix C – Automatic detection – Fathom Geophysics

The appendix is in the accompanying folder entitled ‘Appendix C – Automatic Detection – Fathom Geophysics’, located in the download zip file.

Foreword

The Alberta Geological Survey (AGS) outsourced the geological interpretation of the 2021 high-resolution aeromagnetic survey conducted by the Alberta Energy Regulator (AER) / AGS over the Canadian Shield of northeastern Alberta. This interpretation focused on characterizing the magnetic signature of magnetic rock units, granitoid plutons, dikes, faults, and shear zones and producing a compilation map. Although this report does not identify any mineral occurrences or potential mineral exploration targets, the information will allow for a better understanding of geological features that are linked to increased critical mineral potential.

All production of geophysical products and interpretation of data was conducted by Ronacher McKenzie Geoscience Inc. (RMG), as well as subcontractor Fathom Geophysics LLC, with oversight and approval by the AER and AGS. Using the 2021 aeromagnetic data, RMG synthesized a selection of grid-based filter products and three-dimensional models to aid subsequent interpretation. Additionally, RMG commissioned Fathom Geophysics LLC to produce automatic structure and radial symmetry detection filters, and other geophysical products. By integrating this new information with existing geological data, the authors interpreted five key geological features over the project area, namely magnetic rock units, intrusions, dikes, ductile shear zones, and brittle faults. Subsequently, a compilation map and report were produced by RMG to highlight all new geological interpretations in the Canadian Shield of northeastern Alberta. RMG also included an array of new GIS and geophysical products in their deliverables.

This work was completed under the Mineral Grant provided by the Government of Alberta dated June 22, 2021.

Geological Interpretation of the 2021 Aeromagnetic Data

Canadian Shield, Alberta

Prepared For:
Alberta Geological Survey



Prepared By:
Gloria Lopez, PhD, P.Geo.
Darcy McGill, P.L. (Geo.)
Jenna McKenzie, P.Geo.
Ronacher McKenzie Geoscience Inc.



29 March 2024

TABLE OF CONTENTS

1.0	SUMMARY	4
2.0	INTRODUCTION	6
2.1	RONACHER MCKENZIE GEOSCIENCE QUALIFICATIONS	7
3.0	PROJECT LOCATION	7
4.0	GEOLOGICAL SETTING	9
4.1	TECTONIC HISTORY	9
4.2	REGIONAL GEOLOGY	11
	4.2.1 Crystalline Basement	11
	4.2.2 Athabasca Basin	11
	4.2.3 Western Canada Sedimentary Basin	13
4.3	STRUCTURES	13
4.4	METAMORPHISM	14
5.0	AEROMAGNETIC SURVEY DATA	16
5.1	DATA REVIEW	16
5.2	DERIVATIVE AND FILTER PRODUCTS	16
5.3	AUTOMATIC STRUCTURE DETECTION	29
5.4	3D INVERSIONS	34
	5.4.1 Data Preparation and Inversion Procedures	35
	5.4.2 Inversion Results	35
6.0	METHODOLOGY AND RESULTS	37
6.1	METHODOLOGY	37
	6.1.1 Data Sources	37
	6.1.2 Methods	39
	6.1.3 Workflow	39
6.2	RESULTS	40
	6.2.1 Magnetic Rock Units	40
	6.2.2 Intrusions	44
	6.2.3 Dykes	47
	6.2.4 Ductile Shear Zones	49
	6.2.5 Brittle Faults	53
7.0	INTERPRETATION	55
7.1	INTERPRETATION MAP	55
	7.1.1 Smaller Intrusions	55
	7.1.2 Dykes	56
	7.1.3 Heterogeneities in major plutonic units	56

7.1.4	<i>Shear Zones</i>	58
7.1.5	<i>Basement Features Beneath the Athabasca Basin</i>	58
7.1.6	<i>Basement Features Beneath the WCSB</i>	59
7.1.7	<i>Modifications to Bedrock Geology Map</i>	59
7.2	APPLICABILITY OF MAGNETIC FILTER PRODUCTS.....	59
7.3	APPLICABILITY OF AUTOMATIC STRUCTURE AND INTRUSION DETECTION.....	60
7.4	3D INVERSION.....	60
8.0	CONCLUSIONS	61
9.0	REFERENCES	62

FIGURES

Figure 3-1.	Shield survey area location map.....	8
Figure 4-1.	Tectonic domains for the crystalline basement of the Western Canada Sedimentary Basin and Canadian Shield in Western Canada.	10
Figure 4-2.	Map of the Precambrian Geology of Northeastern Alberta (From Map 537, Panã 2010a).....	15
Figure 5-1.	Residual Magnetic Intensity (“RMI”).....	18
Figure 5-2.	RMI, reduced to pole.....	19
Figure 5-3.	RMI, reduced to pole, 1st vertical derivative.....	20
Figure 5-4.	RMI, reduced to pole, 2nd vertical derivative.....	21
Figure 5-5.	RMI, Analytic Signal.	22
Figure 5-6.	RMI, reduced to pole, total horizontal derivative.	23
Figure 5-7.	RMI, reduced to pole, tilt derivative.....	24
Figure 5-8.	RMI, reduced to pole, pseudo-geology ternary image.....	25
Figure 5-9.	RMI, reduced to pole, pseudo-structure ternary image.....	26
Figure 5-10.	RMI, reduced to pole, standard rainbow (left) and CET i1 isoluminant (right) colour distributions.	27
Figure 5-11.	RMI, pole reduced, 1st vertical derivative, standard rainbow (left), greyscale (center), and CET i1 isoluminant (right) colour distributions.	28
Figure 5-12.	RMI, analytic signal, standard rainbow (left) and CET i1 isoluminant (right) colour distributions.	28
Figure 5-13.	CMY ternary image displaying the 1VD, tilt angle, and HGM results from the RTP.	32
Figure 5-14.	Image showing 1600 m belt-parallel structure detection results for the RTP data. The results highlight lithological contacts and fabric parallel shear zones at inferred depths of 800-1600 m.	33
Figure 5-15.	3D magnetic inversion areas.	34
Figure 5-16.	MVI model (left) and susceptibility model (right), with sections.	36
Figure 5-17.	MVI model (left) and susceptibility model (right), full area with transect models.	36
Figure 6-1.	Location of rock samples with recent whole-rock major and trace element geochemistry.....	38
Figure 6-2.	Interpretation of magnetic rock units.	42
Figure 6-3.	Interpretation of magnetic rock units showing internal subdomains (grey lines).....	43

Figure 6-4. Location of interpreted rounded intrusions.....	45
Figure 6-5. Intrusion detection in Slave and Arch Lake granitoids. Background image is the pseudogeology ternary of the Residual Magnetic Intensity, Reduced to Pole (2021_SHLD_RMI_RTP_Geology.tif).....	46
Figure 6-6. Location of interpreted dykes in Alberta in relation to mapped dykes in Northwest Territories and Saskatchewan.	48
Figure 6-7. Location of interpreted shear zones on first vertical derivative of Residual Magnetic Intensity, Reduced to Pole, aeromagnetic image.....	51
Figure 6-8. Broad zone of magnetite-destructive alteration spatially related to Charles Lake Shear Zone. Background image is the Residual Magnetic Intensity, Reduced to Pole,	52
Figure 6-9. Interpretation of linear features and structure.	54
Figure 7-1. Interpretation map of the magnetic data.	57

TABLES

Table 4-1. Athabasca Basin	12
Table 5-1. Magnetic Filter Products.....	16
Table 5-2. Colour palettes applied to geophysical datasets.....	27
Table 5-3. Additional filter and image products.....	29
Table 5-4. Structure detection products.....	30
Table 5-5. Radial Symmetry products.....	31
Table 5-6. 3D Magnetic Inversion Parameters	35
Table 6-1. General geophysical characteristics of map units of Pană (2010a).....	41

APPENDICES

Appendix 1 – Automatic Detection – Fathom Geophysics Report

DIGITAL APPENDICES

Appendix A – Interpretation and Map Products

Appendix B – Geophysical Inversions

Appendix C – Automatic Detection - Fathom Geophysics Products

1.0 SUMMARY

The Alberta Geological Survey (“AGS”) contracted Ronacher McKenzie Geoscience (“RMG”) to provide a geological interpretation of the 2021 high-resolution aeromagnetic survey conducted over the Canadian Shield of northeastern Alberta, contained within the limits of NTS map sheets 74M and 74L.

The purpose of this report is to present the results of this interpretation which involved the image mapping and characterization of magnetic rock units and lineaments, including the magnetic signature of granitoid plutons, faults, and shear zones. The interpretation of Alberta’s shield includes the subsurface of the Western Canada Sedimentary Basin (“WCSB”) and Athabasca Basin, and inversions of the magnetic data. The report supplements the GIS files produced for this project.

The interpretation was integrated with and calibrated against the existing results of geologic field mapping, rock dating and geochemical studies. The new aeromagnetic data thus provides improved understanding of the geology of the Canadian Shield in Alberta.

The lithotectonic units in the project area are the Archean to Paleoproterozoic metamorphic and igneous rocks of the Alberta Taltson Magmatic Zone (“TMZ”) in the north, the late Paleoproterozoic clastic strata of the western Athabasca Basin in the south, and Middle Devonian strata of the Proterozoic to Phanerozoic Western Canada Sedimentary Basin along the western edge.

Major, generally N- to NNE-trending high- to low-grade shear zones occur in Alberta’s shield area: the Leland Lakes Shear Zone (“LLSZ”) in the west, Charles Lake Shear Zone (“CLSZ”) in the center, and Bayonet Lake Shear Zone in the east, which developed concurrently with granitoid intrusion during the ca. 2.0–1.9 Ga Taltson tectonothermal event.

The AER contracted EON Geosciences Inc. to fly an aeromagnetic survey covering the project area in 2021. RMG reviewed the digital data for completeness and data quality and noted no significant data processing and levelling problems.

RMG calculated grid-based filter products from the total magnetic intensity (“TMI”) and International Geomagnetic Reference Field (“IGRF”)-removed residual magnetic intensity (“RMI”) grids. These products were displayed using a variety of colour schemes to assist with interpretation. All filter products were used for the interpretation. In addition, RMG collaborated with Fathom Geophysics to perform automatic structure and radial symmetry detection and to generate additional magnetic products to assist with the geological interpretation of the shield area. The automatic structure detection filter is a linear feature detection algorithm used to highlight ridges, valleys, or edges in gridded data. Radial symmetry is a filtering process that identifies equant discrete features in the data that may be interpreted as intrusions.

The magnetic data were inverted to produce 3D models of subsurface magnetization, producing both 3D Magnetic Vector Inversion (“MVI”) and susceptibility models. One coarse inversion of the entire Shield area was completed as well as two higher resolution ‘transect’ areas. Data preconditioning parameters are

summarized in the report. Final models were trimmed of extraneous cells using SRTM topography from surface to 5 km depth.

In addition to the geophysical data, the interpretation was supported by geospatial data provided by the AGS.

The analysis of magnetic data follows the methodology developed by Isles and Rankin (2013), which summarizes the interpretation process in three main stages: observations, integration, and interpretation. Observations are recoded directly from the data as form lines. The observations are then integrated with existing geological data and were compared with the automatic structure results. Geologic and geophysical interpretation layers are then generated to present a final geological interpretation map.

Five key geologic features were interpreted from the dataset and incorporated into a 3D model: magnetic rock units, intrusions, dykes, ductile shear zones and brittle faults. GIS files of all interpreted features are provided in a digital appendix.

Magnetic rock units were outlined, and existing geologic data were used to classify magnetic rock units and their subdomains. Classification followed known map units where possible, and geophysical characteristics of interpreted units were tabulated. Relationships to primary heterogeneous fabric or possible secondary geologic processes were noted where possible.

Intrusion detection, using a combination of manual and automatic processes (radial symmetry detection), was conducted to identify smaller rounded intrusive bodies in the project area. These bodies are predominantly noted to be magnetic highs, although four correspond to magnetic lows and may be a result of remanence or alteration. Furthermore, detected intrusions were classified into three main groups: a) individual smaller magnetic features, b) larger rounded intrusions with distinct internal magnetic texture and c) larger intrusions with rims or concentric zonation patterns. Several rounded intrusions are observed in the western part the project, including beneath the WCSB; however, fewer intrusions were detected on the eastern side of the project. Very few small intrusions were detected beneath the Athabasca Basin possibly due to its thick cover which hinders basement interpretation.

Several major dykes are interpreted from the magnetic dataset and are described in detail. These major dykes may either relate to the Mackenzie diabase dyke swarm mapped in Saskatchewan and the Northwest Territories, or Sparrow diabase dykes mapped in the Northwest Territories. Although the orientation is similar to the Mackenzie dykes, it is uncertain that they can be classified as Mackenzie dykes based on age dating.

Shear zones and deeper basin structures were identified from the various filter and structure detection products. The wavelength separation results, particularly the separation of long wavelengths, were useful to interpret the location of deeper structure in the TMZ. Characteristics of shear zones were defined as: broad zones of anastomosing surfaces with curvilinear margins, with either bending noted in magnetic signature or contacts into the shear zone, magnetic mineral alteration, and offsets of units associated with deflection or thinning of magnetic markers. Known and new prominent shear zones are described in detail in the report.

Brittle faults were identified from the various filter and structure detection files. Criteria used to identify brittle structures included: different form line orientations, linear features with angular margins, angular fault jogs or steps, short subtle curvilinear features, narrow zones of demagnetization, and sharp offsets of magnetic rock units.

All interpreted features were compiled and are presented in a summary interpretation map figure that provides a simplified view of the accompanying GIS files. The magnetic domains and linear structure layers form the basis of the interpretation map. This interpretation map supplements the existing mapped geology, and it is not meant to replace it. The interpretation map provides a general framework that includes inferences of structural and geological units based on the results of the observations of magnetic data and integration with existing geological data. The interpretation map shows intrusions and structure in areas hidden by either Quaternary cover, or sedimentary strata from the WCSB and Athabasca Basin.

The magnetic data, the automatic structural detection and the radial symmetry analysis significantly improved the interpretation of the geology of the Shield in northeastern Alberta.

2.0 INTRODUCTION

The Alberta Geological Survey (“AGS”) commissioned Ronacher McKenzie Geoscience (“RMG”) to complete a geological interpretation of the new high-resolution aeromagnetic survey conducted over the Canadian Shield of northeastern Alberta.

The purpose of this report is to present the results of this interpretation which involved the image mapping and characterization of magnetic rock units and lineaments, including the magnetic signature of granitoid plutons, faults, and shear zones. The interpretation of Alberta’s shield includes the immediate subsurface of the Western Canada Sedimentary Basin (“WCSB”) and Athabasca Basin as well as interpretation at depth based on inversions of the magnetic data.

The interpretation was integrated with and calibrated against the existing results of geologic field mapping, rock dating and geochemical studies. The new aeromagnetic data thus provides improved understanding of the geology of the Shield in Alberta.

The main source of information was the AGS. The AGS provided geological and geophysical data including databases, grids, maps, digital data files, and reports. Geological literature was obtained from the public domain.

Universal Transverse Mercator (“UTM”) coordinates are provided in the datum of WGS 84 zone 11N for all digital files (vector and map files) and reprojected in ArcGIS to NAD83 Zone 12N for map figures found in this report.

2.1 Ronacher McKenzie Geoscience Qualifications

RMG is an international consulting company with offices in Toronto and Sudbury, Ontario, Canada. RMG's mission is to use intelligent geoscientific data integration to help mineral explorers focus on what matters to them. We help a growing number of clients understand the factors that control the location of mineral deposits.

With a variety of professional experience, our team's services include:

- Data Integration, Analysis, and Interpretation
- Geophysical Services
- Project Generation and Property Assessment
- Exploration Project Management
- Resource Estimation and Independent Technical Reporting
- Project Promotion
- Lands Management

The primary author of this report is Gloria Lopez, PhD, P.Geo., Senior Geologist at Ronacher McKenzie Geoscience, and a geologist in good standing with the Association of Professional Engineers and Geoscientists of Alberta (#181673) and Newfoundland and Labrador Association of Professional Engineers and Geoscientists (# 11213). Dr. Lopez has over two decades of experience working as an economic geologist.

Co-author of this Report is Mr. Darcy McGill, BSc, P.Geo. (Limited), P.L. (Geo). Mr. McGill is a Senior Geophysicist at Ronacher McKenzie Geoscience and a geophysicist in good standing with the Association of Professional Geoscientists of Ontario (APGO #2010) and Professional Licensee with the Association of Professional Engineers and Geoscientists of Alberta (#316505). Mr. McGill has worked in geophysical data acquisition, processing, and interpretation for mineral exploration since 1995.

A second co-author of this Report is Ms. Jenna McKenzie, Hons BSc, P.Geo. Ms. McKenzie is co-founder and Principal Geophysicist to Ronacher McKenzie Geoscience and a geoscientist in good standing with the Association of Professional Geoscientists of Ontario (APGO #1653) and the Association of Professional Engineers and Geoscientists of Alberta (#315719). Ms. McKenzie has worked as a geophysicist since 2001 in the exploration and mining industry on a variety of exploration properties with specific focus on geophysics surveying and interpretation.

Additionally, Fathom Geophysics completed the automatic structure and intrusion detection on behalf of RMG.

3.0 PROJECT LOCATION

The project area is located in the Canadian Shield of northeastern Alberta, adjoining Saskatchewan and the Northwest Territories. The project area lies between latitudes 58°N and 60°N, and longitudes 110°W and

111°30'W, within the boundaries of NTS map sheets 74M and 74L. An overview of the project area is found in Figure 3-1.

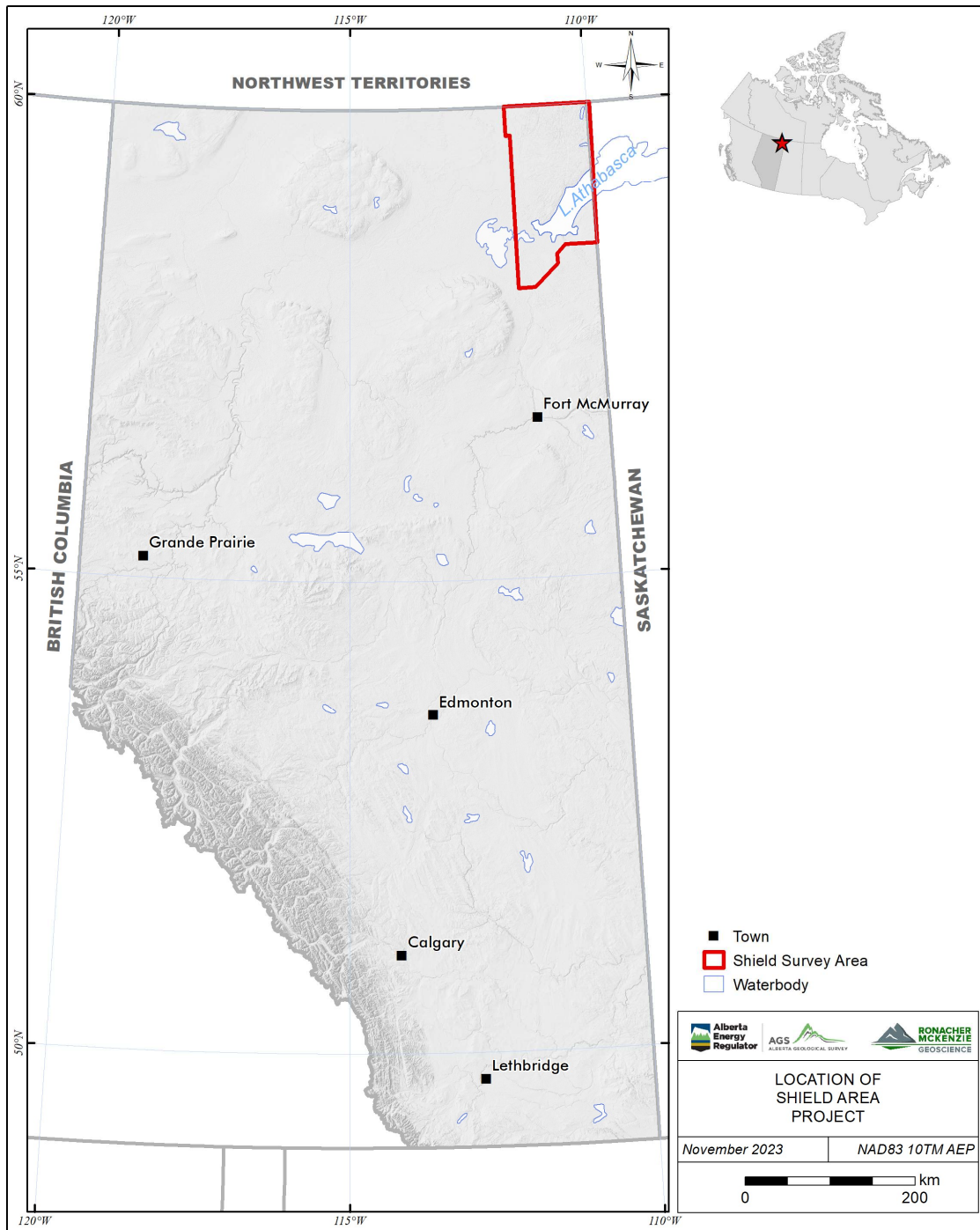


Figure 3-1. Shield survey area location map.

4.0 GEOLOGICAL SETTING

4.1 Tectonic History

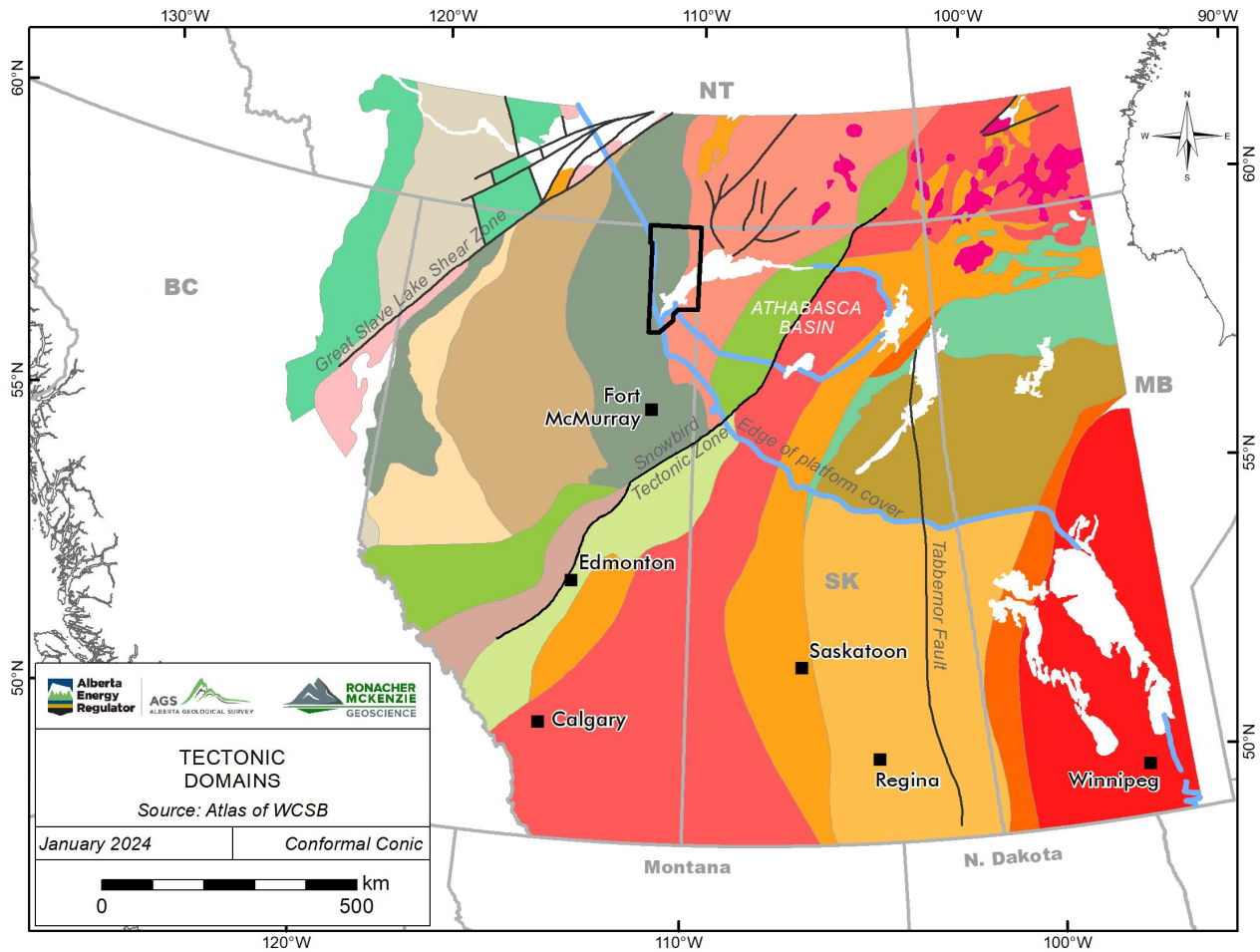
The lithotectonic units in the project area are the Archean to Paleoproterozoic metamorphic and igneous rocks of the Alberta crystalline basement in the north, the late Paleoproterozoic clastic strata of the western Athabasca Basin in the south, and Middle Devonian strata of the Proterozoic to Phanerozoic Western Canada Sedimentary Basin along the western edge.

The crystalline basement in Alberta comprises Archean and Paleoproterozoic terranes (Figure 4-1) welded together between 1.9 and 1.8 Ga during the assembly of Laurentia (e.g., Ross et al., 1994; Ross 2002; Pană et al., 2021). In northeastern Alberta, the crystalline basement is exposed and consists of a basement, intrusive and supracrustal rocks of the Taltson Magmatic Zone (“TMZ”), a ~100 km wide orogenic belt that extends for ca. 600 km from the Great Slave Lake shear zone in the Northwest Territories to the Snowbird tectonic zone in central Alberta (e.g., Pană et al., 2021). The TMZ corresponds to the southern segment of the 3000 km long north-trending Early Paleoproterozoic Thelon-Taltson orogenic belt developed in the Archean to Paleoproterozoic Rae Terrane (Figure 4-1) of western Laurentia.

The TMZ is interpreted to have formed by subduction of oceanic crust beneath a continental margin, followed by terrane collision between the Buffalo Head island arc terrane to the west and the Rae craton to the east (Figure 4-1) (McDonough et al., 2000). Other authors have proposed the TMZ orogen formed by ultra-metamorphism and anatexis in an intracontinental setting in response to distant plate boundary compression (Chacko et al., 2000; De et al., 2000) or in response to mantle downwelling and Rayleigh-Taylor–type flow-induced stress at the base of the Rae crust weakened by high radioactive-heat production, followed by oblique crustal stretching and decompression melting within the TMZ (Pană 2010b, Pană et al., 2021).

The Athabasca Basin represents a post-orogenic intracontinental sag basin with four sub-basins filled between ca. 1740–1730 Ma and 1500 Ma by four unconformity-bounded fluvial sequences (Ramaekers et al., 2007).

The Western Canada Sedimentary Basin developed in three different tectonic settings: 1) Mesoproterozoic (1.50–1.32 Ga) intracontinental rift exposed within the Rocky Mountain fold and-thrust belt of the Canadian Cordillera, 2) Neoproterozoic to Middle Jurassic passive continental margin, and 3) Middle Jurassic to early Eocene foreland basin.



Legend

- City
- Aeromagnetic Survey
- Edge of platform cover
- Fault / Shear
- Archean Hearne Province - Medicine Hat Block
- Archean Rae Province
- Archean Slave Province
- Archean Superior Province
- Belts of mylonitic rock along Snowbird Tectonic Zone - Tantato domain
- Buffalo Head Lower Proterozoic Terrane
- Chinchaga Lower Proterozoic Terrane
- Fort Simpson continental magmatic arch (1.88 – 1.84 Ga)
- Great Bear continental magmatic arch (1.88 – 1.84 Ga)
- Hottah Lower Proterozoic Terrane
- Juvenile island arc rocks and metasediments - Baldock
- Juvenile island arc rocks and metasediments - Snake Indian
- Ksituan continental magmatic arch (1.9 – 1.98 Ga)
- Lower Proterozoic metavolcanic & metasedimentary rocks - Lacombe Domain
- Lower Proterozoic metavolcanic & metasedimentary rocks - Nonacho
- Lower Proterozoic metavolcanic & metasedimentary rocks - Wilson Island terrane
- Lower Proterozoic metavolcanic & metasedimentary rocks - Wollaston belt
- Rapikivi Granite (1.76 Ga)
- Rimbey continental magmatic arch (1.85 – 1.78 Ga)
- Simpson Island terrane
- Taltson continental magmatic arch (1.9 – 1.98 Ga)
- Thorsby Lower Proterozoic Terrane
- Wathamun & Chipewyan continental magmatic arch (1.85 Ga)
- Zones of reactivated Archean crust - Peter Lake
- Zones of reactivated Archean crust - Thompson

Figure 4-1. Tectonic domains for the crystalline basement of the Western Canada Sedimentary Basin and Canadian Shield in Western Canada.

4.2 Regional Geology

4.2.1 Crystalline Basement

The exposed crystalline basement in northeastern Alberta comprises the Taltson Basement Complex, Taltson granitoids, and other metamorphic complexes. The following descriptions of these units were taken from Panǎ (2010a) and Panǎ et al. (2021).

The Taltson Basement Complex (“TBC”) forms a curved north-trending belt of Archean to Early Proterozoic (3.2–2.1 Ga) high- to medium-grade metamorphic tectonites. These tectonites comprise metaplutonic gneisses, interlayered with subordinate supracrustal gneiss, minor amphibolite, and hornblendite, and rare metagabbro. The several distinct, moderately to strongly foliated granitoid plutons with minor roof pendants intrude the TBC, which is considered the westernmost expression of the Rae Terrane.

The Taltson granitoids postdate the Taltson Basement Complex and are petrologically subdivided into two distinct age groups:

- 1.974–1.959 Ga, subduction-related, weakly peraluminous to metaluminous (I-type), diorite–quartz monzonite–granodiorite complexes; includes the Colin Lake granodiorite to quartz diorite (ca. 1971 Ma); the Wylie Lake suite of granodiorite, quartz diorite and quartz monzonite (ca. 1963 Ma), Fishing Creek granodiorite and the Andrew Lake suite of granodiorite to diorite (ca. 1962–1959 Ma), which are located east of the Taltson Basement Complex;
- 1.960–1.934 Ga, collision-related, peraluminous (S-type), monzo-syenogranite complexes; includes the polyphase Slave monzogranite (ca. 1960–1934 Ma) and the Arch Lake quartz monzo- to syenogranite (ca. 1938 Ma) which are located west of the Taltson Basement Complex.

Smaller plutons of uncertain affinity are emplaced within the Taltson Basement Complex, including: the ca. 1.933–1.919 Ga Charles Lake granite and the ca. 1.925 Ga Chipewyan and Thesis Lake quartz monzonite–syenogranite complexes.

Other metamorphic rocks include the Burntwood, Waugh Lake and Rutledge River complexes. The Burntwood Complex (2.1 – 1.93 Ga) consists of high-grade metamorphic tectonites. The Waugh Lake Complex comprises monzonite (1973 Ma), other mafic igneous rocks, and low-grade metamorphic tectonites (2.7 – 2.0 Ga) affected by low grade-shearing (1839 – 1820 Ma). The Rutledge River Complex consists of inliers of high-grade metamorphic tectonites.

The Alberta crystalline basement is overlain by the late Paleoproterozoic to early Mesoproterozoic Athabasca Basin, and dips towards the west beneath the Western Canada Sedimentary Basin (“WCSB”) in the remainder of Alberta.

4.2.2 Athabasca Basin

About ten percent of the western Athabasca Basin is present in northeastern Alberta, overlying the TMZ and possibly the Rae craton. The late Paleoproterozoic to early Mesoproterozoic (ca. 1760 Ma and 1500 Ma)

Athabasca Group comprises four quartzose fluvial sequences, bounded by unconformities, and deposited in distinct stacked NE-trending sub-basins with a total preserved aggregate thickness estimated at 1150 m (e.g., Ramaekers et al., 2007). The following summary table (Table 4-1) lists the main characteristics of the Athabasca Group that may be relevant for the interpretation of the aeromagnetic data. Complete descriptions of Athabasca Group units in Alberta can be found in Post (2004) and Pană (2010a, 2010b):

Table 4-1. Athabasca Basin

Sequence	General characteristics from Pană (2010b) (SK and AB)	Map Units in AB from Post (2004), Pană (2010a, 2010b) (older to younger)
1	Confined to the Jackfish sub-basin (AB-SK), nearby sediment derivation; present in the western part of the Athabasca Basin; estimated preserved thickness of 380 m. Consists of the Fair Point Formation	Fair Point Formation: conglomerate and pebbly quartz-arenite; fining-upward sequence of coarse quartz arenite to granule stone; poorly sorted; generally west-dipping; horizontal and sub horizontal cross-bedding; lag deposits, local lacustrine, upper flow-regime macroforms, crude longitudinal bar forms, and dune forms.
2	Confined to the Cree sub-basin (SK), unconformably overlies sequence 1. Present mostly in the eastern part of the Athabasca Basin, except for a narrow belt along the western Athabasca Basin margin. In Alberta, it consists of distal relatively fine-grained and thin units derived predominantly from the east with a preserved aggregate thickness up to 1100 m. Consists of the Smart Formation in the west, the Red Formation in the east, and overlain by the Manitou Falls Formation	Smart Formation: uniform, well-sorted, fine to coarse quartz arenite, with low-angle cross beds and horizontal bedding in the upper section, but trough-filling cross beds in the lower section. Manitou Falls Formation: cross bedded; abrupt paleocurrent-direction discontinuities; thickest in the southern portion of the basin, ~300 m on AB/SK boundary related to Beatty Trough; dune forms, ripples, and upper flow-regime macroforms; subdivided in two members. Warnes member: medium-grained quartz-arenite with northerly paleocurrent directions. Bird member: conglomeratic quartz-arenite.
3	In the Mirror sub-basin overlying the Cree sub-basin in the central area of the Athabasca Basin, with sediments derived from the south, and an aggregate maximum preserved thickness of about 600 m. Widespread in the central and western parts of the Athabasca Basin. Consists of the Lazenby Lake and Wolverine Point formations.	Lazenby Lake Formation: basal thin conglomerate, and coarse to fine-grained quartz-arenite; common overturned bedding; thickness of 200 m; dune forms, ripples and upper flow-regime macroforms; subdivided into four members (Larter, Shiels, Clampitt, and Hodge)

Sequence	General characteristics from Pană (2010b) (SK and AB)	Map Units in AB from Post (2004), Pană (2010a, 2010b) (older to younger)
4	In the Mirror sub-basin and has both similar sediment derivation (i.e., from south) and paleocurrent patterns than sequence 3. Consists of the Locker Lake and Otherside formations, limited to the central portion of the Athabasca Basin, and the Douglas and Carswell formations, restricted to the Carswell meteorite structure, Saskatchewan	<p>Wolverine Point Formation: recessive thick beds (>50cm) of mudstone, and subordinate medium to fine grained quartz arenite and siltstone; conformably overlies Lazenby Lake Formation; thickness of ~500 m south of Lake Athabasca.</p> <p>Locker Lake Formation: pebbly, medium to coarse grained quartz-arenite, and subordinate thin conglomerate; disconformably overlies Wolverine Point Formation; maximum thickness of 200 m; subcrops south of Lake Athabasca; horizontal and low-angle cross-bedding; subdivided into three members (Marsin, Brudell and Snare)</p> <p>Otherside Formation (Archibald member): quartz-arenite; conformably overlies Locker Lake Formation; thickness < 50 m; subcrops south of Lake Athabasca.</p>

4.2.3 Western Canada Sedimentary Basin

The WCSB consists of Mesoproterozoic to Cenozoic age strata and unconformably overlies Precambrian crystalline basement. The WCSB thickens from an erosional zero edge onto Precambrian Shield in the northeast to more than 20 km within the deformed belt of the Canadian Cordillera in the west. To the east of the Rocky Mountains, the WCSB comprises two major sedimentary basins, the NW-trending Alberta Basin which underlies the Interior Plains with a maximum thickness of 6 km, and the Williston Basin situated in North Dakota, southern Saskatchewan, and southwestern Manitoba.

The WCSB stratigraphy reflects deposition in three different tectonic settings: 1) Mesoproterozoic (1.50–1.32 Ga) intracontinental rift exposed within the Rocky Mountain fold and-thrust belt of the Canadian Cordillera, 2) Neoproterozoic to Middle Jurassic passive continental margin, and 3) Middle Jurassic to Oligocene foreland basin.

4.3 Structures

Major, generally N- to NNE-trending high- to low-grade shear zones occur in Alberta's shield area: the Leland Lakes Shear Zone ("LLSZ") in the west, Charles Lake Shear Zone ("CLSZ") in the center, and Bayonet Lake Shear Zone in the east (Godfrey, 1986a; McDonough et al., 2000b). The crosscutting relationships between shear zones and granitoid bodies indicate concurrent deformation and granitoid intrusion during the ca. 2.0–1.9 Ga Taltson tectonothermal event (e.g., McDonough et al., 2000b; Pană, 2010a).

Two major shear zones are interpreted in Alberta's Athabasca Basin area, the Grease River shear zone (Wilson, 1986; Alberta Geological Survey, 2021) and dextral Black Bay shear zone (Burwash et al, 1994). Both shear zones were mapped in northern Saskatchewan, and project WSW into northeastern Alberta beneath the Athabasca Basin and possibly WCSB (Pană, 2021).

4.4 Metamorphism

Nilsen et al. (1981) interpreted the metamorphic evolution of the Alberta shield in two cycles. A first granulite-grade metamorphic cycle of Archean age and a second cycle that evolved from granulite through amphibolite-grade and finally greenschist-grade metamorphic conditions in the late Aphebian (1900–1790 Ma).

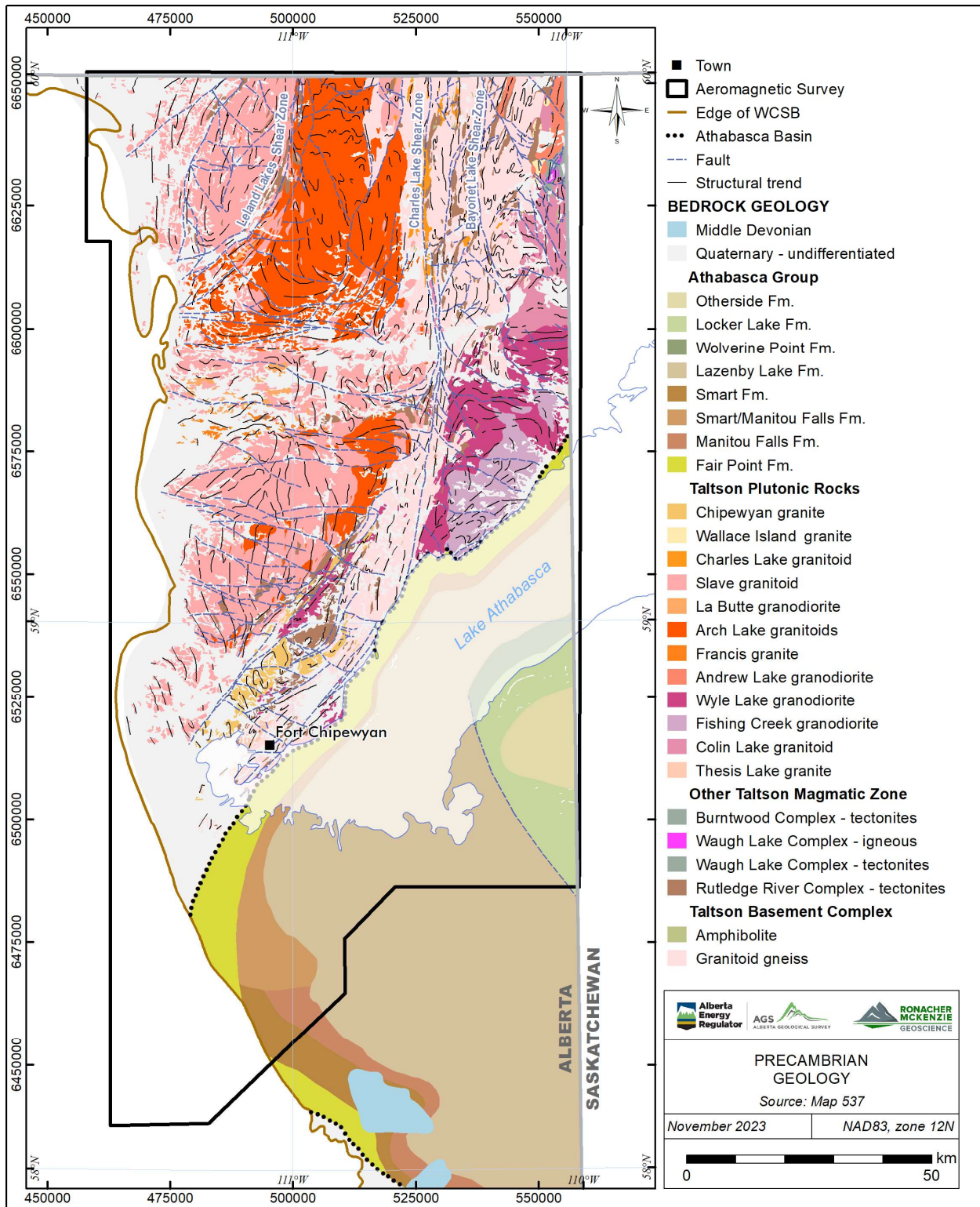


Figure 4-2. Map of the Precambrian Geology of Northeastern Alberta (From Map 537, Pană 2010a).

5.0 AEROMAGNETIC SURVEY DATA

5.1 Data Review

RMG reviewed the digital data available in the AER’s archives, for both completeness and data quality. It was determined that the AER data repository was missing final databases; replacement copies were obtained from the airborne contractor. The dataset was collected by EON Geosciences in 2021 (Alberta Geological Survey 2023).

The final processed data were reviewed with reference to the raw measured data to identify any potential data processing and levelling problems. No significant issues were identified.

The Shield aeromagnetic survey was flown with 400 m spaced survey lines oriented at N87.5°E, at a nominal terrain clearance of 200 m. Tie lines were flown at 2500 m spacing, oriented at N357.5°E (Alberta Geological Survey, 2023).

5.2 Derivative and Filter Products

Grid-based filter products were calculated from the total magnetic intensity (“TMI”) and International Geomagnetic Reference Field (“IGRF”) -removed residual magnetic intensity (“RMI”) grids (Table 5-1). The various filter products are used to enhance and highlight different features in the measured data to aid in geologic interpretation. RGB ternary images were also created from selected filter products to produce pseudo-structure and pseudo-geology maps.

Table 5-1. Magnetic Filter Products.

Product	Abbreviation	Description
Total Magnetic Intensity	TMI	Measured data
Residual Magnetic Intensity	RMI	Measured data, IGRF removed
TMI/RMI, Pole Reduced	RTP	Transform to vertical magnetic field, simplifies anomaly shapes
X Horizontal Derivative	DX	Highlights near surface features in N-S direction
	DY	Highlights near surface features in E-W direction
1st Vertical derivative	VD1	Highlights near surface features
2nd Vertical derivative	VD2	Enhances subtle near surface features
Analytic Signal (Total Gradient)	AS	Highlights discrete magnetic bodies and zones of high gradients
Total Horizontal Derivative	THD	Highlights horizontal changes in the total field

Product	Abbreviation	Description
1st Vertical Derivative of Total Horizontal Derivative	THD_VD1	Enhances THD
Tilt Derivative	TD	Tilt angle between vertical and horizontal derivatives, highlights magnetic contacts, amplitude independent
Total Horizontal Derivative of Tilt Derivative	TD_THD	Used with TD to estimate depth of discrete magnetic sources
Area	AREA	Highlights discrete areas
Edge	EDGE	Highlights edges of discrete areas
Geology	GEOLOGY	Pseudo-geology map. Ternary image only, no grid data
Structure	STRUCTURE	Pseudo-structure map. Ternary image only, no grid data

Selected filter products are presented in Figure 5-1 through Figure 5-9. All filter products are provided to the AGS in a digital appendix to this report.

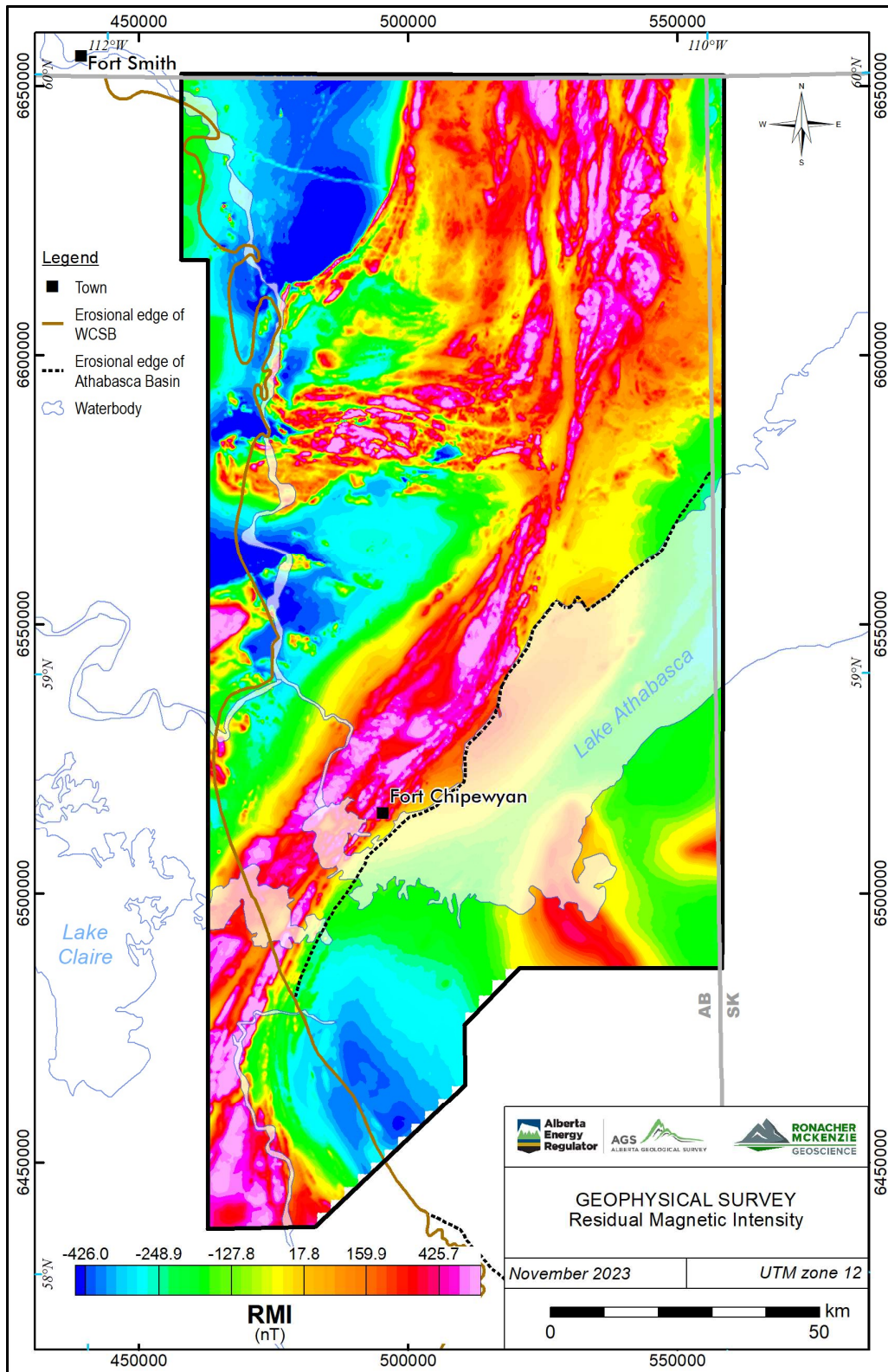


Figure 5-1. Residual Magnetic Intensity ("RMI").

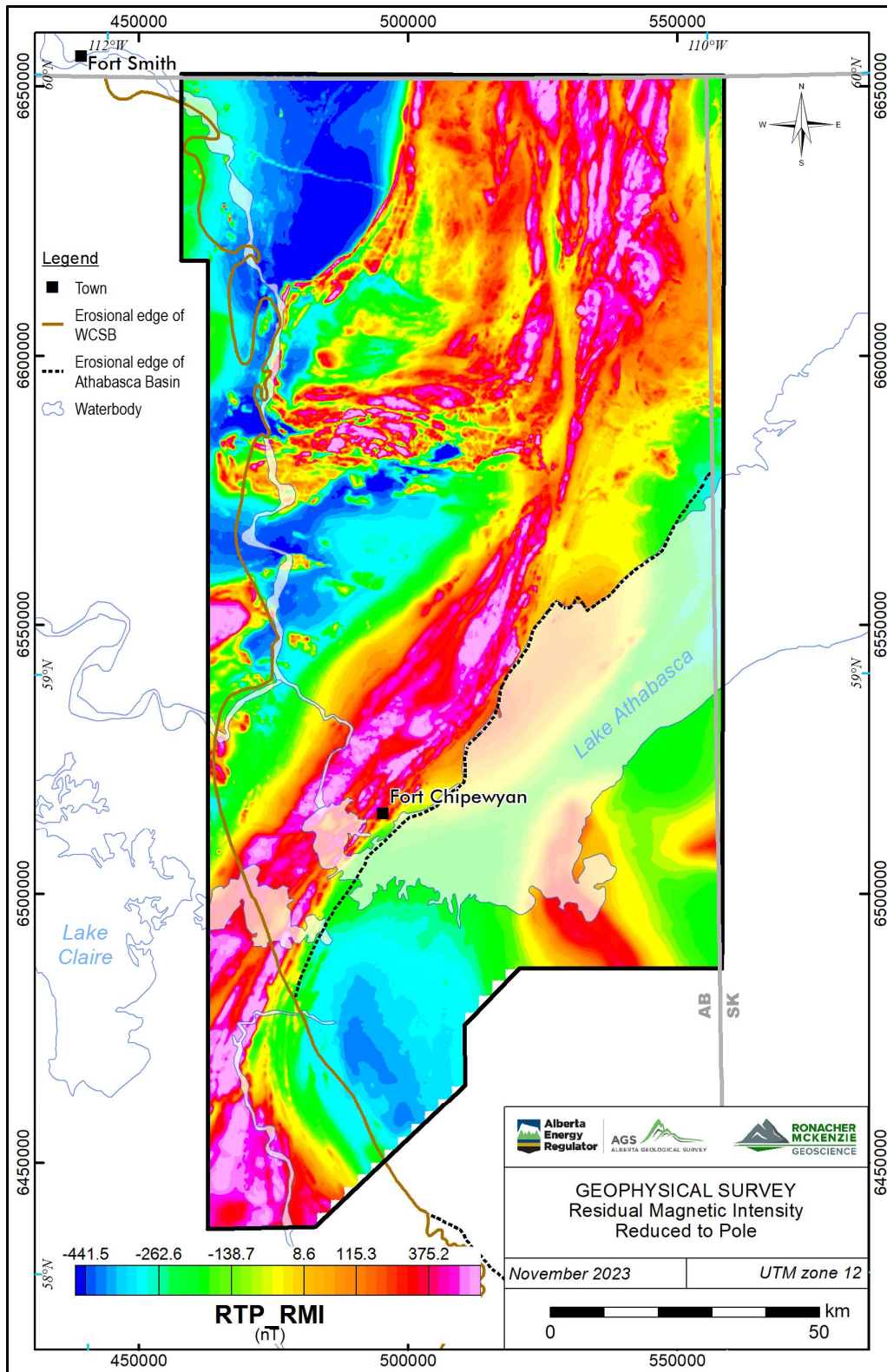


Figure 5-2. RMI, reduced to pole.

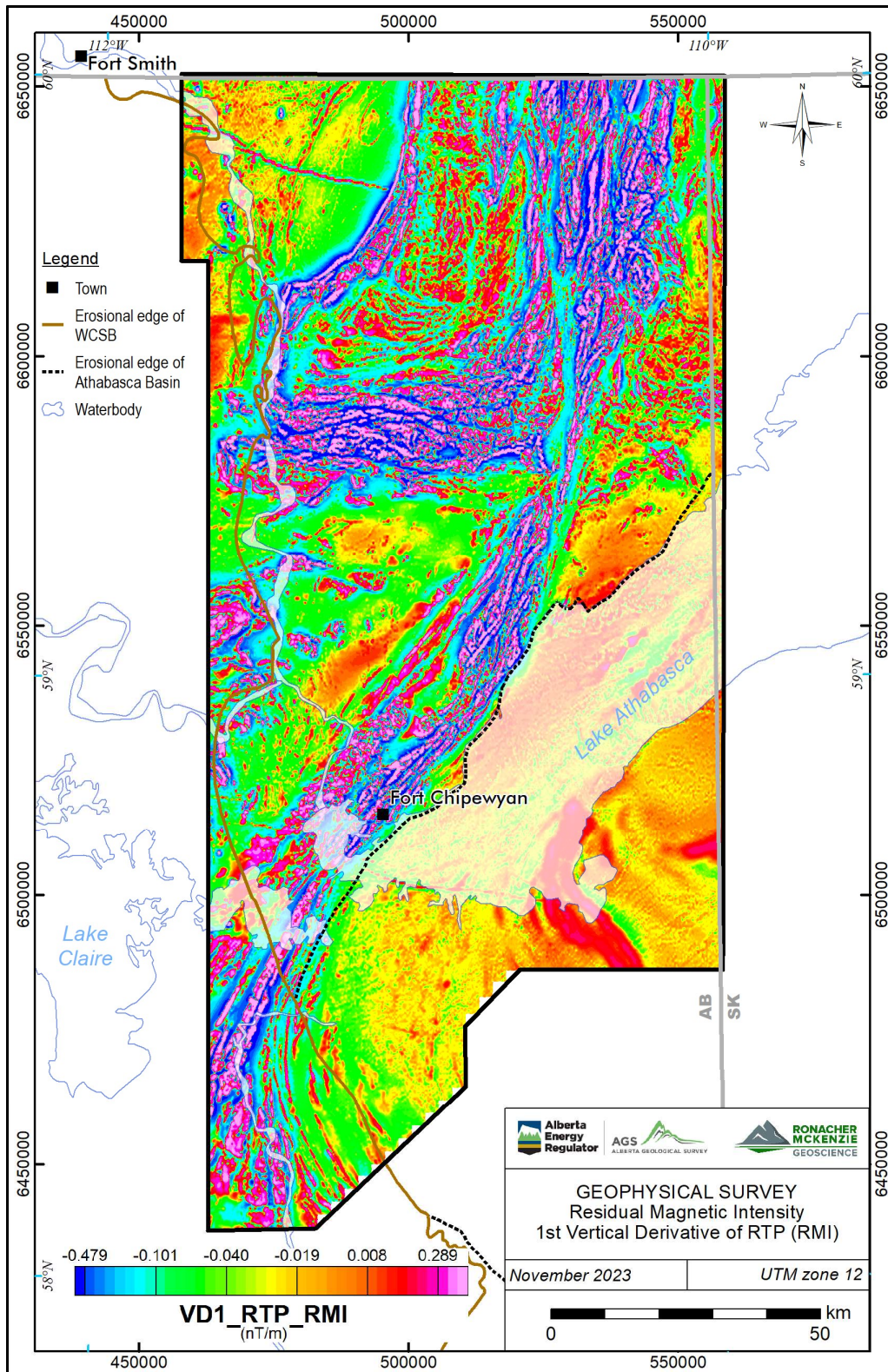


Figure 5-3. RMI, reduced to pole, 1st vertical derivative.

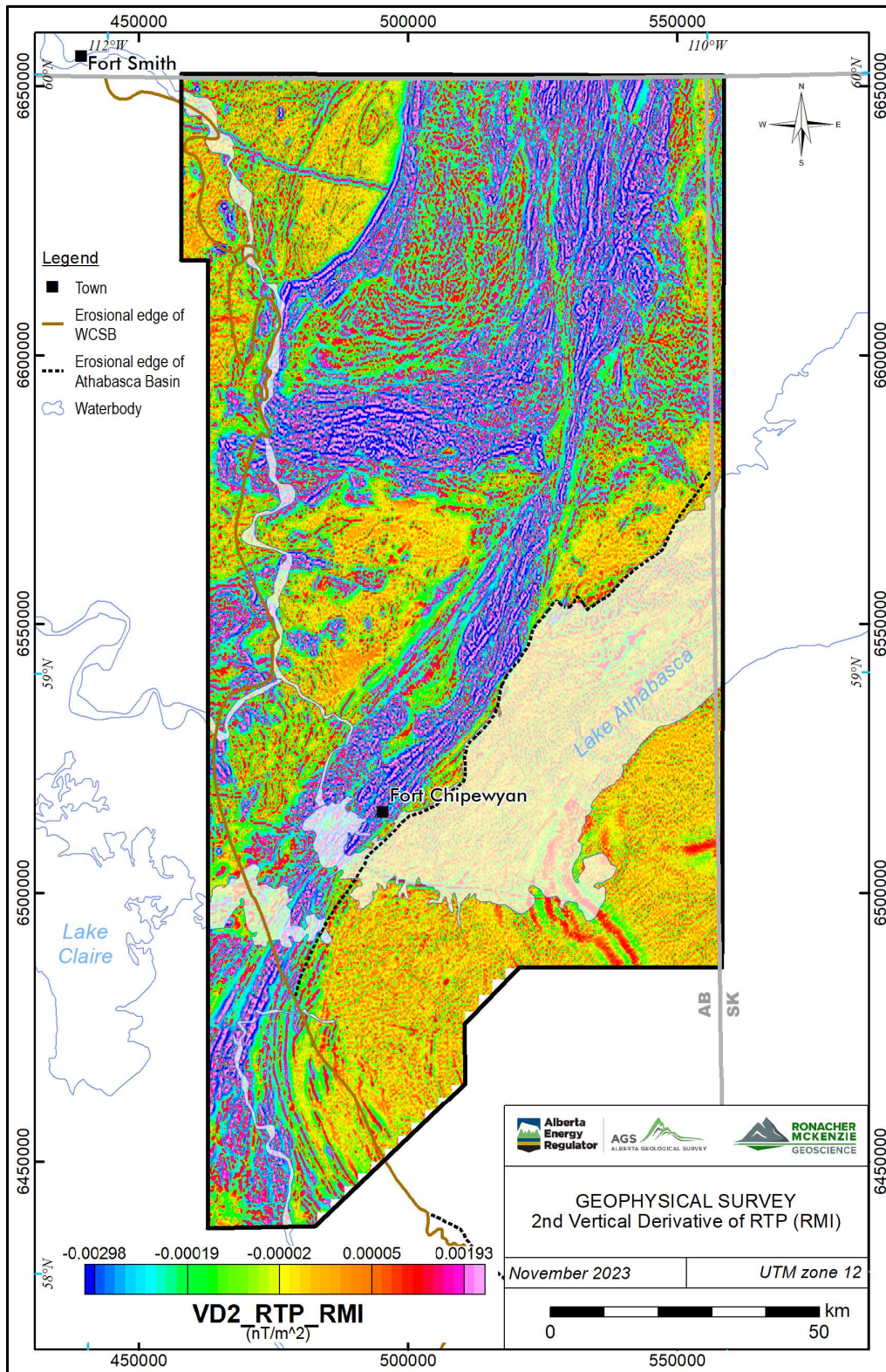


Figure 5-4. RMI, reduced to pole, 2nd vertical derivative.

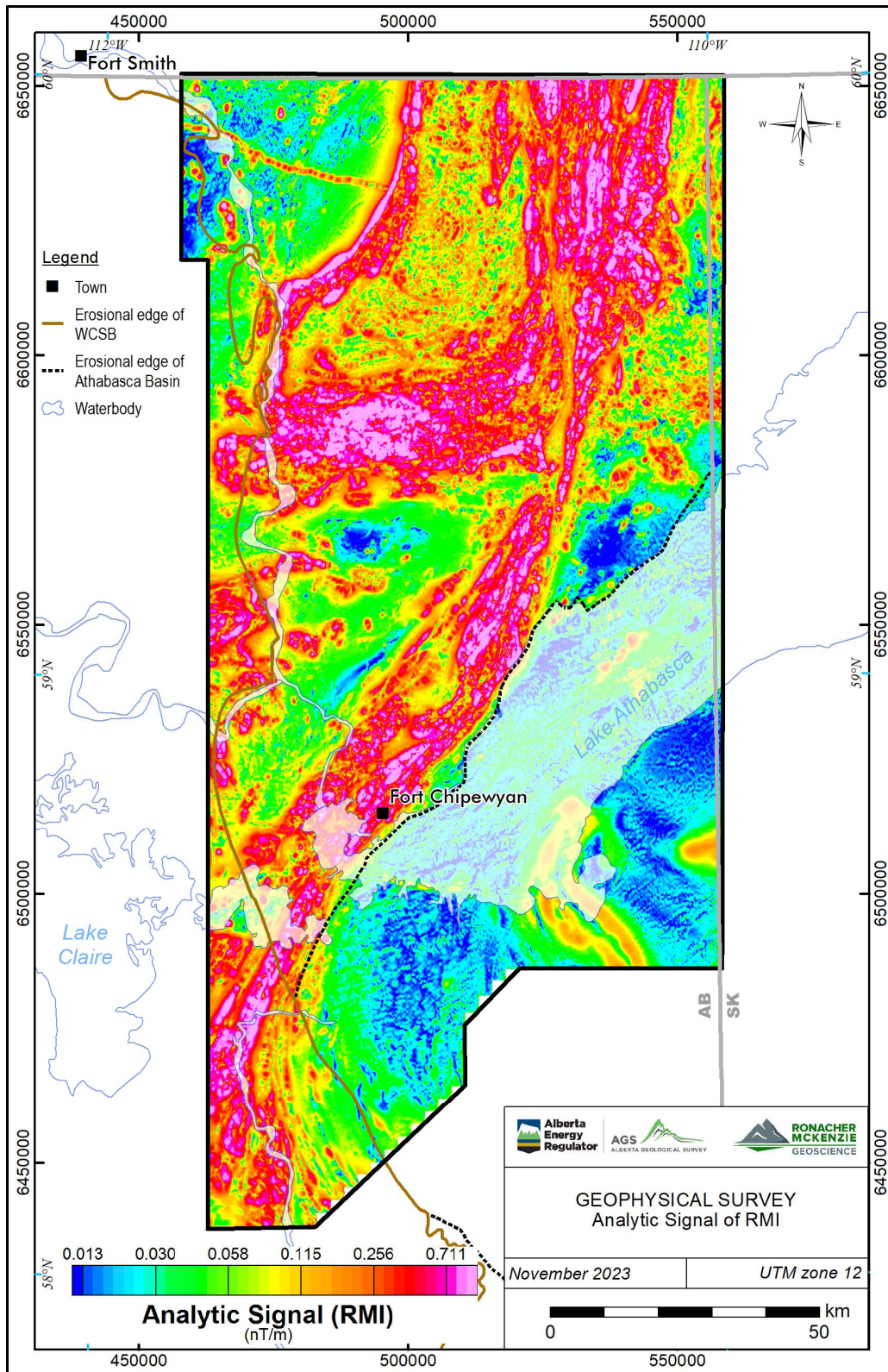


Figure 5-5. RMI, Analytic Signal.

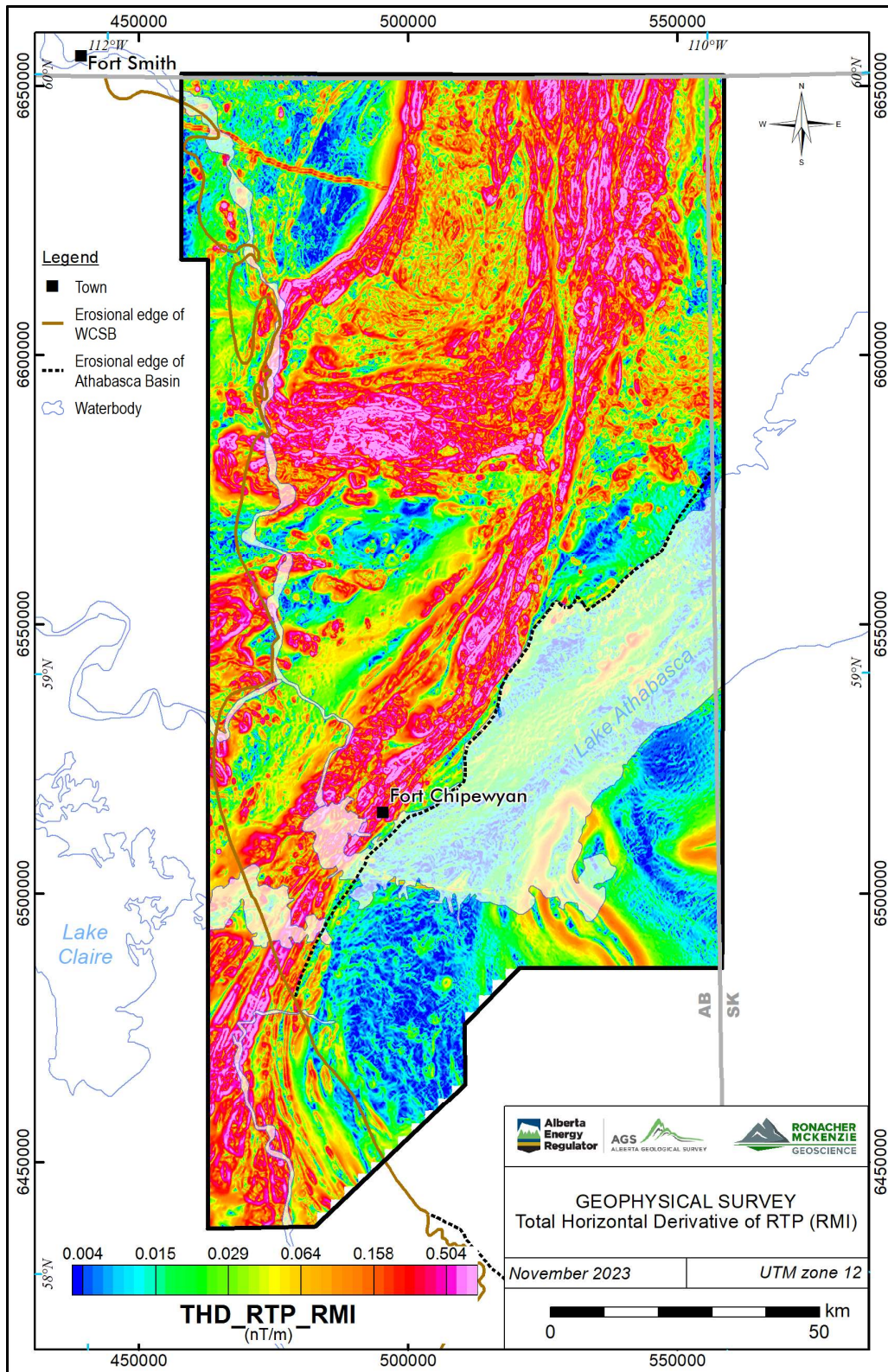


Figure 5-6. RMI, reduced to pole, total horizontal derivative.

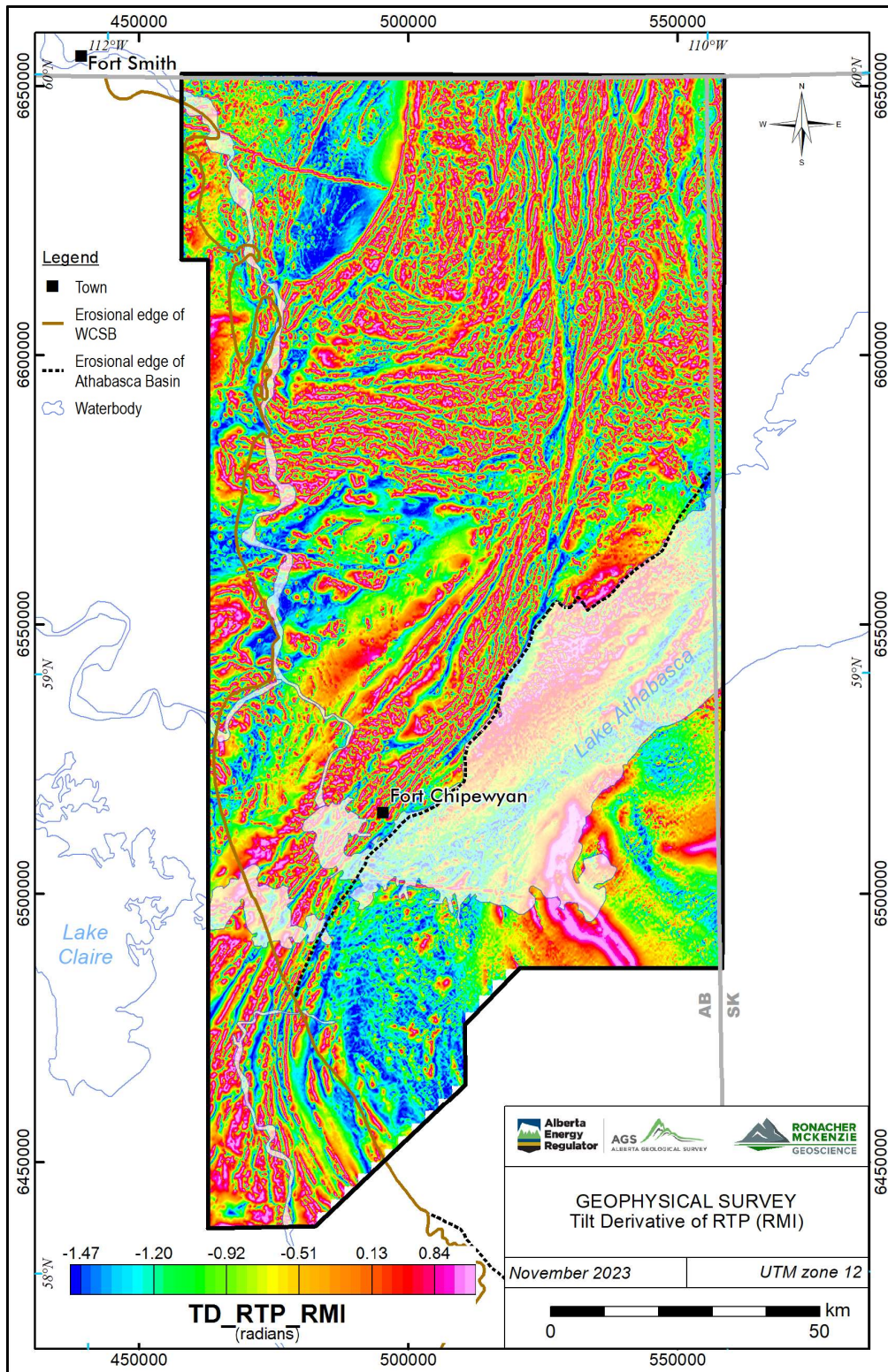


Figure 5-7. RMI, reduced to pole, tilt derivative.

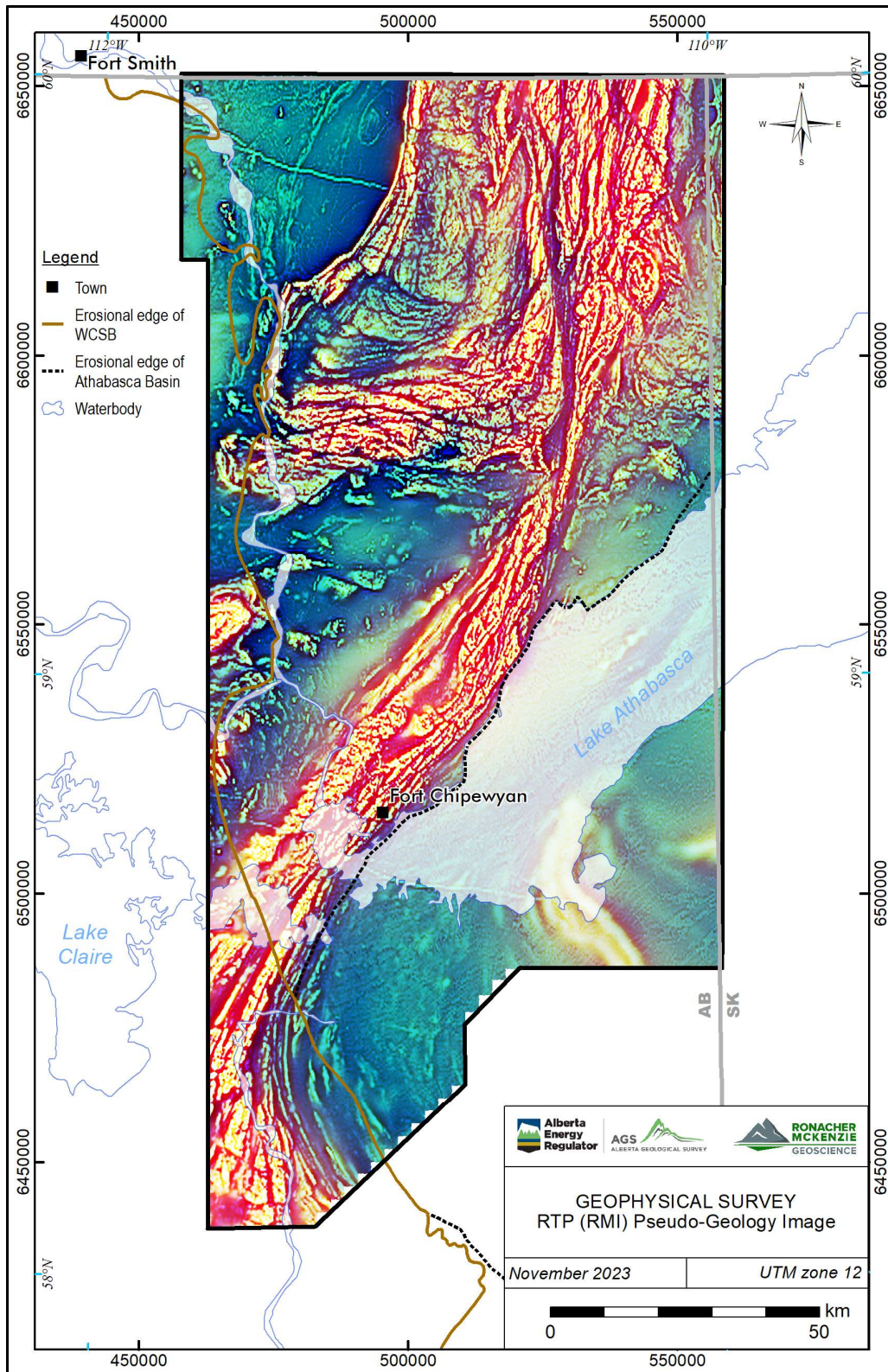


Figure 5-8. RMI, reduced to pole, pseudo-geology ternary image.

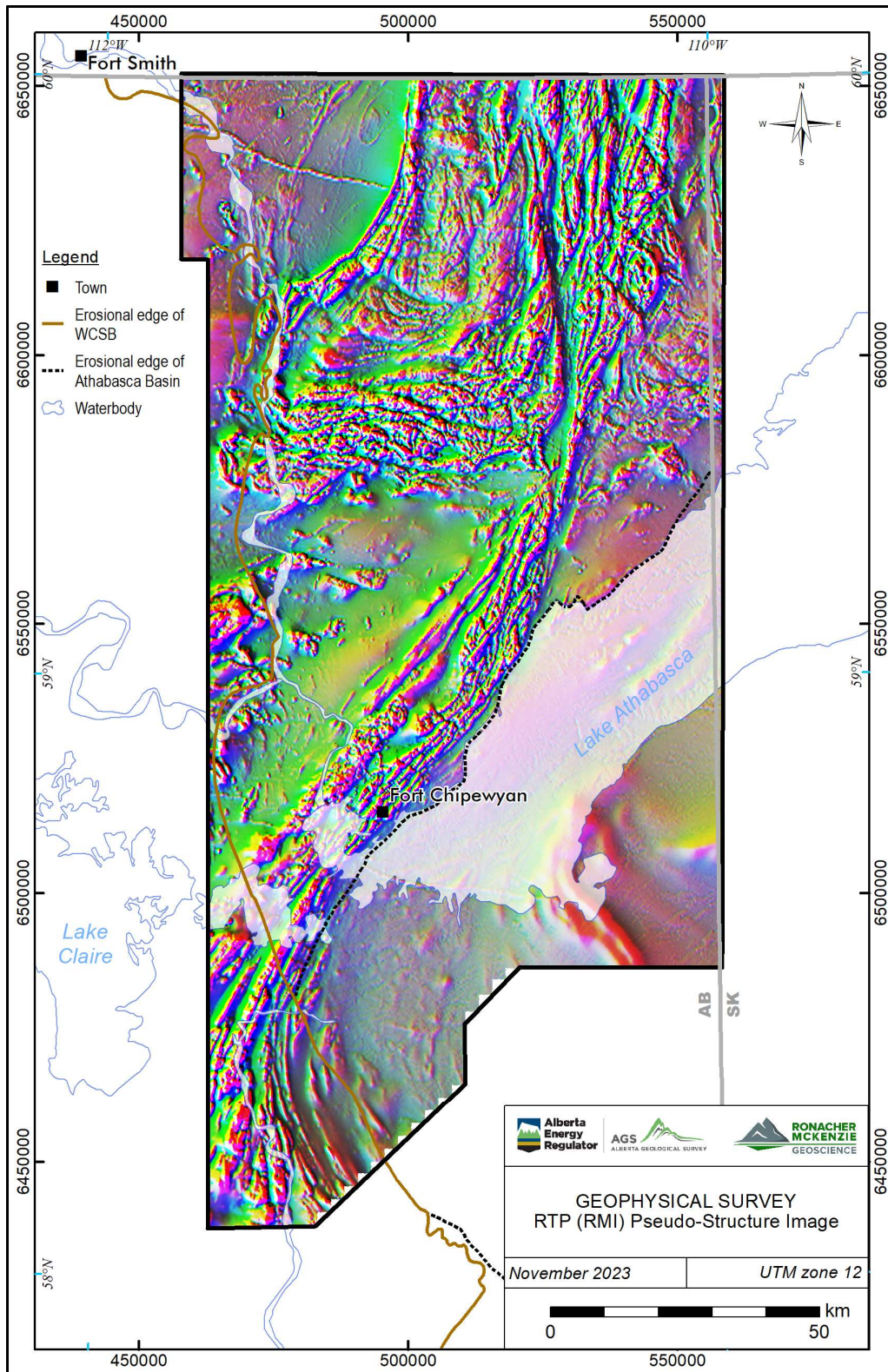


Figure 5-9. RMI, reduced to pole, pseudo-structure ternary image.

The gridded magnetic data are also displayed using alternate colour distributions, to aid in data interpretation (Table 5-2). Different colour distributions are used to help identify structures in the interpretation process. For example, greyscale maps are useful for highlighting high and low areas while minimizing the effects of local amplitudes, and isoluminant palettes (e.g., CET i1 described in Kovesi 2015) mitigate artificial highlighting caused by perceived brighter colours in commonly used rainbow palettes, particularly in the yellow and green ranges.

Table 5-2. Colour palettes applied to geophysical datasets.

Colour Distribution	Abbreviation	Description
Rainbow	(none)	Standard blue through purple colour palette.
Greyscale	BW	Black to white colour range, often easier to see structures.
Centre for Exploration Targeting (I1)	CET	Isoluminant colour range developed by University of Western Australia. No 'bright spots' in the spectrum to artificially attract the eye.

Selected examples of alternate colour distributions are shown in Figure 5-10 through Figure 5-12.

A complete set of georeferenced gridded data including alternate colour distributions is included in the digital appendix delivered with this report.

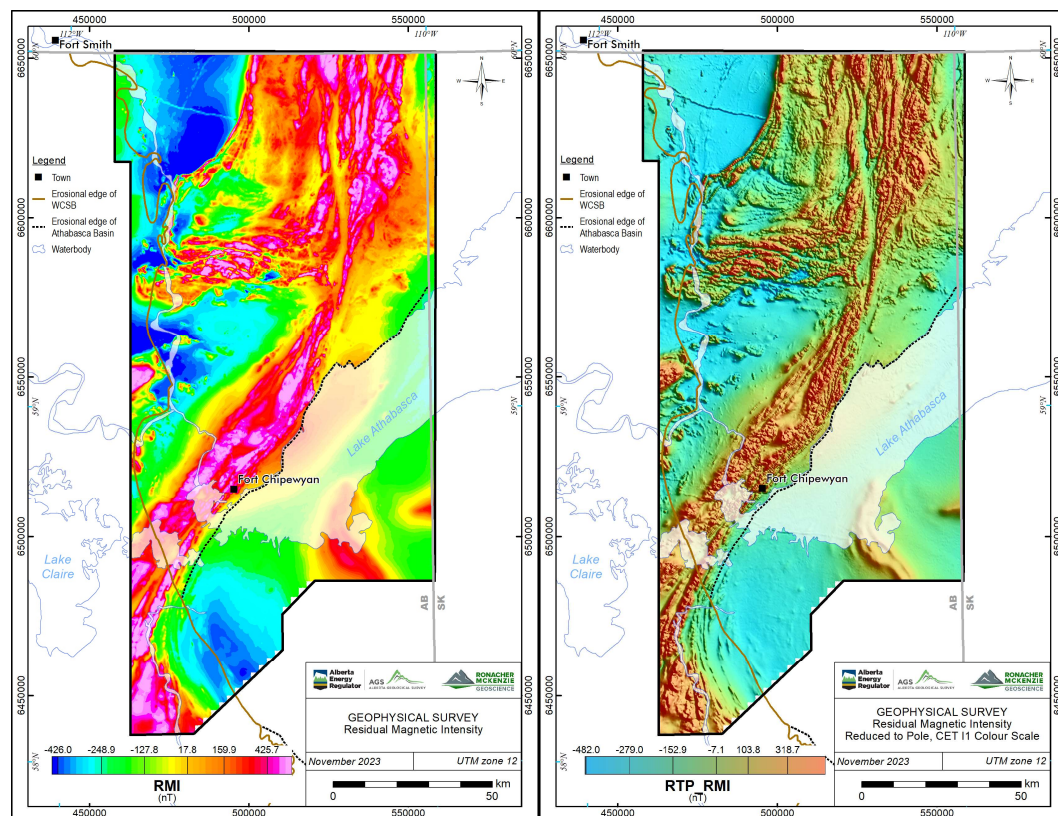


Figure 5-10. RMI, reduced to pole, standard rainbow (left) and CET i1 isoluminant (right) colour distributions.

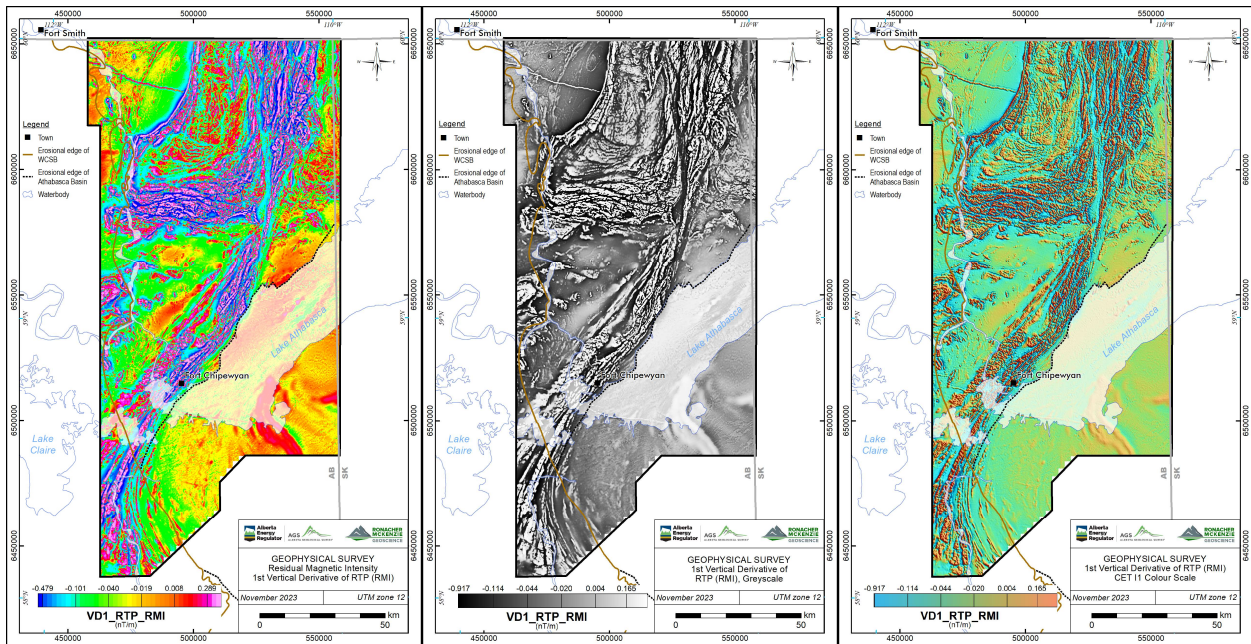


Figure 5-11. RMI, pole reduced, 1st vertical derivative, standard rainbow (left), greyscale (center), and CET i1 isoluminant (right) colour distributions.

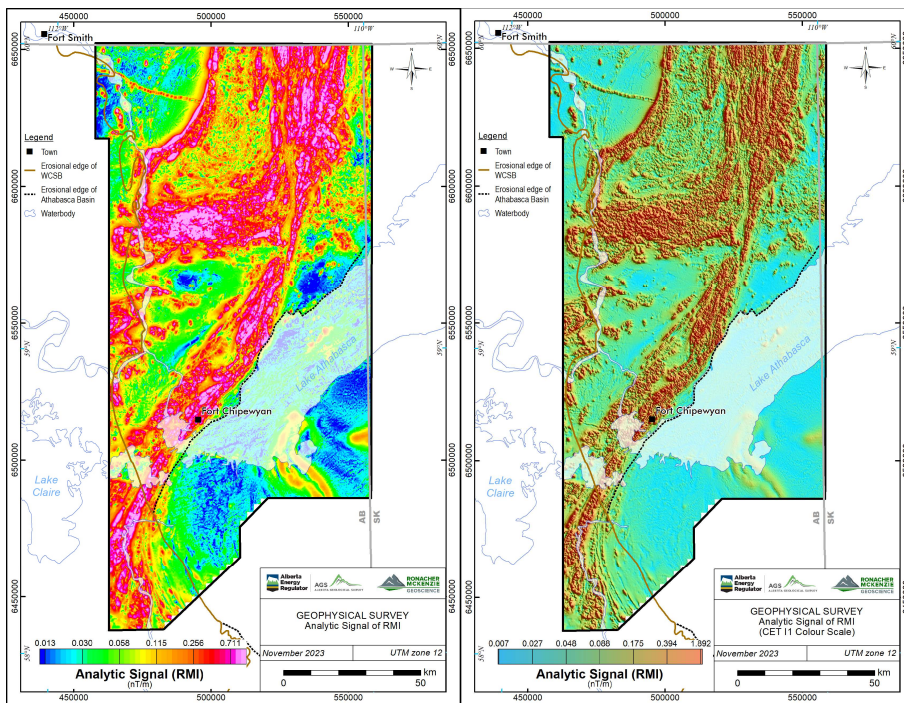


Figure 5-12. RMI, analytic signal, standard rainbow (left) and CET i1 isoluminant (right) colour distributions.

5.3 Automatic Structure Detection

RMG collaborated with Fathom Geophysics to perform automatic structure detection and to generate additional magnetic products to assist with the geological interpretation of the shield area. Automatic structure detection was applied to the gridded magnetic data and the processing included application of standard filters as well as application of Fathom Geophysics' structure detection and radial symmetry filters. The results of this work are presented in Appendix 1 – Automatic Detection – Fathom Geophysics. The final products are in the digital appendix.

The additional filter and image processing products created by Fathom Geophysics are listed in Table 5-3. Grid and image digital files are also attached to this report. An example of an image processing product, a ternary image of 1VD, tilt angle, and horizontal gradient magnitude (“HGM”), is shown in Figure 5-13.

Automatic structure detection filter is a linear feature detection algorithm used to highlight ridges, valleys or edges in gridded data. Automated structure detection is a multi-scale phase congruency algorithm in which features are highlighted either in areas of low or high magnetic contrast, irrespective of amplitude. The method also allows inference of the estimated depth of structures between 0.5 and 1 times the filter wavelength, assuming shorter wavelengths are related to shallow structures and longer wavelengths are related to deeper structures (which may not always be the case). Structure detection products are listed in Table 5-4. An example of belt-parallel structure detection result for the RTP data is shown in Figure 5-14. Given a 1600 m wavelength, these results highlight lithological contacts and fabric parallel shear zones at an inferred depth of 800-1600 m (0.5 to 1 times the filter wavelength).

Radial symmetry is a filtering process that identifies equant discrete features in the data. The algorithm seeks locations around which data values either decrease or increase in all directions. These features may be related to stocks, batholiths, cupolas, alteration haloes, kimberlites, diatremes, steep-plunging mineral lenses, and breccia pipes, although all radial features used in interpretation are correlated manually with other data. Radial symmetry products were calculated using wavelengths from 500-2000 m, starting from a number of different residuals. Radial symmetry products are listed in Table 5-5.

Table 5-3. Additional filter and image products.

Product	Abbreviation	Description
Filter Products		
Automatic Gain Control (standard deviation = 30)	AGC30	Evens anomaly amplitudes to make subtle features more visible, longer wavelengths are suppressed.
Pseudogravity	PGrav	Useful for highlighting large scale features.
Pseudogravity residual	PGravRes	Difference between 0-2000 m upward continued pseudogravity. Longest wavelength features suppressed to highlight intermediate scale features.

Product	Abbreviation	Description
Horizontal gradient of PGravRes	PGravResHGM	Highlights edges of intermediate scale features.
Small-scale residual	Res500_2000	Differential upward continuation residual, 500-2000 m. Highlights sources at 250-1000 m depth.
Medium-scale residual	Res2000_5000	Differential upward continuation residual, 2000-5000 m. Highlights sources at 1000-2500 m depth.
Large-scale residual	Res5000_10000	Differential upward continuation residual, 5000-10000 m. Highlights sources at 2500-5000 m depth.
Vertical derivative minus horizontal derivative	VDMHGM	Accentuates contrast in 1 st vertical derivative, aids in highlighting shallow features.
Vertical integral	VINT	Vertical integral of total field.
Analytic signal of vertical integral.	VIAS	Produces a result with similar amplitudes and wavelengths to total field, with reduced effects of magnetization direction and remanence.
Image Products		
Ternary of directional derivatives	X_Y_Z	Ternary images (CMY+RGB) of 1 st X, Y, and vertical derivatives.
Ternary of 1VD, Tilt, HGM	1VD_Tilt_HGM	Ternary images (CMY+RGB) of 1VD, tilt angle, horizontal gradient.
Ternary of residuals	SmRes_MedRes_LgRes	Ternary images (CMY+RGB) of small, medium, large-scale residuals.
Ternary of RTP, VIAS, Asig	RTP_vias_asig	Ternary images (CMY+RGB) of RTP, analytic signal of vertical integral, and analytic signal. Helps identify remanent zones.
Ternary of pseudogravity	Prav_PGravRes_PGravResHGM	Ternary images (CMY+RGB) of Pseudogravity, pseudogravity residual, and horizontal gradient of pseudogravity residual.

Table 5-4. Structure detection products.

Product	Abbreviation	Description
Fabric Orientation (RTP and AGC)	Fabric_Orientation	Reflects the orientation of long-wavelength features.
Total Structure (RTP and AGC)	StructX_Total	Total structure detected. X = filter wavelength (100 to 3200 m).
Oriented Structural Domains	StructX_OriDom_Th	Total structure (X = filter wavelength), thresholded into orientation domains.
Vectorized Structure	StructX_Total_Vec	Vectorized total structure (X = filter wavelength).

Product	Abbreviation	Description
Belt-parallel structure	StructX_Para	Structure parallel to major belts (X = filter length).
Vectorized belt-parallel structure	StructX_Para_Vec	Vectorized structure parallel to major belts (X = filter length).
Belt-crossing structure	StructX_Cross	Structure crossing major belts (X = filter length).
Vectorized belt-crossing structure	StructX_Cross_Vec	Vectorized structure crossing major belts (X = filter length).

Table 5-5. Radial Symmetry products

Product	Abbreviation	Description
Radial Symmetry Highs	Res_X_Y_RSymZ_mi_Lows	Magnitude-independent radial symmetry at wavelength Z from X to Y residual, lows. Also vectorized.
Radial Symmetry Lows	Res_X_Y_RSymZ_mi_Highs	Magnitude-independent radial symmetry at wavelength Z from X to Y residual, highs. Also vectorized.
Radial Symmetry Highs and Lows	Res_X_Y_RSymZ_mi_Highs_and_Lows	Magnitude-independent radial symmetry at wavelength Z from X to Y residual, highs and lows. Also vectorized.

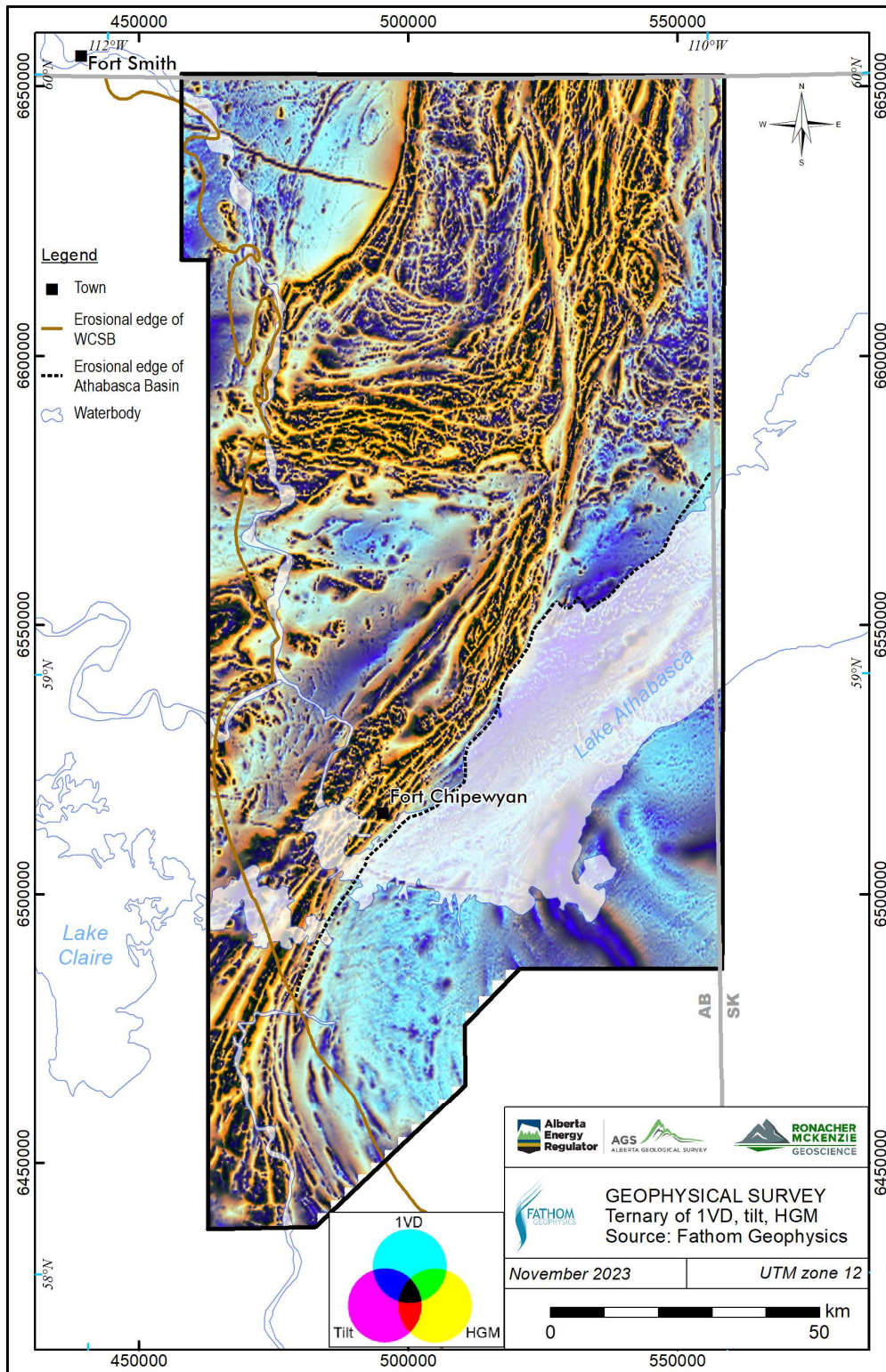


Figure 5-13. CMY ternary image displaying the 1VD, tilt angle, and HGM results from the RTP.

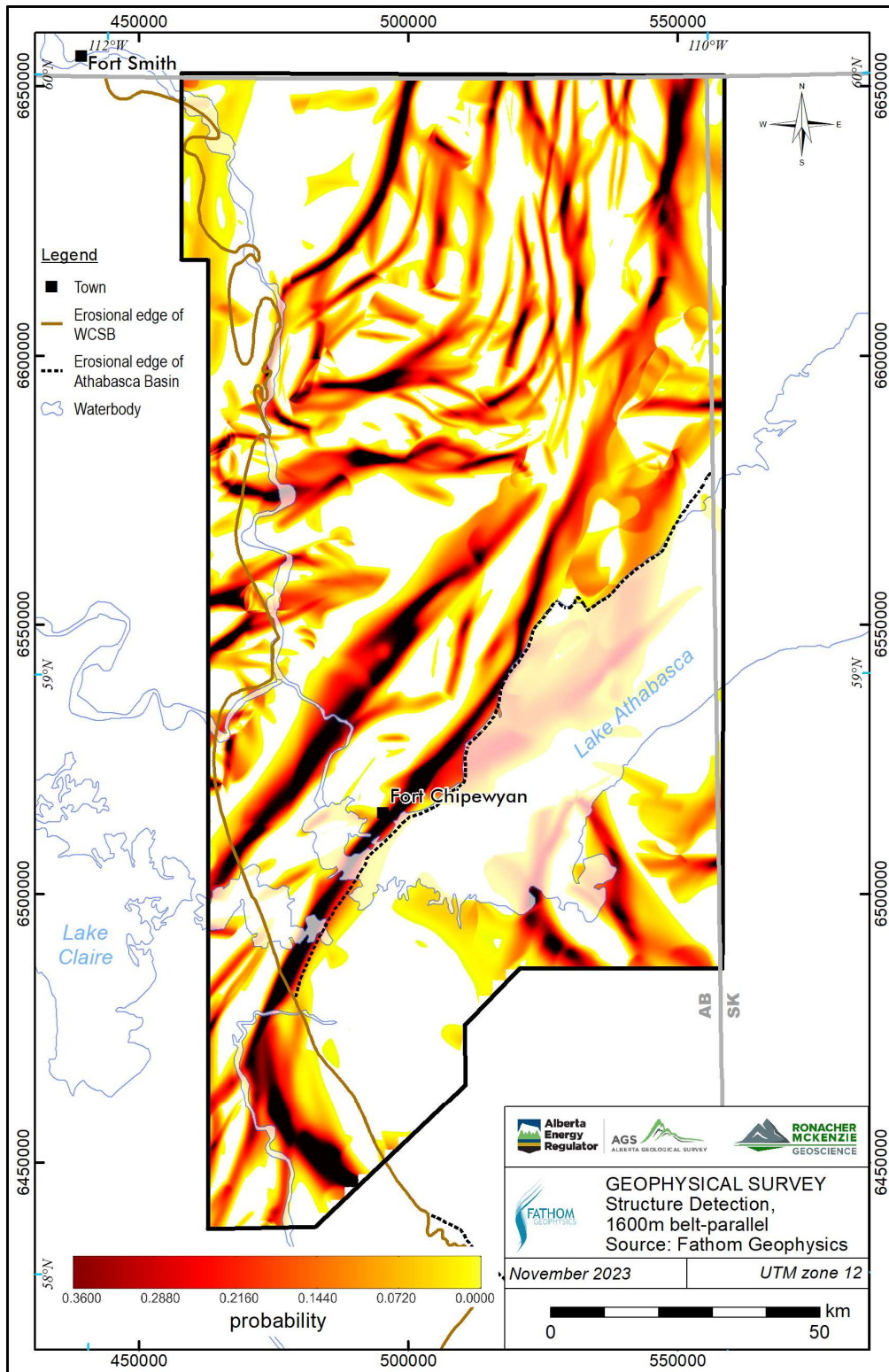


Figure 5-14. Image showing 1600 m belt-parallel structure detection results for the RTP data. The results highlight lithological contacts and fabric parallel shear zones at inferred depths of 800-1600 m.

5.4 3D Inversions

The total magnetic intensity data were inverted using Seequent’s VOXI inversion service to produce 3D models of subsurface magnetization. 3D Magnetic Vector Inversion (“MVI”) and susceptibility models were obtained for the complete Shield survey area at coarse resolution, as well as two 97.5 x 40 km ‘transect’ areas of interest at higher resolution. Areas chosen for inversion are displayed in Figure 5-15.

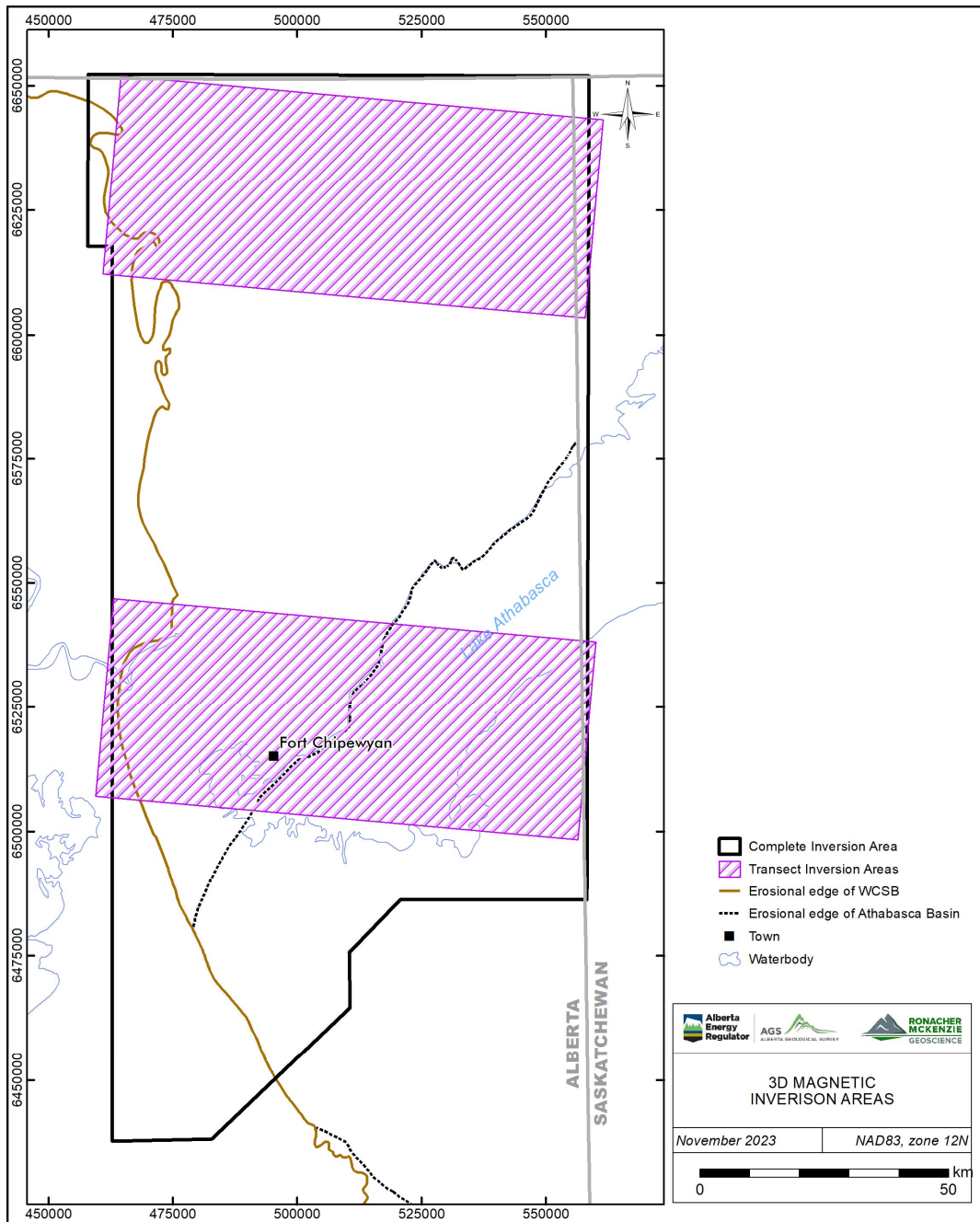


Figure 5-15. 3D magnetic inversion areas.

5.4.1 Data Preparation and Inversion Procedures

Prior to inversion, the data were pre-conditioned to remove long wavelength regional and short wavelength near-surface components, by upward continuation and application of band-pass filtering to the gridded data.

These filtered data were then sampled to a database, which was then de-sampled to the nominal cell size used for inversion. Gaussian noise based on the standard deviation of the low-pass residual of the filtered data was added to create the final data channel used for inversion.

For inversion, an initial error estimate based on the standard deviation of the data was used to generate a first pass inversion model. A new error estimate was calculated based on the misfit from this first pass model and used to run several models to estimate the best regularization parameters for the model. The misfit from the model with the optimal regularization was then used to rescale the estimated error for the final models. For the final models, the inversion was run using the final rescaled error as well as two passes of the VOXI Iterative Reweighting Inversion (“IRI”) focus procedure, which helps to sharpen features in the final model and reduce over-smoothing. The IRI models were compared with models run without IRI to ensure that the results are consistent and plausible.

5.4.2 Inversion Results

The parameters used for each inversion area are summarized in Table 5-6.

Table 5-6. 3D Magnetic Inversion Parameters

Parameter	Full Shield	North Transect	South Transect
Horizontal Cell size:	750 m	250 m	250 m
Vertical Cell size:	375 m	125 m	125 m
Upward Continuation applied:	200 m	200 m	200 m
Band Pass Filter type	Butterworth, 8th order	Butterworth, 8th order	Butterworth, 8th order
Band Pass Filter cutoffs	Low: 700 m High: 127000 m	Low: 700 m High: 55500 m	Low: 700 m High: 55500 m
Gaussian Error added to data:	0.5 nT	0.65 nT	0.4 nT

The final models were trimmed of extraneous cells using SRTM topography from surface to 5 km depth.

The MVI amplitude model reflects only the total magnitude of the magnetization vector, which helps remove effects of ground magnetization not parallel to the Earth’s field. The MVI code also returns scalar models of the magnetization vector magnitude parallel to (Eproj) and perpendicular (Eperp) to the Earth’s magnetic field. The parallel amplitude (Eproj) is analogous to the result returned from a susceptibility inversion.

A 3D vector model is also generated by the MVI process, showing the direction and amplitude of the magnetization vector in the 3D inversion volume.

For comparison, a susceptibility model was also run, using the same noise and regularization parameters as the MVI inversion (Figure 5-16).

The detailed transect models provide enhanced resolution compared to the coarser model run on the full area (Figure 5-17).

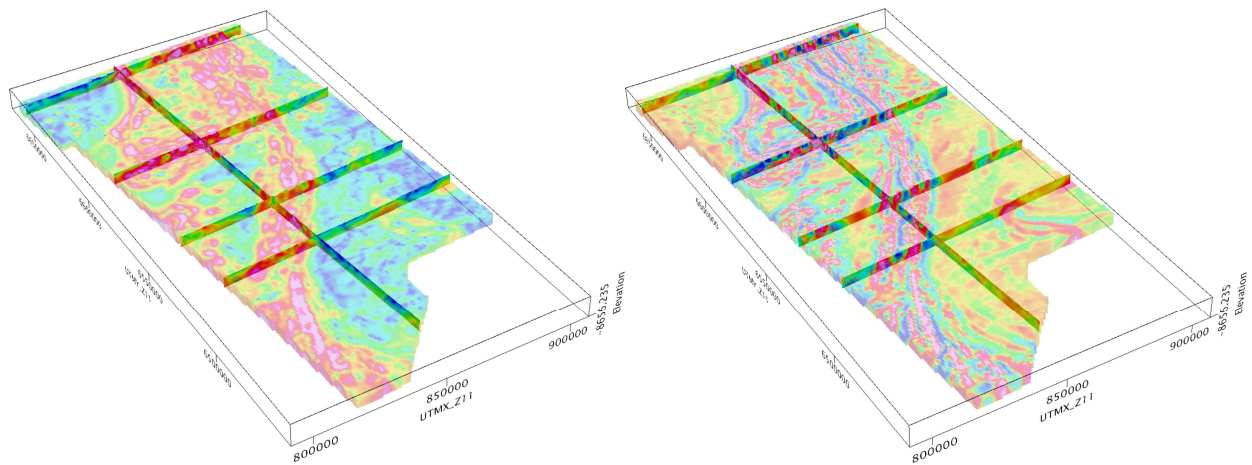


Figure 5-16. MVI model (left) and susceptibility model (right), with sections.

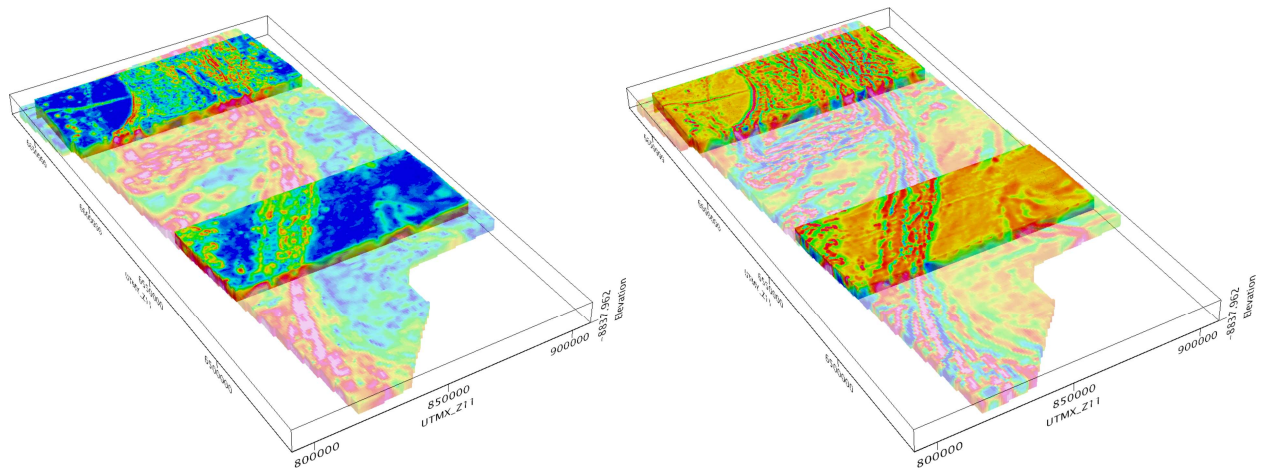


Figure 5-17. MVI model (left) and susceptibility model (right), full area with transect models.

A complete set of inversion products including voxels and elevation plan slices, is included in the digital appendix attached to this report.

6.0 METHODOLOGY AND RESULTS

6.1 Methodology

6.1.1 Data Sources

An aeromagnetic survey was flown over the entire Alberta shield in northeastern Alberta (the “Shield”) in early 2021 by EON Geosciences Inc. (“EON”) on behalf of the Alberta Energy Regulator (“AER”). The survey was flown with 400 m spaced east-west lines, and 2500 m spaced north-south tie lines, at a nominal altitude of 200 m above terrain. This work was completed under the Mineral Grant provided by the Government of Alberta in 2021.

Supporting geological information for the interpretation of the magnetic data are the Precambrian Geology of northeastern Alberta (MAP 537 by Pană, 2010a), the Bedrock Geology of Alberta (MAP 600 by Prior et al., 2013), GIS compilation of structural elements version 3 (Pană and Waters, 2016), Atlas of the Western Canada Sedimentary Basin (Mossop and Shetsen 1994), structural elements in the Alberta Plains (Alberta Geological Survey, 2021, Pană et al., 2021), geochemistry of plutonic and metamorphic rock samples from the Canadian Shield (Lopez et al., 2022; Meek et al., 2023a, 2023b) (Figure 6-1), data compilation from industry assessment reports, various AGS reports (e.g. Langenberg, 1983; Pană, 2010a), and government base layers.

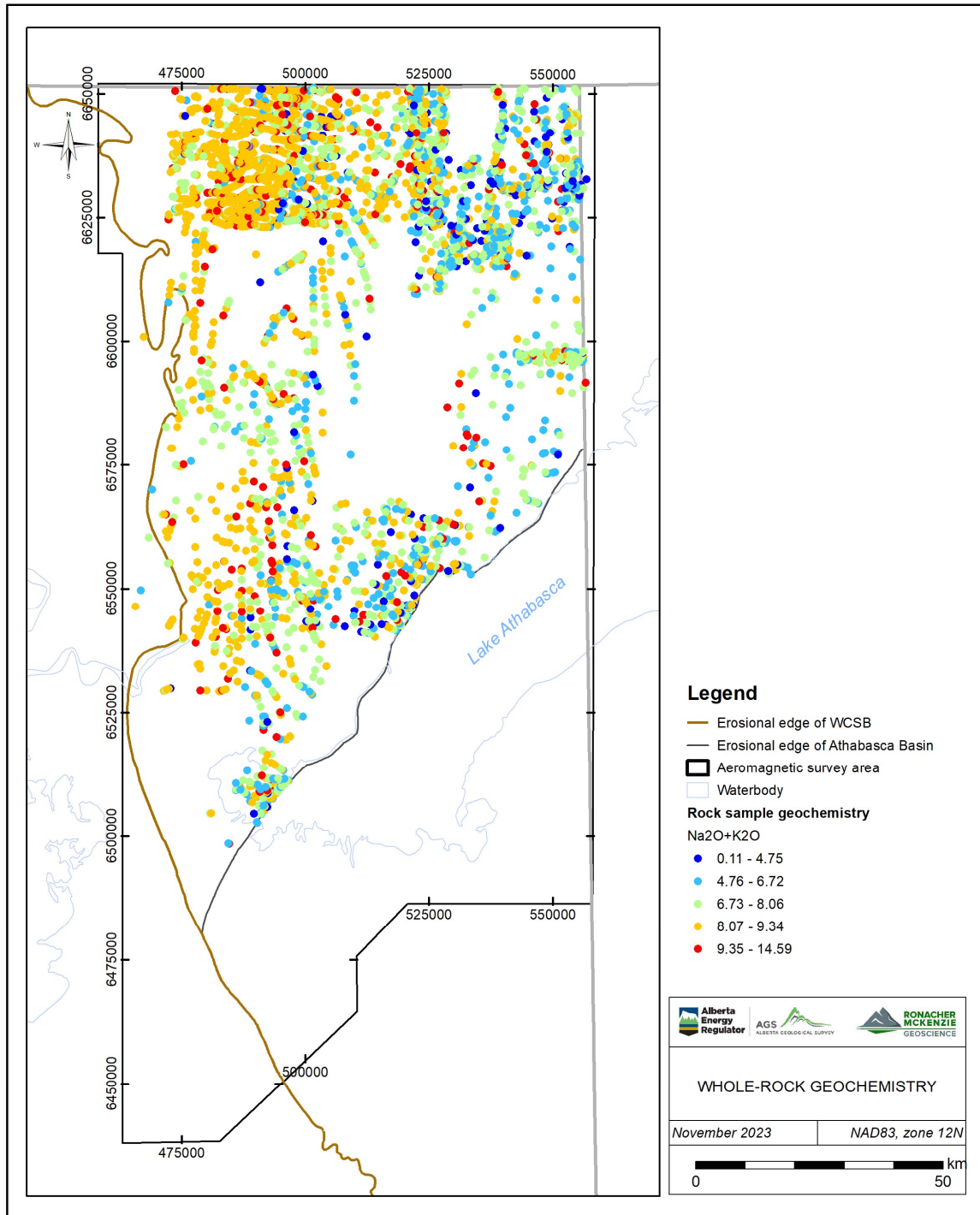


Figure 6-1. Location of rock samples with recent whole-rock major and trace element geochemistry

6.1.2 Methods

The analysis of magnetic data follows the methodology developed by Isles and Rankin (2013). According to this methodology, the interpretation of aeromagnetic data process is broken down in three main stages: observations, integration, and interpretation.

The observation stage is focused on observing features directly from the data. In this stage, the interpreter records linear trends and discontinuities as form line features, and magnetic rocks units from the anomalies that they cause as polygons. Observations are drawn following linear magnetic highs and gradient trends from several magnetic derivative products (e.g., RTP-1VD). Thus, form lines may represent either stratigraphic or structural trends, and line breaks or juxtapositions may represent a structural element (e.g., fault, shear zone, unconformity or intrusive contact). This stage also includes the definition of domains that outline magnetic characteristics of different regions based on combined form line and magnetic rock unit observations.

The integration stage combines observations with existing geological and other types of data. This stage includes identification and definition of structural elements, magnetic rock units, and changes or disruptions in domains with coherent structural or form line trends. Automatic detection results conducted by Fathom Geophysics are evaluated and used in this stage.

The interpretation stage involves the creation of a structural framework that includes inferences of structural and lithotectonic history. This is the final step in generating an integrated geologic and geophysical interpretation of an area to present a final geological interpretation map. The compilation of the domains and structure layers is the basis of the structural framework interpretation.

6.1.3 Workflow

The following workflow is a modified version (adapted to the current project) of the flow chart by Siddorn et al. (2020) which is based on Isles and Rankin's (2013) methodology.

Observation

- a) Observe and record form lines (mainly) from RTP derivative imagery.
- b) Observe and record magnetic rocks units from RMI RTP data.
- c) Observe and record magnetic patterns within magnetic rocks units from RTP derivative imagery.
- d) Observe and record rounded features that may be possible intrusions; use manual detection supported by automatic detection in high amplitude areas where signal is present but obscured.

Integration

- e) Cross-reference aeromagnetic observations with Precambrian Geology of Northeastern Alberta map (MAP 537) to calibrate lithologic subdivisions and their boundaries.

- f) Cross-reference additional data sets (rocks sample geochemistry, geochronology, industry data) with aeromagnetic/geology integration to refine lithologic subdivisions and their boundaries.

Interpretation

- g) Interpret fault and shear zone locations and infer movement senses, timing relationships – use results of quantitative 3D modeling.
- h) Interpret features detected beneath the WCSB and Athabasca Basin
- i) Review and form the geological interpretation map - incorporate modeling results where appropriate.

6.2 Results

6.2.1 Magnetic Rock Units

The residual magnetic intensity, analytic signal and derivative products such as first vertical derivative and total horizontal derivative are used to outline magnetic rock units. Existing geologic data are used to identify and classify magnetic rock units, sequences, and subdomains evident in the interpretation. The geologic information from the Precambrian Geology of Northeastern Alberta map (Pană 2010a), was used as a guide to identify and correlate map units of the Taltson Magmatic Zone and Athabasca Group in the interpretation. Classification follows known map units wherever possible, and the geophysical characteristics of the interpreted units were then tabulated (Table 6-1).

Figure 6-2 displays internal variations in magnetization, which were mapped as magnetic texture, allowing the interpretation of subdomains (Figure 6-3).

The interpreted magnetic rocks units include subdomains with a change in magnetic character in relation to the surrounding rock. These changes may be related to primary heterogeneous fabric or possible secondary geologic processes. Possible processes are metamorphism, metasomatism, deformation, weathering, and other forms of alteration that create, introduce, or destroy magnetic minerals. The enclosed GIS vector files include observations regarding a change in character of a given map unit, for example, a broad zone of magnetite-destructive alteration possibly due to low-grade metamorphism along the Charles Lake Shear Zone.

The GIS files provided in the digital Appendix show the details of the interpreted magnetic rock units.

Table 6-1. General geophysical characteristics of map units of Pană (2010a).

Tolson Magmatic Zone Parent 1	MAP 537 Unit	Magnetic characteristics
Plutonic rocks	Chipewyan Granite	High magnetic intensity (RMI_RTP) with elongate shape and high-frequency grainy texture in derivative maps (e.g., RMI_VD1) without significant interval variations.
	Wallace Island Granite	Moderate magnetic intensity and high gradients (e.g., RMI_VD1, THD), distinct from surrounding units.
	Charles Lake granitoid	Narrow or small unit not apparent in the magnetic products. Moderate to weakly magnetic intensity undistinguishable from surrounding units.
	Slave granitoid	Both strong and weakly magnetic intensity variants. Weakly magnetic variant displays flat lowest total magnetic intensity where few form lines can be interpreted. Form lines are better seen on enhanced derivative products; linear features are either dykes or narrow bands with relatively higher susceptibility. Strongly magnetic variant is in the middle section of the granitoid at ~58.5 latitude N where high-magnitude EW-trending magnetic subunits occur; suspected to be units of Arch Lake granitoids instead of Slave granitoid.
	La Butte Granodiorite	Higher magnetic intensity body intruding Arch Lake granitoids.
	Arch Lake granitoids	High-frequency grainy magnetic anomalies in RMI_AS on relatively low to medium magnetic intensity unit
	Francis Granite	Moderate magnetic intensity and high gradients (e.g., RMI_VD1, THD), distinct from surrounding units.
	Andrew Lake Granodiorite	Moderate to weak magnetic intensity, with rare internal anomalies
	Wyle Lake Granodiorite	Moderate magnetic intensity, and both moderate and high gradient variants. Moderate gradient variant displays several internal heterogeneities and anomalies. High gradient variant displays higher frequency grainy texture and few internal variations.
	Fishing Creek Granodiorite	Weak magnetic intensity and few internal rounded anomalies.
	Colin Lake granitoid	Both moderate and weak magnetic intensity variants. Weakly magnetic variant with rare internal anomalies. Moderately magnetic variant with high frequency internal variations in intensity, mostly grainy texture in derivative products (e.g., RTP_AS) and both round and elongate anomalies.
Thesis Lake Granite	Moderate magnetic intensity, small and narrow only distinguishable with enhanced derivative products (e.g., RMI_RTP_THD_VD1)	
Tectonites	Burntwood Complex	Narrow or small unit not apparent in the magnetic products, but narrow elongate anomalies interpreted as tectonites are spatially related to this map unit along a branch of the Charles Lake Shear Zone.
Waugh Lake Complex	Waugh Lake Complex	Strong to moderate magnetic intensity with high-frequency anomalies. Distinct from surrounding units. Displays internal heterogeneities.
Tectonites	Rutledge River Complex	Moderate to weak magnetic intensity, with rare internal anomalies. Internal heterogeneities only enhanced products (e.g., RMI_RTP_THD_VD1, THD_TD, asig_HSI_NE). Two variants with different internal texture.
Basement Complex	Amphibolite	Not visible in the magnetic products.
	Granitoid gneiss	High-frequency magnetic anomalies on relatively high magnetic intensity unit.

In the Athabasca Basin area, a curvy north-northeast trending basement magnetic high anomaly is interpreted as a basement topographic high underneath the Athabasca Basin (Figure 6-2). The 3D MVI model supports the interpretation of a basement magnetic high in the subsurface (Figure 5-16 and Figure 5-17). This basement high underlies the Larter member of the Lazenby Lake Formation and based on mapped geology it separates the Lazenby Lake lower members to the west from the Locker Point Formation units to the east.

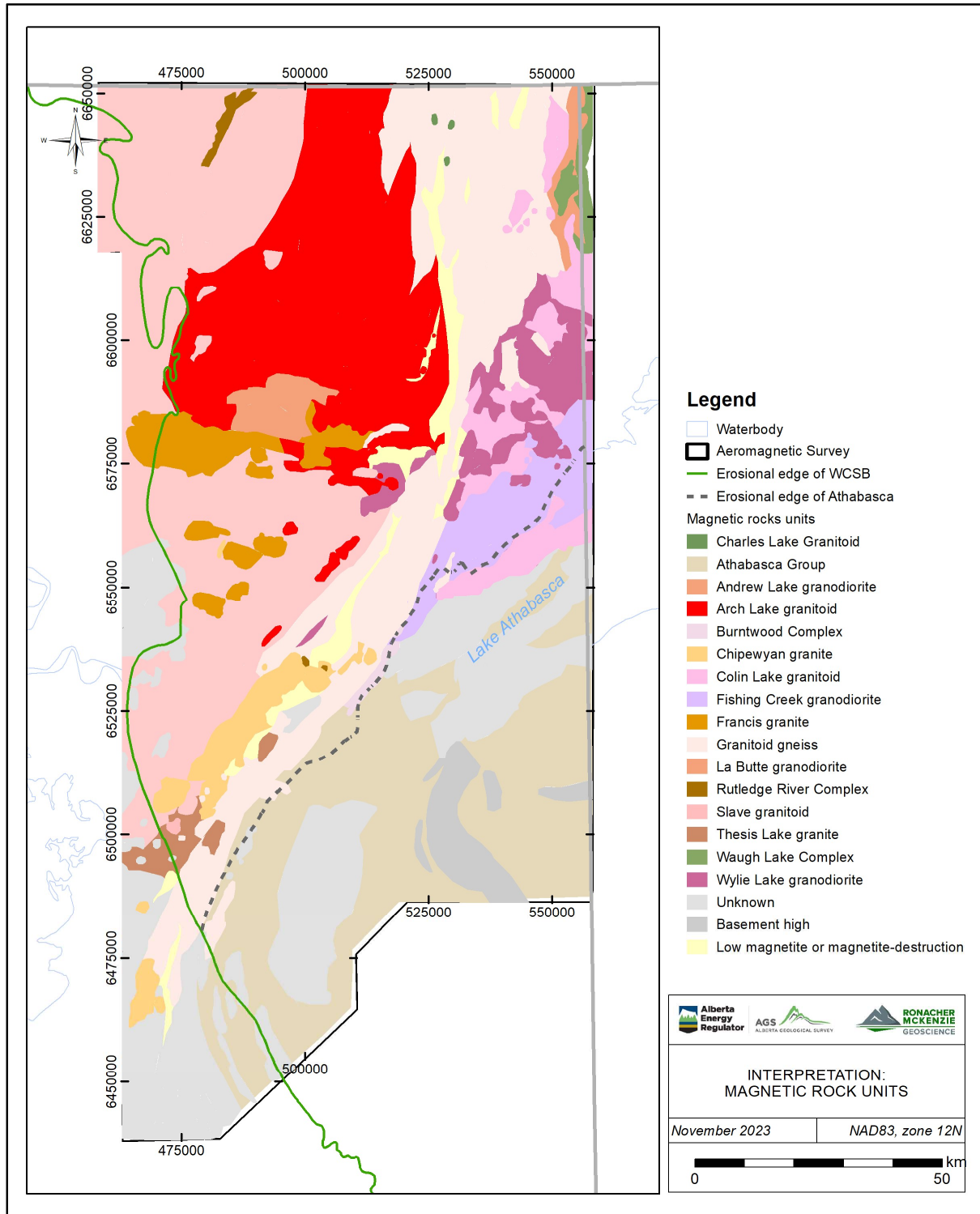


Figure 6-2. Interpretation of magnetic rock units.

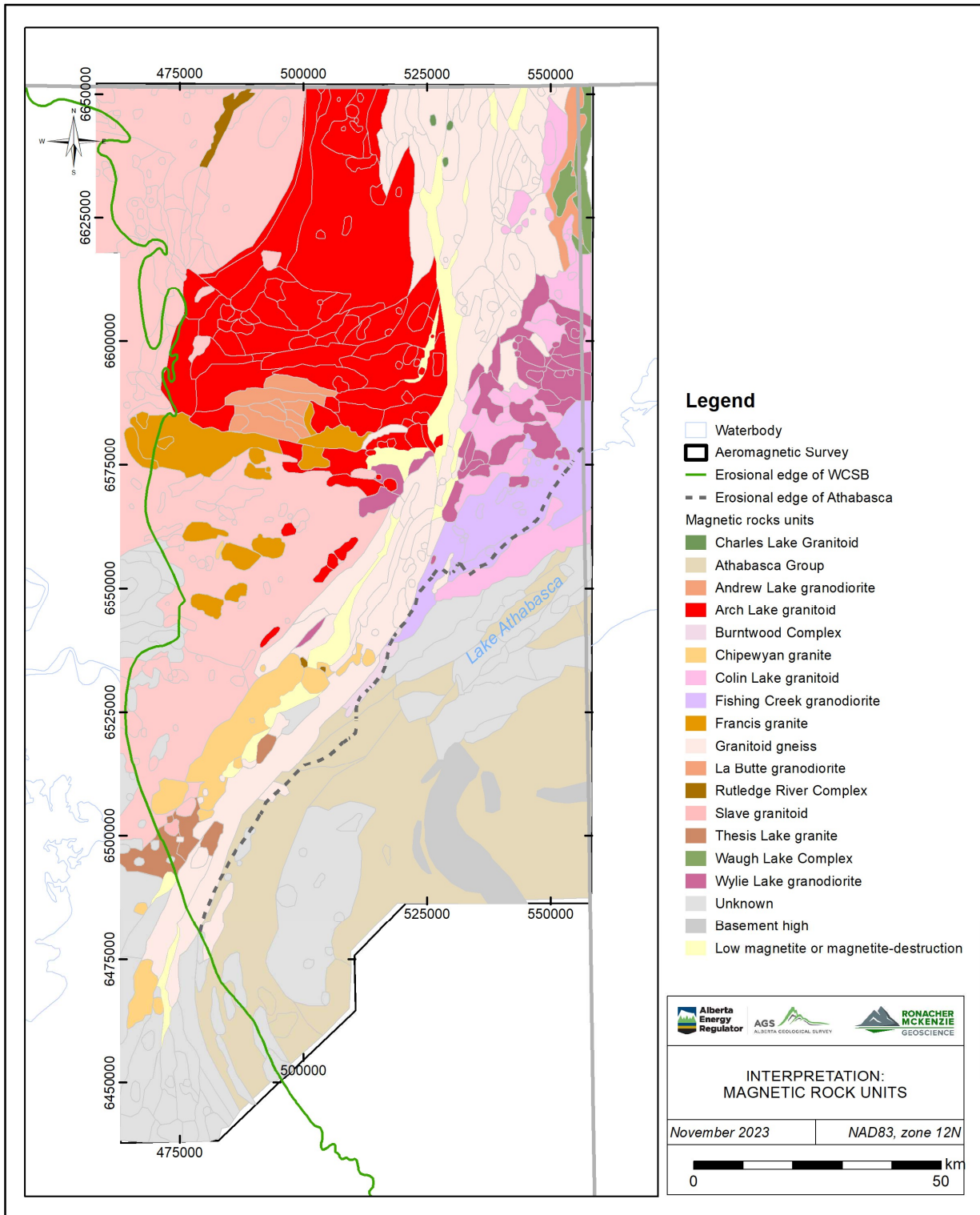


Figure 6-3: Interpretation of magnetic rock units showing internal subdomains (light grey lines).

6.2.2 Intrusions

Intrusion detection using a combination of manual and automatic processes was conducted to identify smaller rounded intrusive bodies in the project area. This section summarizes the results of the detection of smaller rounded intrusions, whereas the mapping of larger heterogeneous batholiths is described in the previous section (section 6.2.1)

Several small to medium size rounded magnetic anomalies were observed in the magnetic data. High-pass filters such as vertical, tilt and horizontal magnetic derivative products were used to outline the boundaries of these rounded anomalies. The results of the combined manual and automatic interpretation yielded a total of 206 interpreted intrusions, of which 88 were obtained with the support of automatic detection. Most of the anomalies correspond to magnetic highs, whereas four correspond to magnetic lows (Figure 6-4), which can be explained either due to remanence or alteration. The list of intrusions detected is provided in the accompanying digital files.

These interpreted intrusions may be stocks, cupolas, kimberlites, diatremes, or breccia pipes among other possible interpretations. Some of these rounded features may be interpreted as alteration haloes.

Intrusion detection was conducted manually by interpreting rounded equant and elliptical features. The process was assisted by the results of radial symmetry automatic detection, which highlighted simple discrete magnetic features with radial symmetry at different scales. All results from the automated process were verified against the geophysical and geological data before they were interpreted as intrusions. Thus, the automated products were used as a guide to help identify smaller anomalies outside and inside of major map units of the TMZ and Athabasca Group.

Detected intrusions can be separated in three main groups: a) individual small circular or elliptical magnetic highs, which occur either in clusters or isolated.; b) larger rounded intrusions with distinct internal texture either intruding low intensity or high intensity magnetic rocks throughout the project area; c) larger intrusions with rims or concentric zonation patterns (Figure 6-5). A larger elliptical magnetic low was interpreted in Slave granitoid (Figure 6-5B) which displays a well-defined elliptical rim of higher magnetic intensity. This rim defines the intrusion boundary and an internal domain of distinct magnetic texture relative to the outside. This anomaly may represent a dome or other structural feature (e.g., folding, impact crater). A larger intrusion displaying magnetic zonation was interpreted beneath the WCSB (Figure 6-5C). The outer zone of the intrusion is either a distinct intrusive or an alteration halo that modifies and magnetizes the intrusion rim or the host-rock.

Several rounded intrusions are clearly visible in the western part the project in the Slave granitoid in exposed shield rocks or beneath the WCSB cover; however, fewer intrusions were detected on the eastern side of the project area possibly because they are sheared, therefore more difficult to differentiate from the sheared and modified older plutonic units in the central and eastern parts of the project area. Very few small intrusions were detected beneath the Athabasca Basin (Figure 6-4) possibly due to its thick cover that hinder the interpretation of the basement.

The GIS files provided in the digital Appendix show the details of the interpreted intrusions.

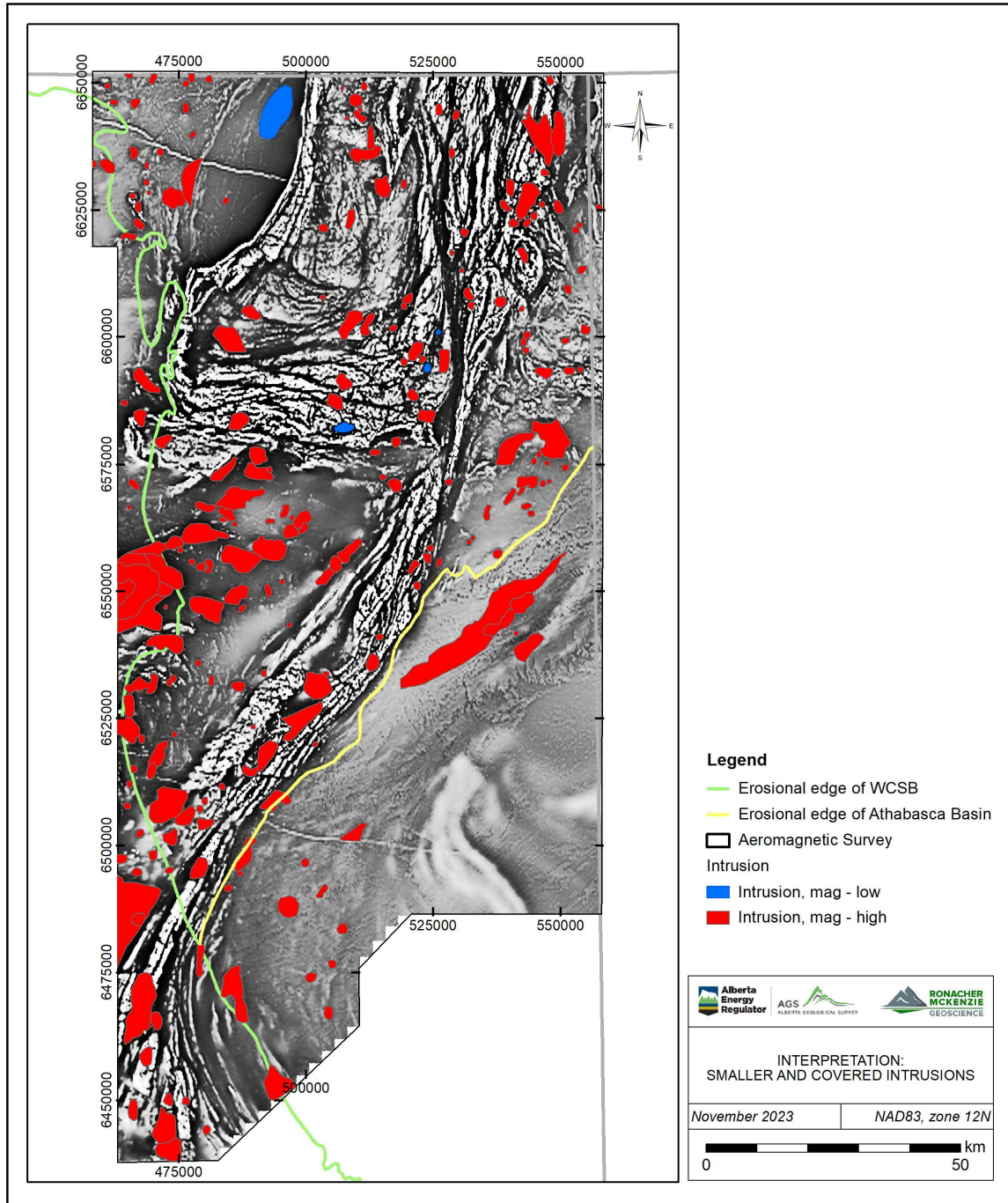


Figure 6-4. Location of interpreted rounded intrusions. Background image is the First Vertical Derivate of the Residual Magnetic Intensity, Reduced to Pole, in greyscale color distribution (2021_SHLD_RMI_RTP_VD1_BW.tif).

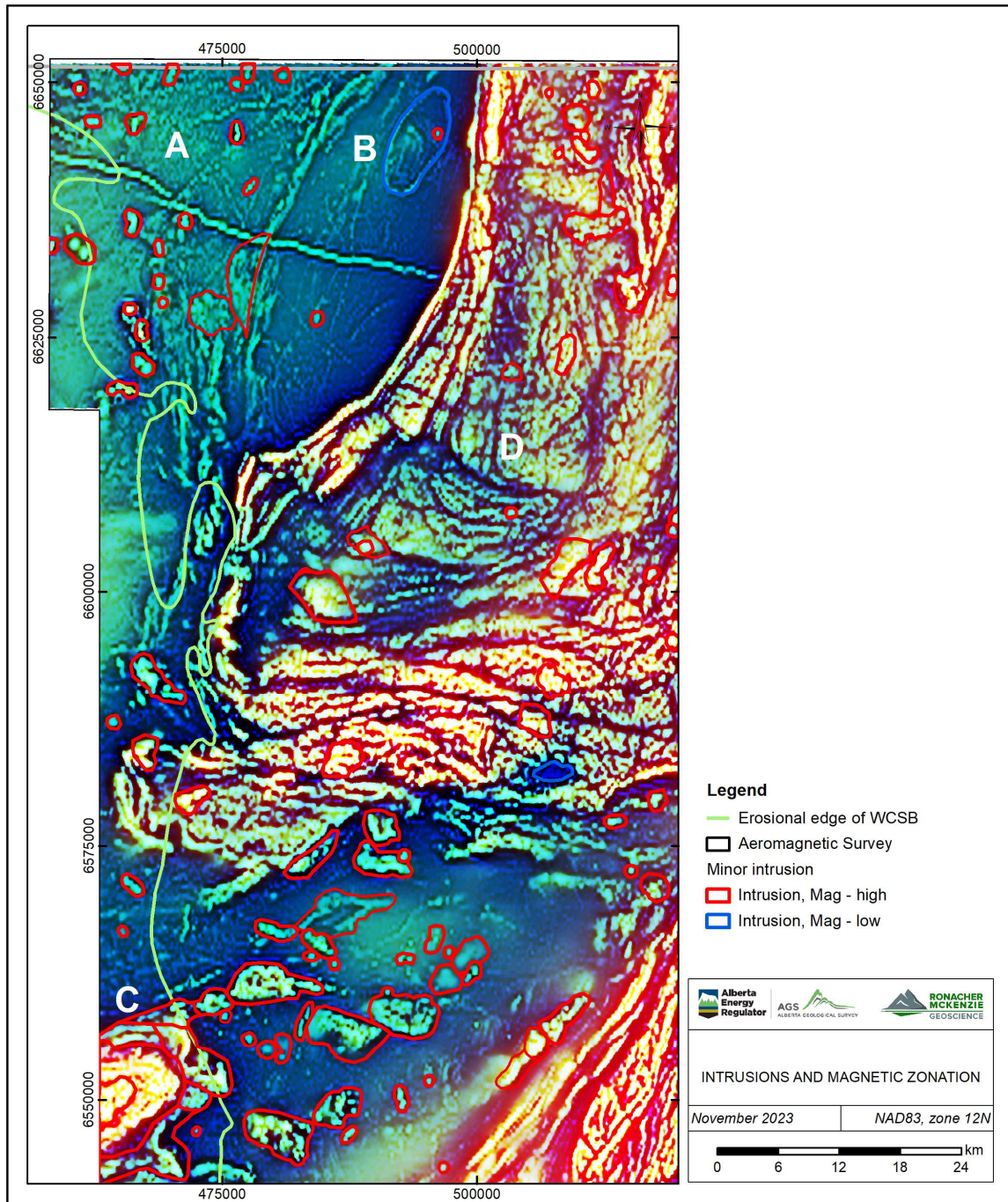


Figure 6-5. Intrusion detection in Slave and Arch Lake granitoids. Background image is the pseudogeology ternary of the Residual Magnetic Intensity, Reduced to Pole (2021_SHLD_RMI_RTP_Geology.tif). A. Clusters of minor rounded intrusions in Slave granitoid, B. Elliptical magnetic low in Slave granitoid and few minor rounded intrusions in Slave and Arch Lake granitoids. The magnetic low displays an elliptical rim of higher intensity that defines the intrusion boundary. C. Concentric zonation pattern around an interpreted intrusion showing homogeneous high-intensity core and a middle zone of intermediate intensity both interpreted as part of the intrusion, and an outer zone of lower intensity that may be part of the intrusion or an alteration halo developed in the host-rock around the intrusion.

D. Transitional magnetic zonation in Arch Lake granitoids that may reflect prolonged intrusion or metasomatism in oxidized conditions.

6.2.3 Dykes

The aeromagnetic data show prominent ESE-trending linear features that are over 40 km in length crosscutting the Slave granitoid, the Arch Lake granitoid, and the Athabasca Group. These features are interpreted as major dykes. The major dyke in the northwest corner of the project area appears in all magnetic products (including TMI and RMI; Figure 5-1), intrudes the Slave and Arch Lake granitoids, strikes 099° to the east, and extends for 49 km. This dyke runs across the Leland Lakes Shear Zone without showing apparent offset and ends in the Arch Lake granitoid, where it shows a 6.7 km apparent offset by a NW-trending brittle dextral fault and continue in the southeast for additional 10 km. The major dyke in the southeast corner of the project area appears only in derivative end other enhanced magnetic products (Figure 5-2 to Figure 5-13), strikes 094° to the east and extends for 40.5 km. This dyke intrudes the Fair Point, Smart/Manitou Falls (undifferentiated) and all members of the Lazenby Lake Formation and dies out at a prominent, wide and curvy magnetic high interpreted as a basement high. This dyke does not appear to intrude the Locker Point Formation units to the east. The western end of the dyke dies out at a branch of the Charles Lake Shear Zone, where it shows an apparent dextral offset of 2 km.

These major dykes may either relate to the Mackenzie diabase dykes ($1267 \pm 2\text{Ma}$; LeCheminant and Heaman 1989) mapped in Saskatchewan and Northwest Territories, or Sparrow diabase dykes ($1827 \pm 4\text{Ma}$; Bostock and van Breemen, 1992) mapped in Northwest Territories (Figure 6-6). The orientation of interpreted dykes is similar to that of the Mackenzie dykes. However, rock samples analyzed from Slave and Arch Lake granitoids that are spatially overlapping the interpreted major dykes are of felsic composition ($\text{SiO}_2 > 69\text{ wt.}\%$). Either the samples provided with geochemistry data were collected from the felsic host-rocks or the dyke does not outcrop.

The GIS files provided in the digital Appendix show the details of the interpreted dykes.

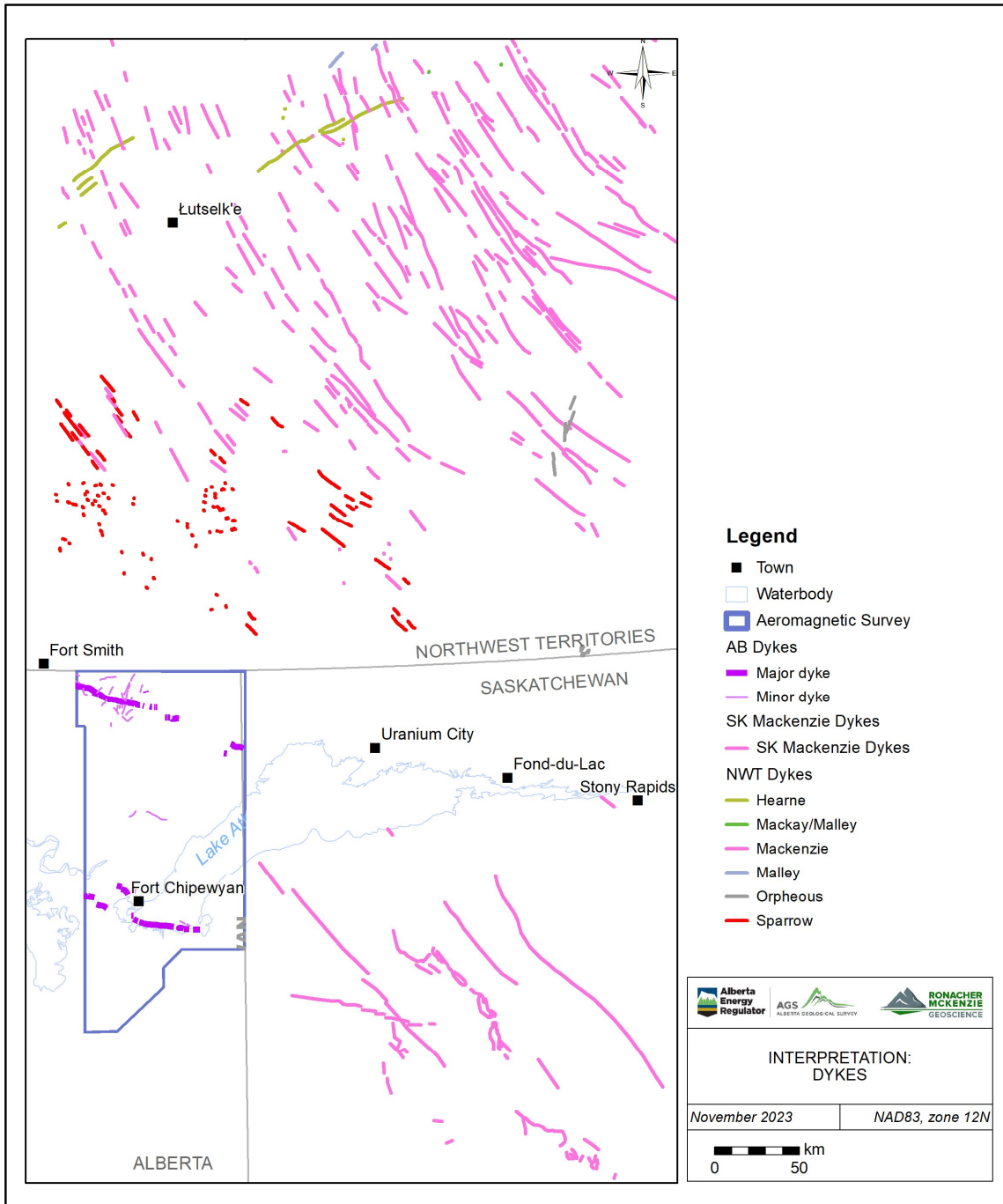


Figure 6-6. Location of interpreted dykes in Alberta in relation to mapped dykes in Northwest Territories and Saskatchewan.

6.2.4 Ductile Shear Zones

High-pass filters (e.g., derivatives, tilt) completed by RMG combined with the results from the structure detection completed by Fathom Geophysics were used to identify deeper basin structure and shear zones. The wavelength separation results, particularly the separation of long wavelengths (Figure 5-14), were useful to interpret the location of deeper structure in the TMZ. The results of the interpretation are shown on Figure 6-7.

Shear zones in the project area are characterized by the following:

- broad zones of anastomosing surfaces, with curvilinear margins
- bending of magnetic units or contacts into the shear zone
- magnetic mineral alteration that may be destructive, additive, or both; or
- offset of units associated with deflection or thinning of magnetic markers as they enter the shear zone.

The magnetic signature of the Leland Lakes Shear Zone is a continuous highly magnetic linear feature that relates to magnetite addition along a narrow zone of high gradient between the Slave Granitoid and Arch Lake granitoids. The geometry of the shear zone and the asymmetry of the edge of the anomaly indicates dip to the west. The detailed 3D voxel model across northern shield confirms the dip of the Arch Lake granitoid towards the west (Figure 5-17).

The Charles Lake Shear Zone has a complex magnetic signature consisting of braided shear zones, with narrow to wide deformation zones (sheared?) and overlapping brittle faults. Deformation zones include broad areas of magnetite destruction (Figure 6-8), or narrow areas of magnetite addition. In the southern end of the project area, sheared rocks of the Charles Lake Shear Zone curve towards the south-southeast following the edge of the Athabasca Basin where it dips to the east (Figure 5-17). In the northern part of the project area, the 3D MVI model shows the Charles Lake Shear Zone area as the center of opposite verging subsurface magnetic units. Units to the east of the shear zone dip to east, whereas units to the west of the shear zone dip to the west.

The Bayonet Shear Zone is a prominent narrow north-northeast-trending and east-dipping magnetic feature coincident with the mapped shear zone and related mylonites. The 3D MVI model shows a narrow low magnetic zone also dipping in an easterly direction.

The Black Bay Shear Zone is subtle in the magnetic data and follows a trend parallel to ESE-trending magnetic high and intrusions beneath the Athabasca Group.

The Grease River Shear Zone is not apparent in the magnetic data except for a small EW-trending basement high.

Other shear zones are interpreted in the west and east of the project area.

- a) In the west, an irregular deformation zone trending north-south occurs in the Slave granitoid. Mapped geology indicates the presence of the Rutledge River Complex tectonites over this zone near the provincial border with NWT. The magnetic signature indicates that this magnetic rock unit extends to the south with a curved geometry towards the southeast where it meets with the Leland Lakes Shear Zone. The center of this zone shows apparent N-trending stretching. The 3D model section view shows a deep vertical demagnetized zone that it is open at depth (Figure 5-17).
- b) In the north-central area an additional shear zone is interpreted between Charles Lake and Leland Lakes shear zones. This shear zone strikes to the north-northeast, and curves towards the southwest running parallel to the Leland Lakes Shear Zone. This shear zone flanks the western margin of a Slave Arch pluton in the north and bisects the Arch Lake granitoid towards the southwest. The 3D MVI model shows a deep vertical magnetic low between units interpreted as Slave pluton and basement complex (Figure 5-17).
- c) In the Andrew Lake area, a continuous linear feature interpreted as a shear zone characterized by the addition of magnetite separates the Rutledge River Complex in the west from Andrew Lake granitoids in the east. This shear zone defines a sharp boundary, steeply dipping to the east, observed in the 3D susceptibility model. The interpreted shear zone projects at depth for the entire section. However, the MVI model shows a moderate dip of the structure and no continuation at depth where it is underlain by a subsurface high magnetic anomaly (Figure 5-16). The presence of a major-scale shear zone in the Andrew Lake area is therefore uncertain.
- d) In the east, a 2 km wide N-trending shear zone with short NW-trending splays is interpreted flanking the Waugh Lake Complex in Saskatchewan and running parallel to the AB/SK provincial boundary.

The GIS files provided in the digital Appendix show all interpreted shear zones.

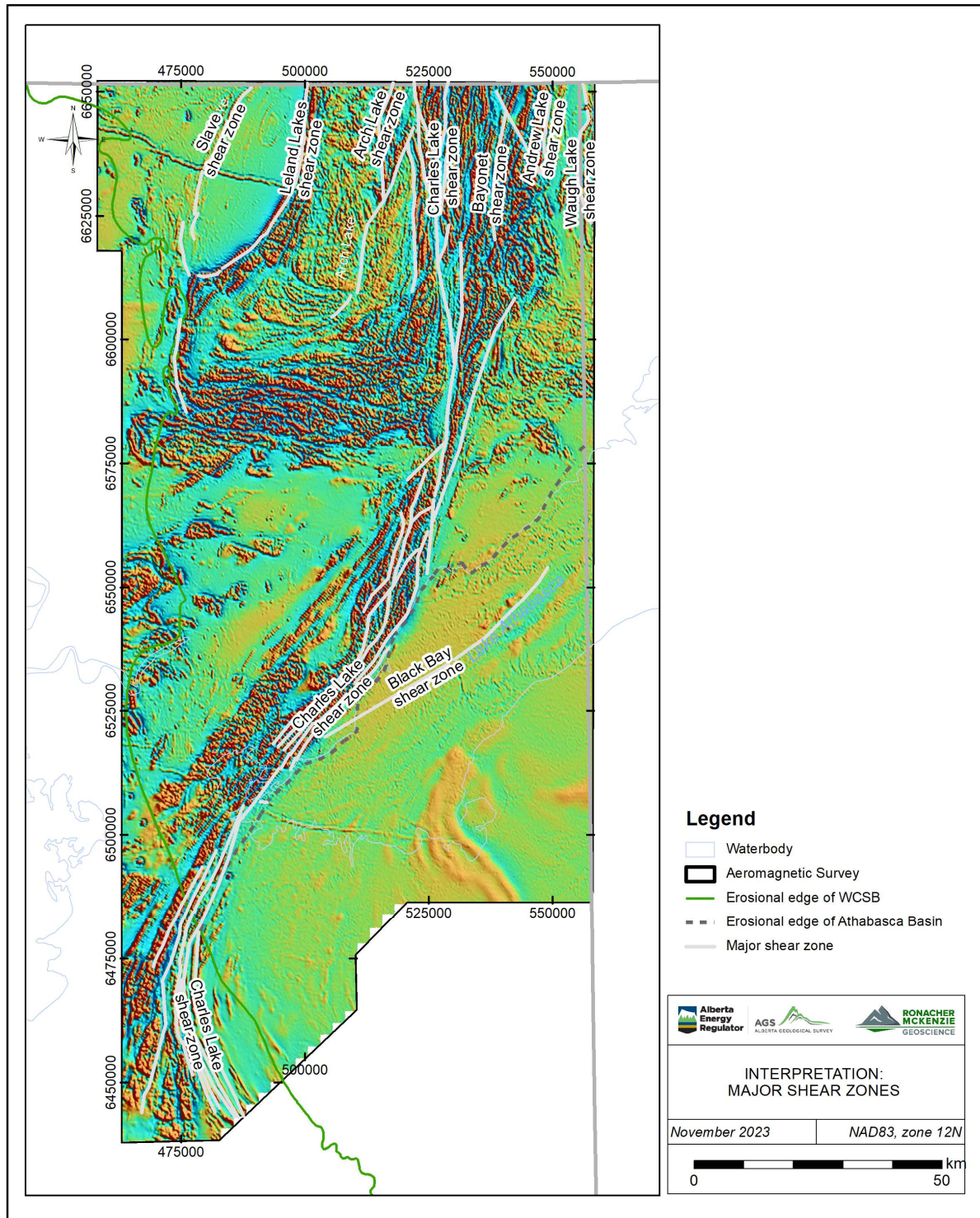


Figure 6-7. Location of interpreted shear zones on first vertical derivative of Residual Magnetic Intensity, Reduced to Pole, aeromagnetic image.

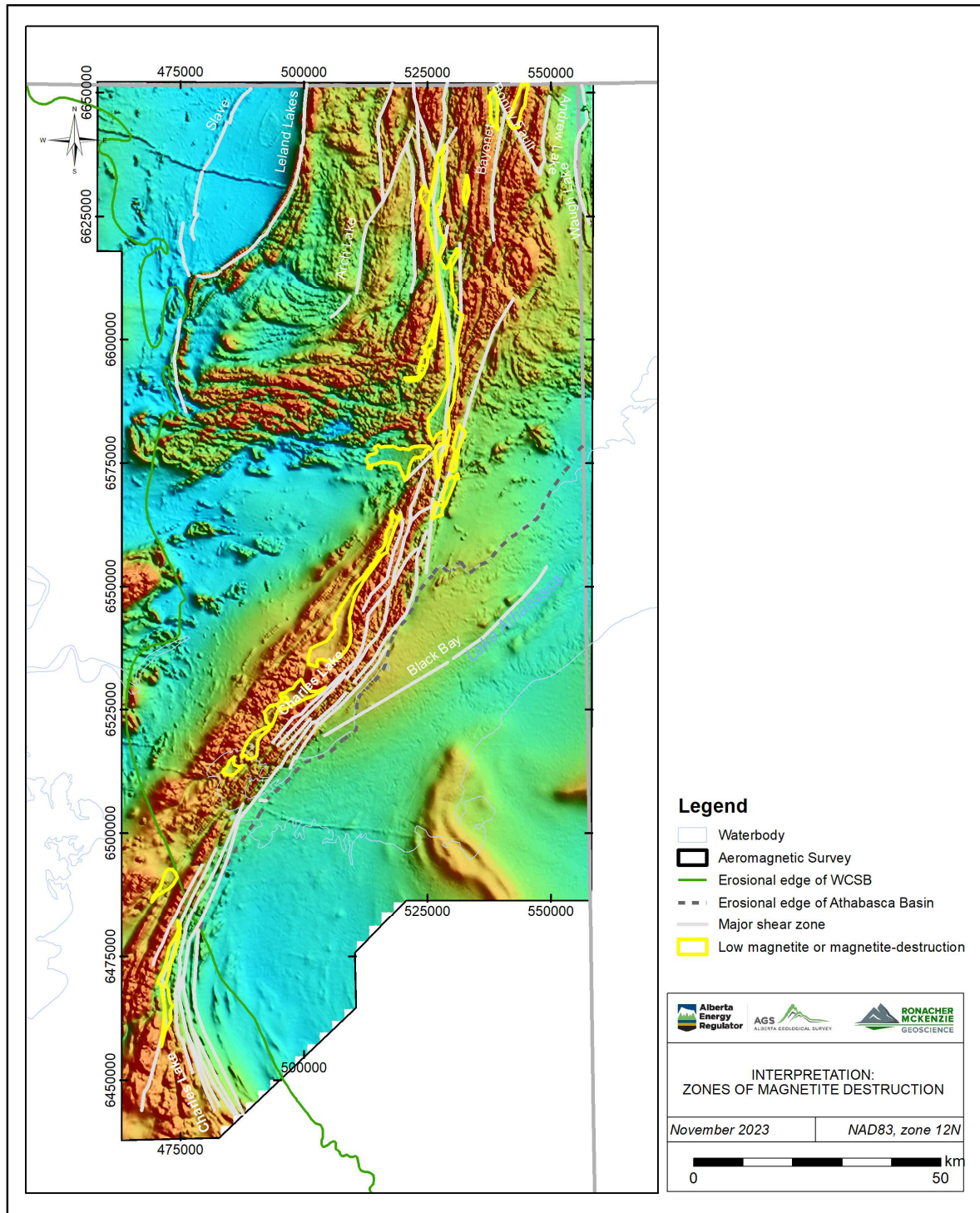


Figure 6-8. Broad zone of magnetite-destructive alteration spatially related to Charles Lake Shear Zone. Background image is the Residual Magnetic Intensity, Reduced to Pole,

6.2.5 Brittle Faults

High-pass filter products (e.g., derivatives, tilt, automatic gain control) and the results for short wavelengths from the structure automatic detection were used to emphasize shallow and detailed brittle structure in the project. Criteria to identify brittle structures included the following:

- juxtaposition of different form line orientations
- linear features, with angular margins
- angular fault jogs or steps
- short subtle curvilinear linear features (for sub-horizontal sedimentary strata)
- narrow zones of demagnetization (due to low temperature oxidation of magnetic minerals)
- offset of magnetic rock unit

Offsets and relative timing defined by crosscutting relationships and fault terminations were recorded in the accompanying GIS vector files where possible. Because of the 2-D plan nature of aeromagnetic data, mapped offsets are apparent offsets.

Fault azimuth was calculated for every feature. Several brittle faults were interpreted in the Taltson Magmatic Zone (outside the Charles Lake Shear Zone), which can be grouped in five sets (older to younger): a) north-northeast, b) north-northwest, c) east-northeast, d) west-northwest, and e) east-west.

Automatic gain control and structure detection are essential for delineating brittle faults in the Athabasca Basin where the cover is very thick.

On the Shield, derivative products are suitable for identifying faults. Automatic Gain Control provides greater detail on the location of the faults.

The GIS files provided in the digital Appendix show all interpreted brittle faults.

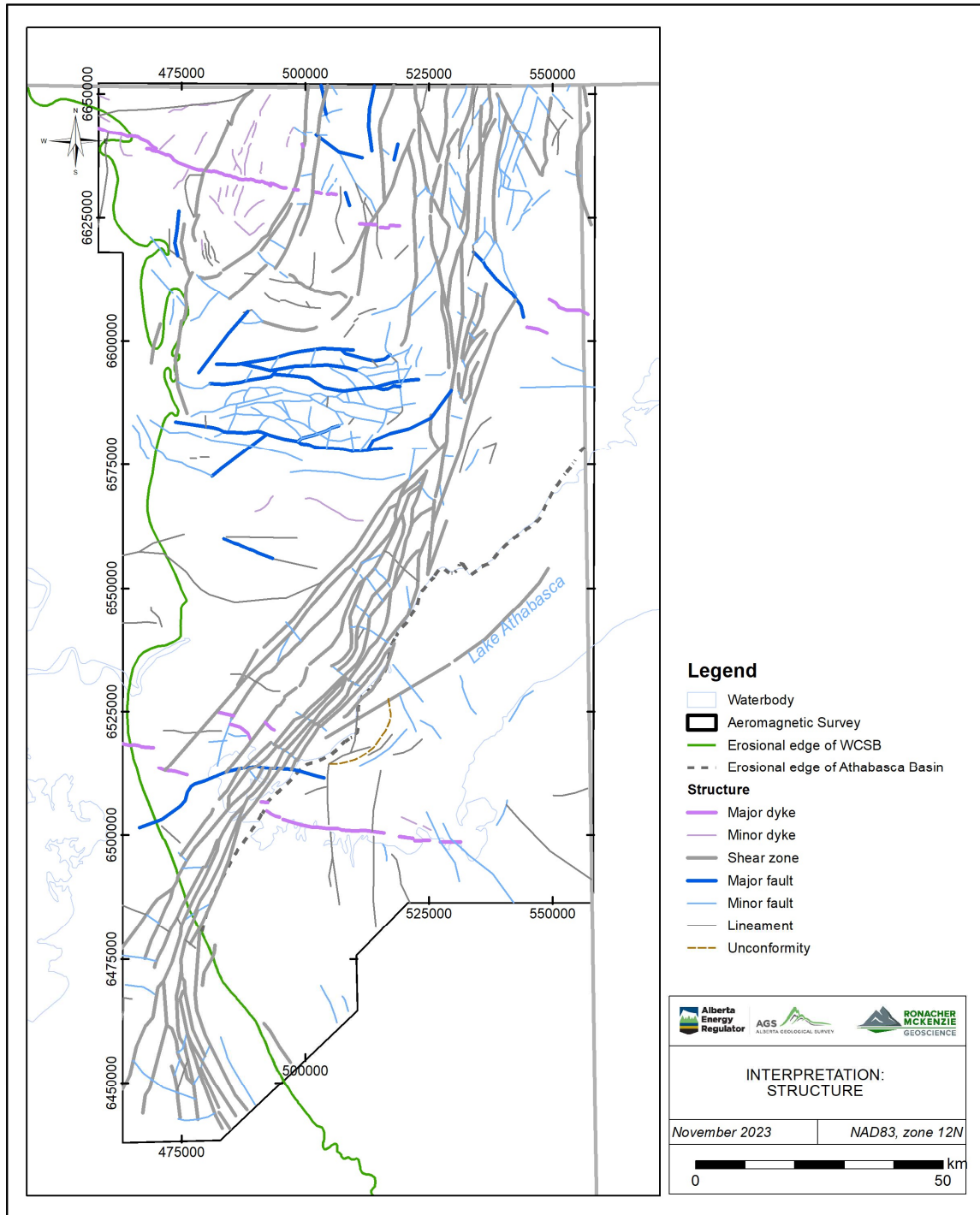


Figure 6-9. Interpretation of linear features and structure.

7.0 INTERPRETATION

The final interpretation of the aeromagnetic data is presented in Figure 7-1. This map is a simplified view of the accompanying vector files found in the digital files delivered with this report. The compilation of the magnetic domain and linear observation layers are the basis of the interpretation map. This interpretation map supplements the existing mapped geology and is not meant to replace it. The interpretation map provides a general framework that includes inferences of structural and geological units based on the results of the observations and integration of magnetic data with existing geological data.

7.1 Interpretation Map

The interpretation map shows intrusions and structures in areas hidden by either Quaternary cover or sedimentary strata from the WCSB and Athabasca Basin. Major dykes and additional shear zones were identified and compared to the known geology. Major rocks units were reinterpreted in some areas to remain consistent with the magnetic signature and geochemistry.

The resolution of the magnetic data is high and therefore, the interpretation found in GIS files is very complex. In areas where less detailed geological data is available, the resolution of the magnetic data was appropriate to outline heterogeneity within geological map units, particularly within plutonic units. However, in areas with detailed geology, the resolution of the magnetic data cannot resolve the smaller mapped units, such as small intrusions (e.g., Charles Lake granodiorite) and narrow slivers of metamorphic complexes along fault zones. Furthermore, the magnetic signature of the plutonic units obscures the more subtle magnetic signatures of overlying metamorphic complexes' roof pendants.

New features that the interpretation identified from the geophysical products are listed in the following sections (Sections 7.1.1 to 7.1.7).

7.1.1 *Smaller Intrusions*

Intrusion detection using a combination of manual and automatic processes was conducted to identify smaller rounded intrusive bodies in the project area. Intrusions are interpreted from rounded to elliptical features with significant magnetic contrast with host rocks. Larger heterogeneous intrusions were successfully mapped on edge and texture enhancing products to delineate subdomains. Interpreted intrusions are predominantly noted to be magnetic highs although four interpreted intrusions correspond to magnetic lows and may be a result of remanence or alteration. Furthermore, detected intrusions were classified into three main groups: a) individual smaller magnetic features, b) larger rounded intrusions with distinct internal magnetic texture and c) larger intrusions with rims or concentric zonation patterns. Several rounded intrusions are observed in the western part the project area, including beneath the WCSB; however, fewer intrusions were detected on the eastern side of the project area. Few small intrusions were detected beneath the Athabasca Basin possibly due to its thick cover which hinders basement interpretation.

7.1.2 Dykes

The aeromagnetic data show two ESE-trending major dykes that are over 40 km in length and crosscut the Slave granitoid and the Arch Lake granitoid in the northwest, and the Athabasca Group in the southeast of the project area.

These major dykes may be related to some of the Mackenzie diabase dykes mapped in Saskatchewan and Northwest Territories. Although their orientation is similar to some of the Mackenzie dykes (SE and ESE-trending), it is uncertain that they can be classified as Mackenzie dykes without age dating.

7.1.3 Heterogeneities in major plutonic units

The Arch Lake granitoid displays a distinct grainy magnetic signature and a zonation in magnetic intensity from moderate in the center to high towards the edges (Figure 6-5). This zonation may be the result of prolonged oxidizing intrusive events or metasomatism of the pre-existing rocks.

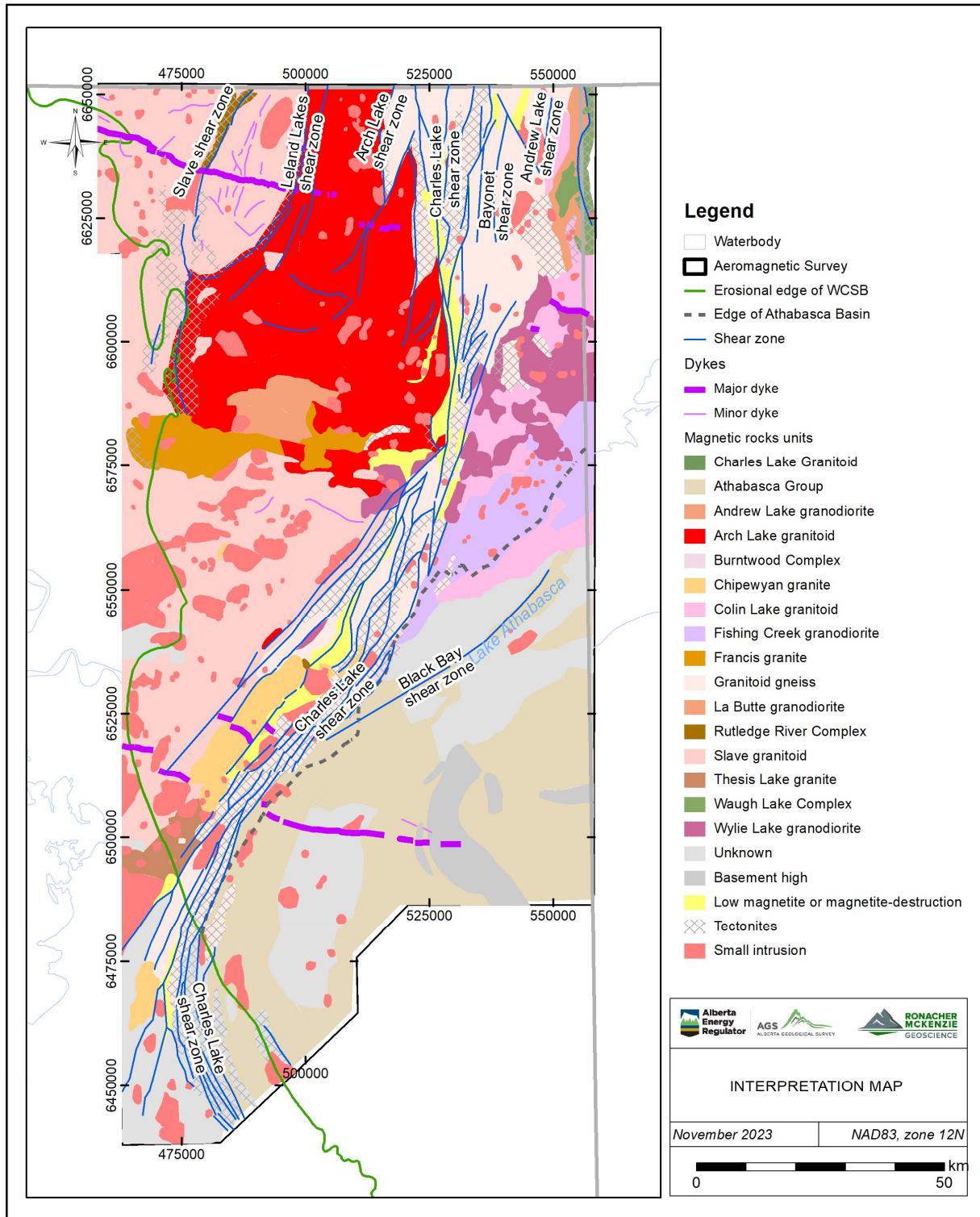


Figure 7-1. Interpretation map of the magnetic data.

7.1.4 *Shear Zones*

Shear zones in the project area are characterized by broad zones of curvilinear margins, bending of form lines in the magnetic signature into the shear zone, preferred orientation of form lines, and magnetic mineral alteration that may be destructive or additive. Shear zones and deeper basin structures were identified from the various filter and structure detection products. The wavelength separation results, particularly the separation of long wavelengths, were useful to interpret the location of deeper structure in the TMZ. Generally north-trending major shear zones were interpreted in the northern part of the project area. These shear zones show continuous curvilinear trends of high magnetic intensity that are interpreted as magnetite concentration along a deformation zone. New major shear zones detected include:

- Shear zone in Slave granitoid
- Shear zone in Arch Lake granitoid
- Shear zone in Andrew Lake area
- Shear zone in Waugh Lake Complex

7.1.5 *Basement Features Beneath the Athabasca Basin*

The magnetic data in the Athabasca Basin mostly reflect a complex mixed pattern of basin features with limited magnetic variation within the basement. Basement and shallower magnetic features are difficult to separate without the aid of structure detection results to identify lineaments and structural patterns. The muted basement signature is likely due to a combination of the thickness of the Athabasca Group strata in trough shaped subbasins and the generally low magnetic variation in the basement rocks. Only few smaller basement intrusions, local magnetic texture patterns and structural trends were clearly identified (Figure 7-1). The largest intrusion under the Athabasca Group cover is interpreted as the Wylie Lake granodiorite because of similar magnetic signature and proximity to exposed units of the Wylie Lake granodiorite in the northern rim of Athabasca basin. The outlines of rounded single intrusions away from the northern rim were identified from magnetic derivative products, ternary images and radial symmetry results. They are too small to be linked to any known intrusions in the project area. Regarding noticeable structural trends, a curvy north-northeast trending basement magnetic high is interpreted as a basement topographic high underneath the Athabasca Basin (Figure 7-1). The 3D MVI model supports the interpretation of a basement magnetic high. This basement high underlies the Larter member of the Lazenby Lake Formation and separates the Lazenby Lake lower members to the west from the Locker Point Formation units to the east. The 3D MVI model also shows that this magnetic high is disconnected from intrusions in the north and displays a distinct texture. A second and smaller east-trending magnetic high is interpreted in the east and is not connected with the north-northeast trending magnetic high. These magnetic highs were recognized in older aeromagnetic data and were interpreted in the 1970-1980s as granitoid gneiss of the Taltson Basement Complex (e.g., Wilson, 1986). The reduced to pole tilt (RTP_TD) image shows a magnetic fabric consistent with mostly tectonites for the larger basement high. A local intrusion is only visible in the analytic signal of the vertical integral (VIAS) image.

7.1.6 *Basement Features Beneath the WCSB*

Beneath the WCSB, the magnetic data predominantly reflect changes in basement geology rather than the overlying sedimentary units and it is generally straightforward to interpret basement anomalies in the project area. The recognizable magnetic response of the basement may be due to the distinct magnetic signature of the basement, the limited thickness and the low magnetic response of the sedimentary cover.

Previously unrecognized plutons were interpreted in the Slave granitoid below the WCSB strata. The magnetic signature of some of the intrusions in the west-central part of the project area resemble the Francis Granite units located immediately to the east, whereas intrusions in the southwest resemble the Chipewyan Granite units near the Charles Lake Shear Zone. Other intrusions show a distinct signature and zonation patterns that do not match plutonic units found in the rest of the project area and therefore were labeled as unknown.

Tectonites were interpreted under the WCSB spatially related to the Charles Lake Shear Zone in the southwest of the project area as well as in the Slave Granitoid spatially approaching to the southern segment of the Leland Lakes Shear Zone in the northwest.

7.1.7 *Modifications to Bedrock Geology Map*

The Slave granitoid to the west of Leland Lakes Shear Zone has a magnetic texture characterized by low intensity and few internal variations. This texture extends to the south along the western part of the project area. The Slave granitoid also has a dominant more alkaline composition (higher $\text{Na}_2\text{O}+\text{K}_2\text{O}$) than the Arch Lake granitoids based on the normalized whole-rock geochemical data. Map units from MAP 537 of the Slave granitoid located south of the Arch Lake granitoid map units do not match the underlying magnetic texture and geochemistry characteristic of Slave granitoid in the northwest. Therefore, the Slave granitoid map units in the south are reinterpreted as variations of the Arch Lake granitoids; alternatively, they are either assigned to the Francis Granite or La Butte Granodiorite according to exposed map units.

Other modifications to the geology are in the eastern part of the project area where the boundaries between Colin Lake, Wylie Lake and Fishing Creek granitoids are reinterpreted.

7.2 **Applicability of Magnetic Filter Products**

High-pass magnetic filter products that were used for the interpretation of the basement include first vertical derivative, horizontal derivative, automatic gain control, and tilt angle. These filters allow for accurate mapping of faults and fault patterns, and analysis of the internal structure of granitoids. The second derivative magnetic filter was useful to detect subtle changes due to alteration. For interpretation of the basement beneath the WCSB and Athabasca Basin, high-pass filter products are less effective and low-pass filters that retain low frequencies related to deeper structure are more appropriate for interpretation. Low-pass filters for this project were provided by Fathom Geophysics and the most useful for the shield area are differential upward

continuation residuals (particularly small-scale residual) and wavelength separation. These products allow the separation of surficial faults from major shear zones and their splays, and other major lineaments.

7.3 Applicability of Automatic Structure and Intrusion Detection

The automatic structural detection and the radial symmetry analysis significantly improved the interpretation of the geology of the project area.

Automatic structure detection was useful for the interpretation of surficial short wavelength faults from deeper long wavelength faults and shear zones, as well as identifying major lithotectonic boundaries. For example, the main branch of Charles Lake Shear Zone was mapped using the long 1600 m wavelength of structure detection Parallel Cross Reduced to Pole images (e.g., Figure 5-14), whereas the short, 100 to 400 m wavelength products were used to outline domains with different structure patterns in the Athabasca Basin to infer units beneath the basin.

Manual detection was successful at identifying several anomalies interpreted as intrusions mostly in the western half of the project area, where higher magnetic gradients exist between high-magnetic rounded anomalies and the low-magnetic surrounding rocks. However, manual intrusion detection was challenging or nearly impossible in domains of high magnetic intensity and high frequency or in domains with subtle to nearly plain signature. The results of automatic detection with the radial symmetry algorithm were useful to revisit areas with anomalies that visual detection had missed. About 40% of the anomalies interpreted to be intrusion were obtained with the support of automatic detection.

Interference patterns between the noisy Athabasca Group and weakly magnetized basement are difficult to separate without the aid of structure detection results to identify major structural trends and separate higher from lower frequencies. Structure detection by wavelength separation in combination with a detailed review of high and low-pass magnetic products was essential to identify lineaments, units, subbasins, and detect internal structure patterns, which would otherwise have remained undiscovered. Depth-to-basement analysis of the magnetic data, while out of scope for this report, may be effective for further basement topography beneath the Athabasca Basin and the WCSB.

7.4 3D Inversion

Inversions of the magnetic data for two transect regions across the project area were successful at matching the regional amplitude and trends of rock magnetization by showing major plutonic bodies, bounding shear zones, and their general dip at depth. The MVI models show narrow low magnetization zones extending up to 5 km depth that correlate with the known Leland Lakes, Charles Lake and Bayonet shear zones, and the newly interpreted steeply-dipping shear zone in the Slave granitoid. The 3D MVI model also shows the interpreted shear zone in the Andrew Lake area as a shallow dipping feature. However, the geometry results are considered uncertain because the modeled areas are broad and contain complex assemblages of magnetic rocks units.

The 3D inversion results are consistent with the observations from the measured data. Several structures and interpreted intrusions have an expression in the subsurface.

8.0 CONCLUSIONS

The aeromagnetic data flown in 2021 over the Canadian Shield in Alberta were interpreted using a combination of manual and automatic methods in combination with existing geological information to delineate and characterize the magnetic signature of major map units, intrusions, dykes, brittle faults and shear zones. The interpretation also includes the subsurface of the portions of the Western Canada Sedimentary Basin and the Athabasca Basin covered by the survey area.

Manual interpretation of the data was supported by automated structure and intrusion detection methods, as well as 3D inversion models of magnetic vector amplitude and susceptibility. The magnetic interpretation was integrated with and calibrated against existing geological data to map existing features and to identify covered or previously unknown features. 3D inversions of magnetic vector amplitude and susceptibility also helped to identify complex structures and geometry within shear zones.

Automated structure detection aided in identification and interpretation of often complex linear structures, while radial symmetry analysis aided in identification of intrusions. Wavelength separation using differential upward continuation was essential in identifying lineaments and magnetic texture changes which may have otherwise remained undetected.

The integrated interpretation of the new magnetic data from 2021 has identified a number of previously unrecognized features, including shear zones, intrusions, dykes and structures underneath the WCSB and Athabasca Basin. In addition, a number of modifications to existing bedrock geology maps have been proposed.

9.0 REFERENCES

- Alberta Geological Survey. 2023. "Alberta Aeromagnetic and Gravity Survey, Southern Alberta, Northern Alberta and Gap + Shield Surveys." <https://geology-ags-aer.opendata.arcgis.com/pages/aeromag-gravity-survey>.
- Alberta Geological Survey. 2021. "Structural Elements in the Alberta Plains Interactive App and Map." Accessed November 15, 2023. <https://ags.aer.ca/publication/iam-011>.
- Berman, R. G., and H. H. Bostock. 1997. "Metamorphism in the northern Taltson magmatic zone, Northwest Territories." *Canadian Mineralogist*, p. 1069-1091.
- Burwash, R. A., C. R. McGregor, J. A. Wilson, and S. C. O'Connell. 1994. "Precambrian Basement Beneath the Western Canada Sedimentary Basin." *Alberta Energy Regulator*. Accessed October 30, 2023. <https://ags.aer.ca/atlas-the-western-canada-sedimentary-basin/chapter-5-precambrian-basement>.
- Chacko, T., K.S. De, R.A. Creaser, and K. Muehlenbachs. 2000. "Tectonic setting of the Taltson magmatic zone at 1.9–2.0 Ga: a granitoid-based perspective." *Canadian Journal of Earth Sciences* 37: p. 1597–1609.
- De, S.K., T. Chacko, Creaser R., and K. Muehlenbachs. 2000. "Geochemical and Nd-Pb-O isotope systematics of granites from the Taltson Magmatic Zone, NE Alberta: implications for early Proterozoic tectonics in western Laurentia." *Precambrian Research* 102, Issues 3-4: p. 221-249.
- Isles, D. J., and L. R. Rankin. 2013. *Geological interpretation of aeromagnetic data*. Australian Society of Exploration Geophysicists, 365 p.
- Kovesi, P. 2015. *Good Colour Maps: How to Design Them (colorcet.com)*. Accompanying Document, Crawley, Western Australia: Centre for Exploration Targeting, The University of Western Australia. <https://colorcet.com/>.
- Langenberg, W. C. 1983. *Polyphase deformation in the Canadian Shield of northeastern Alberta*. Bulletin 45, Alberta Research Council, 33 p.
- LeCheminant, A.N., and L.M. Heaman. 1989. "Mackenzie igneous events, Canada: Middle Proterozoic hotspot magmatism associated with ocean opening." *Earth and Planetary Science Letters* 96, Issues 1-2: p. 38-48.
- Lopez, G. P., J. A. Weiss, G. L. Smerek, and S. N. Massey. 2022. *Geochemistry of plutonic and metamorphic rock samples from Taltson magmatic zone Canadian Shield, Northeastern Alberta (74M)*. Alberta Energy Regulator/Alberta Geological Survey, AER/AGS Digital Data 2021-0011.
- McDonough, M. R., V. J. McNicoll, E. M. Schetselaar, and T. W. Grover. 2000. "Geochronological and kinematic constraints on crustal shortening and escape in a two-sided oblique-slip collisional and magmatic

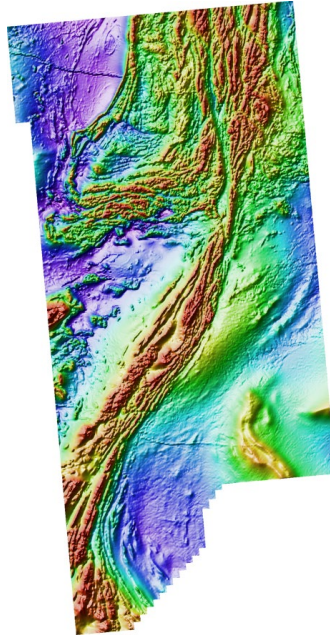
- orogen, Paleoproterozoic Taltson magmatic zone, northeastern Alberta." *Canadian Journal of Earth Sciences* 37, no. 11: p. 1549-1573.
- McGlynn, J., G. Hanson, E. Irving, and J. Park. 2011. "Paleomagnetism and Age of Nonacho Group Sandstones and Associated Sparrow Dikes, District of Mackenzie." *Canadian Journal of Earth Sciences* 11: p. 30-42.
- Meek, D. M., G. P. Lopez, and C. Knudson. 2023a. *Geochemistry of plutonic and metamorphic rock samples from the Canadian Shield, northeastern Alberta (74L, 74M) version 2 (tabular data, tab-delimited format)*. Alberta Energy Regulator / Alberta Geological Survey, AER/AGS Digital Data 2023-0015.
- Meek, D. M., G. P. Lopez, and C. Knudson. 2023b. *Geochemistry of plutonic and metamorphic rock samples from the Canadian Shield, Northeastern Alberta (tabular data, tab-delimited format)*. Alberta Energy Regulator / Alberta Geological Survey, AER/AGS Digital Data 2022-0048.
- Mossop, G. D., and I. Shetsen. 1994. "Geological atlas of the Western Canada Sedimentary Basin." *Alberta Geological Survey*. Canadian Society of Petroleum Geologists and Alberta Research Council. Accessed October 30, 2023. <http://ags.aer.ca/reports/atlas-of-the-western-canada-sedimentarybasin.html>.
- Nilsen, P.A., C.W. Langenberg, H. Baadsgaard, and J.D. Godfrey. 1981. "Precambrian metamorphic conditions and crustal evolution, northeastern Alberta, Canada." *Precambrian Research* 16: p. 171–193.
- Pană, D. I. 2007. "A two-stage thermotectonic model for the Athabasca unconformity-type uranium deposits; in Digging deeper." *Society for Geology Applied to Mineral Deposits*. Dublin, Ireland: C.J. Andrew (ed.) v. 2. p. 1133-1136.
- Pană, D. I. 2010b. "Overview of the geological evolution of the Canadian Shield in the Andrew Lake area based on new field and isotope data, northeastern Alberta." Energy Resources Conservation Board, ERCB/AGS Open File Report 2009-22, 76 p.
- Pană, D. I. 2010a. "Precambrian geology of northeastern Alberta (NTS 74M, 74L and part of 74E)." Energy Resources Conservation Board, ERCB/AGS Map 537.
- Pană, D. I., and E. J. Waters. 2016. *GIS compilation of structural elements in Alberta, version 3.0*. Alberta Energy Regulator/Alberta Geological Survey, Digital Data 2003-0012.
- Pană, D. I., J. Waters, and M. Grobe. 2001. "GIS compilation of structural elements in northern Alberta, release 1.0." Alberta Energy and Utilities Board, EUB/AGS Earth Sciences Report 2001-01, 60 p.
- Pană, D. I., R. Elgr, E. J. Waters, J. A. Warren, G. P. Lopez, and J.G. Pawlowicz. 2021. "Structural elements in the Alberta Plains." Alberta Energy Regulator/Alberta Geological Survey, AER/AGS Open File Report 2021-01, 33 p.

- Post, R. T. 2004. "Stratigraphy and sedimentology of the Athabasca Group in the Net Lake-Maybelle River area, northeastern Alberta." Alberta Energy and Utilities Board, EUB/AGS Earth Sciences Report 2003-01, 103 p.
- Prior, G. J., B. Hathaway, P. M. Glombick, D. I. Pană, C. J. Banks, D. C. Hay, C. L. Schneider, M. Grobe, R. Elgr, and J. A. Weiss. 2013. "Bedrock geology of Alberta." Alberta Energy Regulator / Alberta Geological Survey, AER/AGS Map 600.
- Ramaekers, P., C. W. Jefferson, G. M. Yeo, B. Collier, D. G.F. Long, O. Catuneanu, S. Bernier, et al. 2007. "Revised geological map and stratigraphy of the Athabasca Group, Saskatchewan and Alberta; in EXTECH IV: geology and uranium EXploration TECHnology of the Proterozoic Athabasca Basin." Bulletin of the Geological Survey of Canada 588, p. 155-191.
- Ross, G.M. 2002. "Evolution of Precambrian continental lithosphere in Western Canada: results from LITHOPROBE studies in Alberta and beyond." *Canadian Journal of Earth Sciences* 39: p. 413–437.
- Ross, G.M., J. Broome, and W. Miles. 1994. "Potential fields and basement structure – Western Canada Sedimentary Basin." In *Geological Atlas of the Western Canada Sedimentary Basin*, by Canadian Society of Petroleum Geologists and Alberta Research Council G.D. Mossop and I. Shetsen (comp.), p. 41–47.
- Siddorn, J. P., P. R. Williams, D. J. Isles, and L. R. Rankin. 2020. "Chapter 9: Integrated Geologic-Geophysical Interpretation of District-Scale Structural Frameworks: Systematic Approaches for Targeting Mineralizing Systems." *Reviews in Economic Geology*, p. 271-313.
- Wilson, J. A. 1986. "Geology of the basement beneath the Athabasca Basin in Alberta." Alberta Research Council, ARC/AGS Bulletin 55, 66 p.

Appendix 1 – Automatic detection - Fathom Geophysics Report

Processing of magnetic data over the Northern Shield area, Alberta for Ronacher McKenzie Geoscience

October 2023



**by Dan Core[†], Eric Core, and Lisa Lombardi
Fathom Geophysics**

[†]Corresponding author: dan@fathomgeophysics.com

www.fathomgeophysics.com

DOCUMENT SECTION	PAGE
Introduction	2
Processing summary	2
File formats and image types delivered	6
List of acronyms and abbreviations	7
Figure 1: Project location map	9
Magnetic data-processing results images	10
<i>Figure 2: Residual magnetic intensity (RMI)</i>	10
<i>Figure 3: Reduction-to-pole (RTP)</i>	11
<i>Figures 4 – 22: Standard filtering</i>	12
<i>Figures 23 – 26: Total structure detection</i>	31
<i>Figures 27 – 32: Belt-parallel & belt-crossing structure detection</i>	35
<i>Figures 33 – 34: Radial symmetry analysis</i>	41
Appendix 1: Structure detection algorithm	43
Appendix 2: Radial symmetry detection algorithm	45

Introduction

The project area for this work is the Northern Shield magnetic survey from the Alberta Geological Survey (AGS) covering the Canadian shield in northeastern Alberta (**Figure 1**). The goal of this work is to process the magnetic data to generate products that can assist with interpretation of structure and lithology based on the magnetic data.

The magnetic data are from a survey flown in March 2021 by EON Geosciences Inc on behalf of the Alberta Energy Regulator. Gridded data provided with the survey were good quality and were supplied to us with coordinates in WGS84 UTM Zone 11N (**Figure 2**). All outputs of our work use this coordinate system. Survey data have 400m line-spacing. All gridded products use a cell size of 100m.

The processing completed includes application of a suite of standard filters as well as application of Fathom Geophysics' structure detection and radial symmetry filters.

Processing summary

Reduction to the pole (RTP)

RTP processing produces a magnetic field that is equivalent to what would be generated if the data were collected at the magnetic north pole. This shifts magnetic highs to be directly over their sources and creates symmetric anomalies over the top of symmetric magnetic sources. The RTP filter for these data uses an inclination of 79.0° and a declination of 13.8° (**Figure 3**).

Note that in general RTP processing is not valid for remanent bodies unless the remanence is directly opposed to the present-day field. The dataset almost certainly contains some remanent bodies that will not be corrected properly using the RTP filter. However, it is worthwhile applying the filter because most of the anomalies in the area are normally magnetized or reversely magnetized with relatively few anomalies possessing an apparent magnetization direction at a high angle to the present-day field.

Magnetic standard filtering

The RTP grid was filtered with a suite of standard geophysical filters including the analytic signal and vertical derivative. These grids were imaged using our in-house software to produce shaded images with the sunlight coming from the northeast or northwest (NE or NW in the filename). Unshaded images were also produced so that the geographic location of pertinent features in the data can be readily defined (because shaded images can 'fool the eye' in this respect).

Processing summary — Magnetic data

Magnetic standard filtering (continued)

Figures 4 to 22 show images of most of the standard filtering results supplied. Standard filtering results have been included in this report because of their capacity to help the reader who might be new to the delivered processing results files to quickly grasp the project area's overall magnetic susceptibility changes/contrasts.

Magnetic total structure detection

Structure detection was applied to highlight edges in the RTP magnetic data and the AGC of the RTP data. Edges in potential field data are locales that are more likely to be faults, contacts or other structures. The structure detection algorithm and processing are described in more detail in **Appendix 1**.

Representative images of the total structure detection filtering are shown in **Figures 23 and 24** for the RTP data and **Figures 25 and 26** for the AGC of the RTP. Further results files were delivered in addition to those visualized within this report, and we urge the reader to explore the entire series of results files to ensure full familiarity with the results of total structure detection processing and their possible exploration ramifications.

Total-structure detection filtering was applied to the RTP grid at minimum wavelengths of 100m, 200m, 400m, 800m, 1600m, and 3200m. The RTP-derived total-structure detection results are good at depicting relatively long-wavelength features. Structure intersection images were supplied alongside structure images.

This filtering was also applied to the AGC grid at minimum wavelengths of 100m, 200m, 400m, 800m, 1600m, and 3200m. The AGC-derived total-structure detection results are good at depicting relatively detailed features as well as highlighting features in quiet parts of the dataset. Structure intersection images were supplied alongside structure images.

The larger-scale structures observed in the RTP data show a dominant belt-parallel structural orientation that is NE-trending in the south and almost due north-trending in the north. Northwest-trending cross structures are present throughout the area. In the north, ENE-trending cross structures are also present.

The AGC results show a lot of detail allowing interpretation of individual units in many cases. They also show features in the quiet parts of the dataset that suggest some stratigraphic units may be present in the magnetically quiet areas.

Processing summary — Magnetic data (continued)

Magnetic total structure detection (continued)

The intersection maps show where structures of different orientations are collocated. Areas with a high density of intersections are likely to be more structurally complex and therefore may be more likely to host mineralization.

Magnetic belt-parallel and belt-crossing structure detection

In many greenstone belts, the fabric-parallel and fabric-crossing structures can be different structure types and may have different timing. The fabric-parallel features tend to be contacts or belt-parallel shear zones. The cross structures are usually not contacts and are more likely to be faults. Any sense of motion is possible on the cross structures. If clear lateral offset of the units is present, the faults are likely strike-slip faults. Normal and reverse faults are often represented by a change in amplitude or frequency content of the magnetic data.

The first step in extracting fabric-parallel and fabric-crossing structures is to extract the fabric orientation. The fabric was extracted separately from the RTP data (**Figure 27**) and the AGC of the RTP data (**Figure 30**). The results are broadly similar. The only major disagreements occur in quiet parts of the dataset where long-wavelength features dominate the RTP signature and more detailed features dominate the AGC. Most of the greenstone units have a fabric that strikes NE to north. Some small areas in the west-central part of the area have a nearly east-west strike,

Representative images of the results of parallel and cross structure detection are shown in **Figures 28 and 29** for the RTP data and **Figures 31 and 32** for the AGC of the RTP data. The wavelengths that were run are the same as for the total structure except that no 3200m scale was run for the RTP data. The structure results at that scale lack a strong fabric. At longer wavelengths, the original fabric orientation maps are smoothed so that larger-scale structures do not get broken up by rapid changes in the fabric orientation.

The fabric-parallel structures should be useful for highlighting lithological contacts and fabric parallel shear zones. The AGC results appear to be useful for highlighting lithological boundaries. The fabric-crossing structures are likely to be faults. The RTP results are likely more useful for cross structures because there is a lower density of features meaning that the features that are present are more likely to be significant.

Further results files were delivered in addition to those visualized within this report, and we urge the reader to explore the entire series of results files to ensure full familiarity with the results of belt-parallel and belt-crossing structure detection processing and their possible exploration ramifications.

Processing summary — Magnetic data (continued)

Magnetic radial symmetry

The radial symmetry detection filter can highlight discrete, equant magnetic features with different radii. Radial symmetry detection was completed on the RTP magnetic data. The radial symmetry algorithm is described in greater detail in **Appendix 2** of this report.

Representative images of the radial symmetry results are shown in **Figures 33** and **Figure 34**. Further results files were delivered in addition to those visualized within this report, and we urge the reader to explore the entire series of results files to ensure full familiarity with the results of radial symmetry analysis processing and their possible exploration ramifications.

Radial symmetry detection processing was applied to the RTP grid in magnitude-independent mode at minimum-radius runs of 500m, 1000m, and 2000m. Radii smaller and larger than these did not appear to be useful on this dataset. Both magnetic highs and magnetic lows represent meaningful/useable results and therefore are presented in images.

Note that in order to obtain optimal results it was necessary to take a residual (i.e., carry out differential upward continuation) prior to running radial symmetry detection at a given minimum radius. It was found that a residual involving levels going from on quarter the minimum radius to four times the minimum radius enable the production of satisfactory radial symmetry detection results (e.g., for the 500m radial symmetry detection run, a 125m-2000m residual was carried out first). In the case of radial symmetry processing applied to the AGC, the residual was performed on the RTP data, then AGC filtering was applied, and then radial symmetry detection was carried out.

The view of the full project area shown in **Figure 33** shows that round features are more common in the western half of the project area than the eastern half. The greenstone in the eastern half appears to be more sheared with more linear features.

Figure 34 shows a zoomed in view of part of the project area to show the kinds of anomalies that are highlighted by the radial symmetry analysis. The highest scoring features in the radial symmetry grids are the most likely to be discrete bodies and therefore more likely to be intrusions. The radially symmetric features that are strongly magnetic are more likely to be mafic intrusions and the less magnetic features are more likely to be felsic.

Reversely magnetized bodies will be highlighted as radially symmetric lows in this analysis. Any lows that correspond with highs in the analytic signal are likely to be reversely magnetized.

File formats and image types delivered

The grids for this work have been delivered in ER Mapper ERS format. All images have been provided in GeoTIFF format with associated MapInfo TAB files and ESRI world files. Vectors have been delivered in ESRI shapefile format.

Structure detection results have been supplied as grids, images (GeoTIFF), and polylines (vectorization of the gridded results). The polylines have been attributed with the values from the structure detection grid and the orientation of the structure calculated based on the vectorized result.

Structure images were made in an unshaded fashion using a warm color bar (yellows through to reds) and a linear color stretch. Shaded structure images cycle through colors starting from purple and blue (lows) through to reds (highs) and were made with a histogram-equalized color stretch. Dominant orientation images use a wraparound colorbar palette that produces the same color for 0 and 180 with a rainbow distribution for colors in between. Those orientation images that have been thresholded display only significant features and are white in locales that essentially lack structure.

Radial symmetry 'lows and highs' images were made using a blue-and-red color bar possessing no intermediate colors. Highs-only images use the red side of that same color bar, and lows-only images use the blue side.

Several ternary images were also created for this work. These images are generated using three separate grids to represent the red-green-blue (RGB) or cyan-magenta-yellow (CMY) channels of the output image. RGB ternary images involve color addition, analogous to how different-colored light beams combine on a performance stage. When all three channels are present in full strength, pure white is the result. (Pure black indicates all three channels are absent.) CMY ternary images involve color subtraction, similar to colors resulting from the mixing of paint pigments. When all three channels are present in full strength, pure black is the result. (Pure white indicates all three channels are absent.)

Figure 17 explains in more detail how to interpret the full gamut of colors that can turn up in ternary images.

See also the list of abbreviations and acronyms supplied in this report to help decode the information contained within a given grid/image filename.

List of acronyms and abbreviations

agc	automatic gain control (appears in delivered file names)
agc30	AGC when standard deviation=30 (in file names)
asig	analytic signal (appears in delivered file names)
colorbar	numerical values associated with image's color range (in file names)
Cross	structures that are perpendicular or oblique to the magnetic stratigraphic fabric
CMY	cyan-magenta-yellow ternary (appears in delivered file names)
hgm	horizontal gradient magnitude (appears in delivered file names)
Highs	positive anomalies-only radial symmetry image (in file names)
HSI	hue, saturation and intensity (appears in delivered file names)
HTh	hysteresis thresholding was used during vectorization (in file names)
Int	structural intersections image (appears in delivered file names)
LgeRes	large-scale residual (appears in delivered file names)
lin	linear-stretch image (appears in delivered file names)
Lows	negative anomalies-only radial symmetry image (in file names)
LowsAndHighs	negative and positive anomalies radial symmetry image (in file names)
md	magnitude dependent radial symmetry result (in file names)
MedRes	medium-scale residual (appears in delivered file names)
Mi	magnitude independent radial symmetry result (in file names)
NS	Northern Shield project area (appears in delivered file names)
OriDom	dominant orientation image (appears in delivered file names)
Para	Structures that are parallel to the magnetic stratigraphic fabric
Pgrav	pseudogravity (appears in delivered file names)
PgravRes	residual of pseudogravity (appears in delivered file names)
PgravResHGM	HGM of residual of pseudogravity (appears in delivered file names)
res	residual (appears in delivered file names)
res25_100	25m-100m residual (appears in delivered file names)
RGB	red-green-blue ternary (appears in delivered file names)
RMI	residual magnetic intensity (appears in delivered file names)
RSym	radial symmetry image (appears in delivered file names)
RSym100	100m minimum radius radial symmetry image (in file names)
RTP	reduced-to-pole (appears in delivered file names)
SmRes	small-scale residual (appears in delivered file names)
Struct	structure image (appears in delivered file names)
Struct100	100m minimum wavelength structure image (in file names)
tern, ternary	ternary image (appears in delivered file names)
Thresh, thr, Th	image made via thresholding (appears in delivered file names)
tilt	tilt angle (appears in delivered file names)
TMI	total magnetic intensity (appears in delivered file names)
Total	total structure image (appears in delivered file names)
vd	vertical derivative (a.k.a. 1VD) (appears in delivered file names)

List of acronyms and abbreviations (continued)

vdmhgm	vertical derivative minus HGM (appears in delivered file names)
Vec	vectorized results file (appears in delivered file names)
vias	analytic signal of vertical integral (appears in delivered file names)
vint	vertical integral (appears in delivered file names)
X	directional derivative along X axis (appears in delivered file names)
Y	directional derivative along Y axis (appears in delivered file names)
Z	directional derivative along Z axis (i.e., vertical derivative) (in file names)

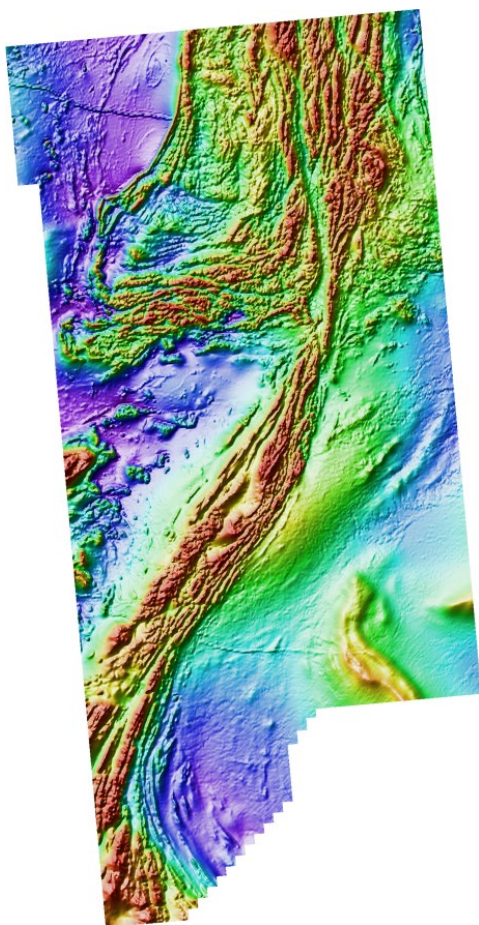
Project location map



Figure 1: Location map for this project showing the outline of the survey area as a red outline.

Magnetic data-processing results images

► Residual magnetic intensity (RMI)



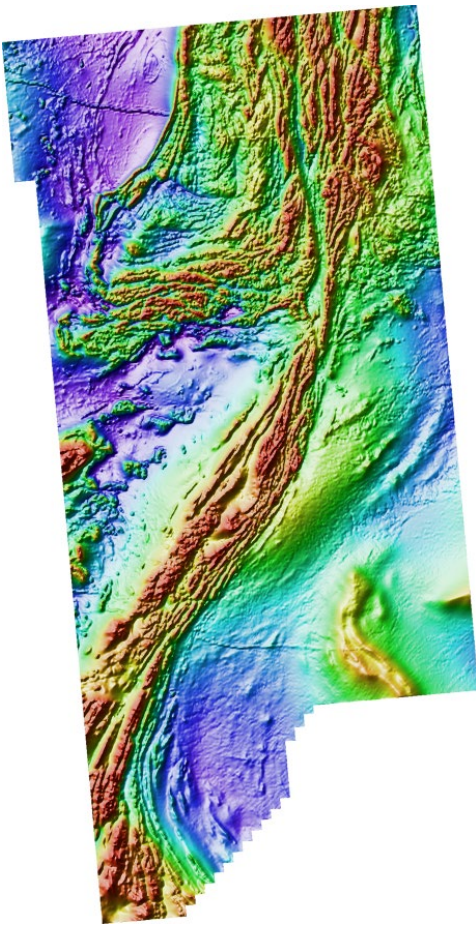
NS_RMI_HSI_NW



Figure 2: Residual magnetic intensity data for the project area. The indicative colorbar shown applies to all magnetic data-processing results images involving the HSI (hue, saturation, intensity) color display system.

Magnetic data-processing results images

► Reduction-to-pole (RTP)

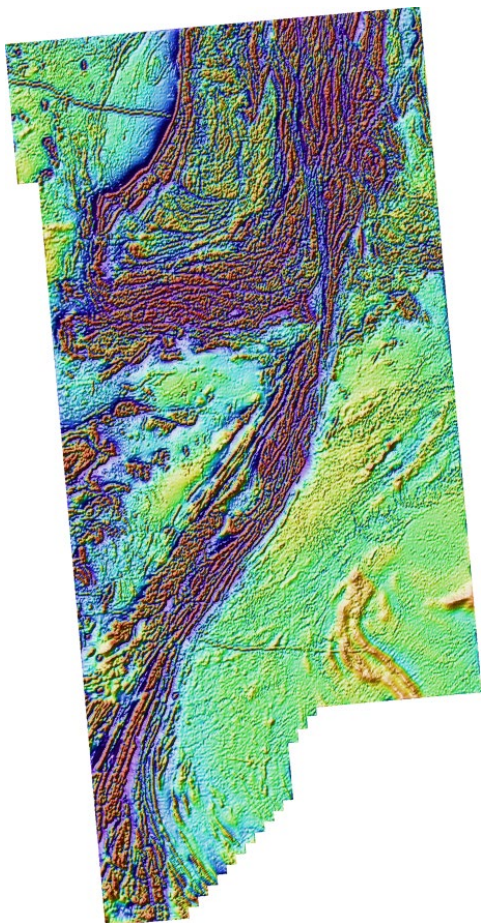


NS_RMI_RTP_HSI_NW

Figure 3: Reduced-to-the-pole magnetic data for the project area. The RTP filter attempts to produce the magnetic field that would be expected if the data were collected at the magnetic pole.

Magnetic data-processing results images (continued)

► Standard filtering — First vertical derivative

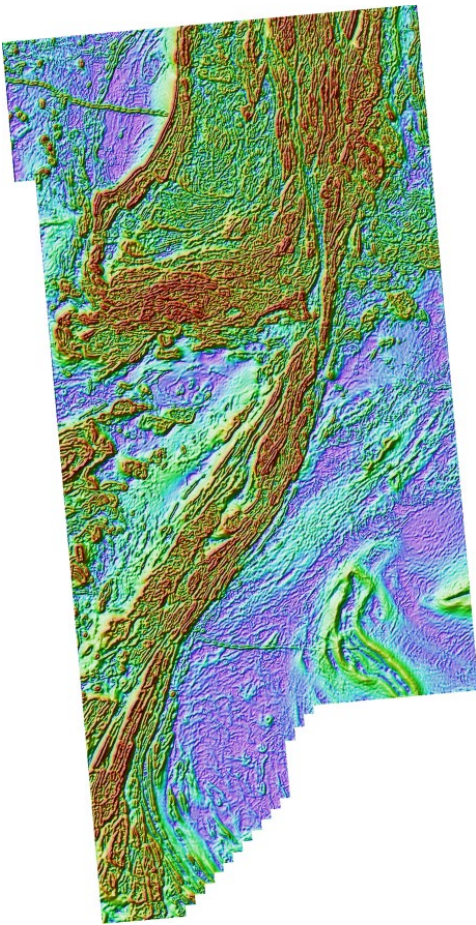


NS_RMI_RTP_vd_HSI_NW

Figure 4: The first vertical derivative (1VD) transform is the rate of change of the potential field in the vertical direction. Application of this filter has the effect of accentuating the shorter wavelength (higher frequency) components at the expense of longer wavelength (more regional) features.

Magnetic data-processing results images (continued)

► Standard filtering — Horizontal gradient magnitude

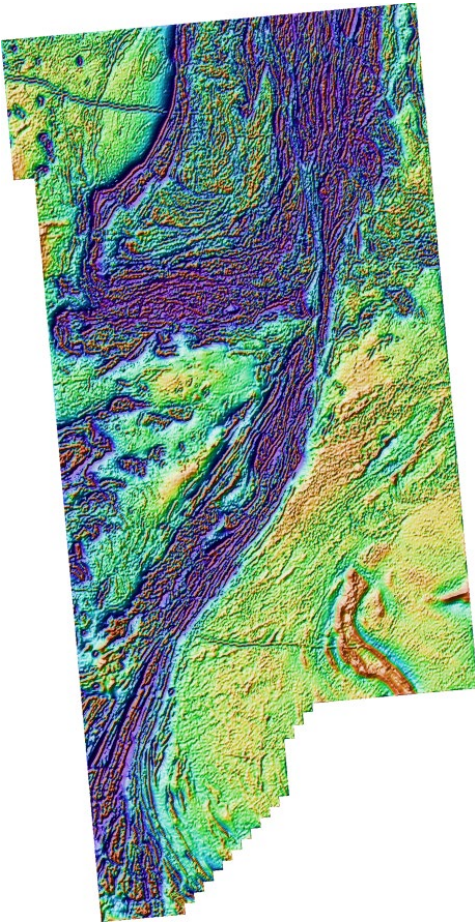


NS_RMI_RTP_hgm_HSI_NW

Figure 5: The horizontal gradient magnitude is calculated from the x- and y-derivatives of the data ($\sqrt{dx^2 + dy^2}$). This filter highlights the location of steep gradients in the data. Peaks in the HGM should occur at susceptibility contrasts in magnetic data and density contrasts in gravity data. These are likely to be locations of faults or contacts. Peaks will be offset in the down-dip direction for dipping bodies. The results are affected by remanent magnetization.

Magnetic data-processing results images (continued)

► Standard filtering — Vertical derivative minus HGM

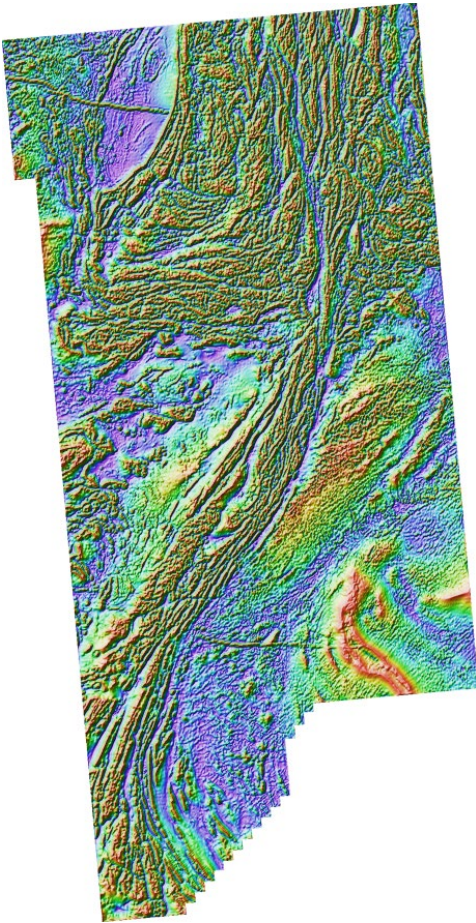


NS_RMI_RTP_vdmhgm_HSI_NW

Figure 6: The vertical derivative minus the HGM (VDMHGM) is a filter that accentuates the contrast in the first vertical derivative. This is useful for highlighting shallow sources in potential field data. It can also be useful when trying to pick the exact location to place a narrow magnetic unit or a narrow dense unit.

Magnetic data-processing results images (continued)

► Standard filtering — Tilt angle

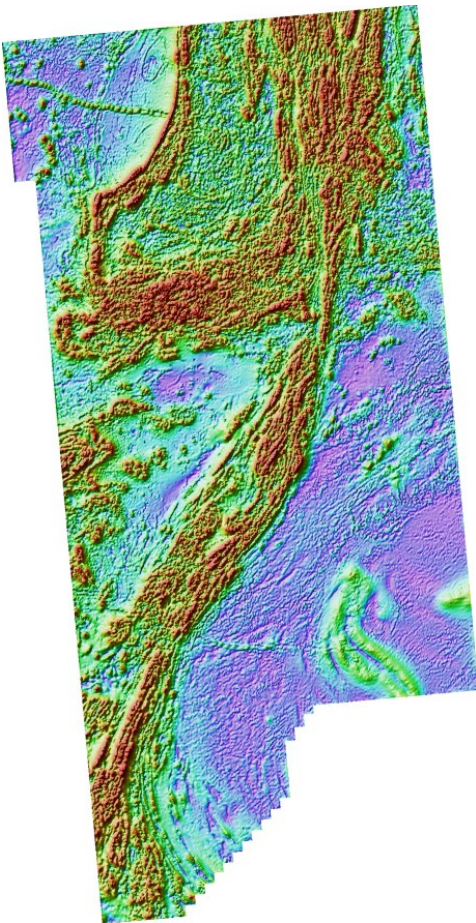


NS_RMI_RTP_tilt_HSI_NW

Figure 7: The tilt angle filter is the arctangent of the ratio of the vertical derivative to the horizontal gradient magnitude. This filter removes information about the amplitude of the signal, making the heights of peaks the same regardless of the susceptibility or density of the causative body. Structure and depth information are preserved. This makes it easier to see subtle features and some structures.

Magnetic data-processing results images (continued)

► Standard filtering — Analytic signal

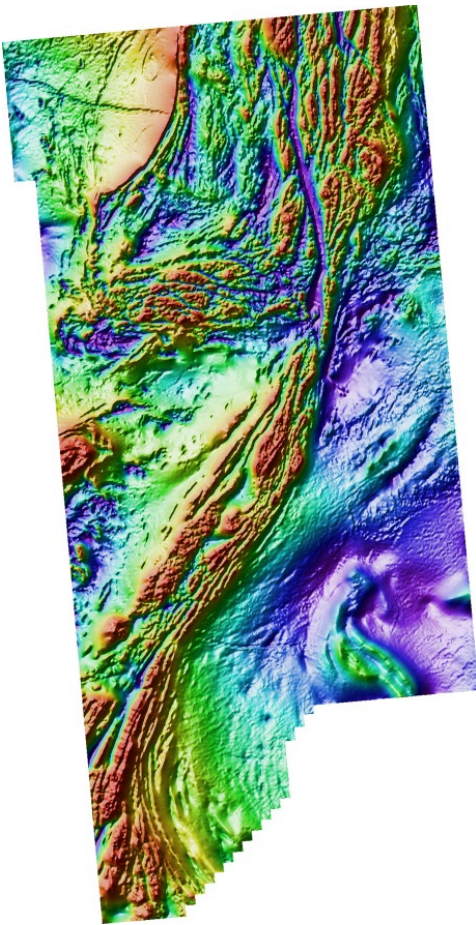


NS_RMI_RTP_asig_HSI_NW

Figure 8: Analytic signal of the RTP data. The analytic signal (also known as the total gradient magnitude) is calculated as $\sqrt{dx^2 + dy^2 + dz^2}$. This filter highlights the location of rapid changes in the data. Highs in the analytic signal correspond to high amplitudes in the vertical derivative (positive or negative) or high amplitudes in the horizontal gradient magnitude. Highs will occur over the top of small bodies with high susceptibility or high density contrast or at the edge of large-scale susceptibility or density contrast. Long-wavelength features are suppressed by this filter since it is based on derivative filters. This filter is relatively independent of magnetization direction and remanent magnetization.

Magnetic data-processing results images (continued)

► Standard filtering — Analytic signal of vertical integral

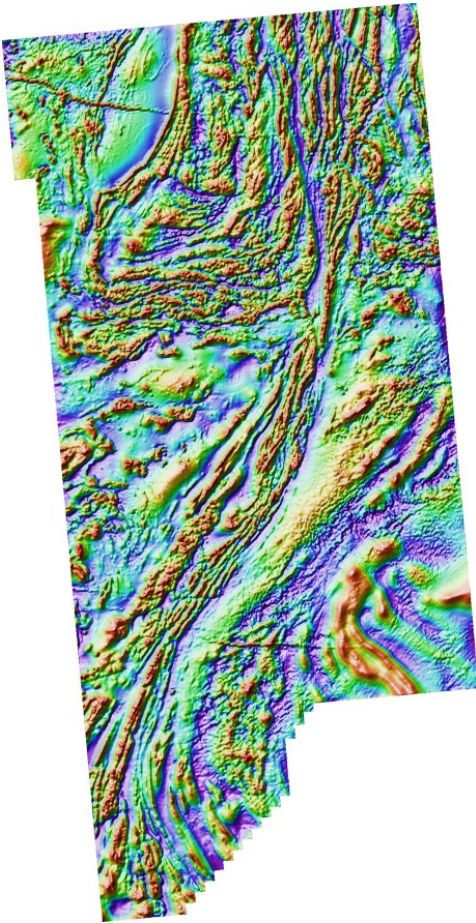


NS_RMI_RTP_vias_HSI_NW

Figure 9: The analytic signal filter was applied to the vertical integral of the magnetic data to produce this VIAS result. The analytic signal filter is described in the caption of **Figure 8**. Produces a grid with wavelength and amplitude characteristics that are similar to the RTP grid, but with reduced effects of remanent magnetization and magnetization direction.

Magnetic data-processing results images (continued)

► Standard filtering — Automatic gain control

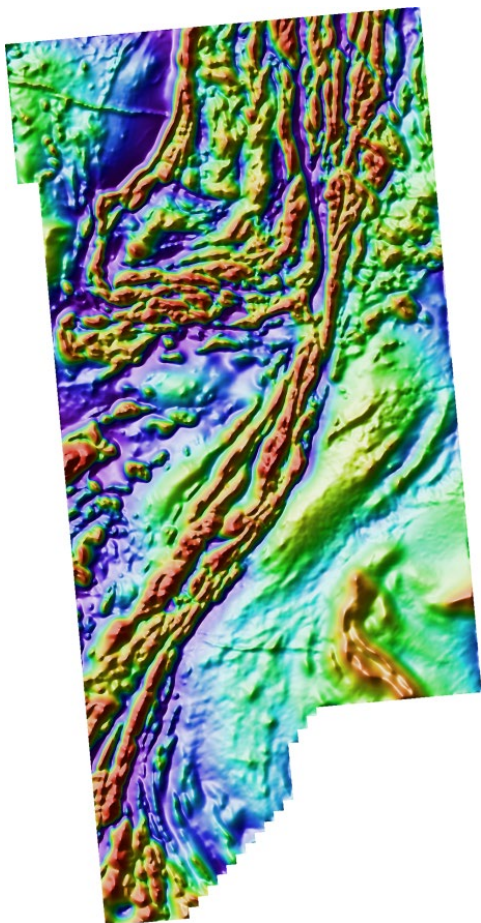


NS_RMI_RTP_AGC30_HSI_NW

Figure 10: The automatic gain control filter (AGC) is a means of evening out the amplitudes of anomalies. This makes more subtle features in the data visible. The filter also acts as a high-pass filter by suppressing the longer wavelengths.

Magnetic data-processing results images (continued)

► Standard filtering — Small-scale residual

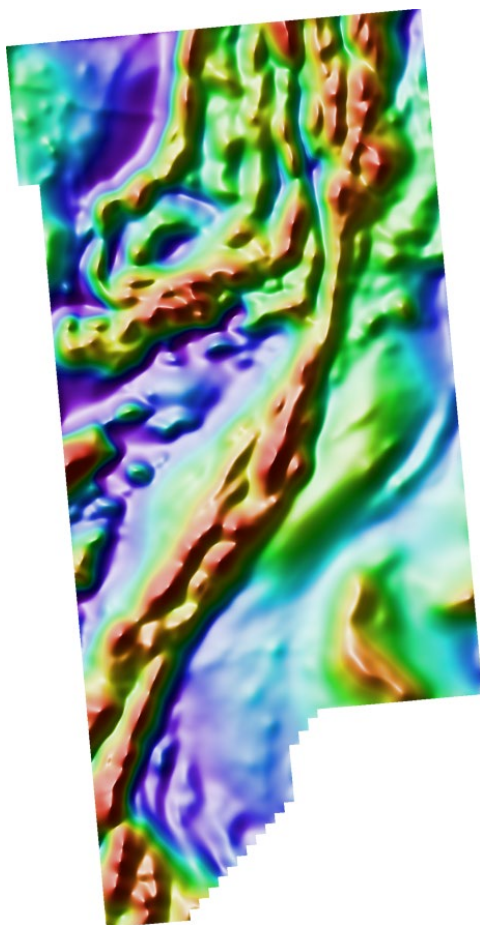


NS_RMI_RTP_res500_2000_HSI_NW

Figure 11: Differential upward continuation was applied to calculate the 500m-2000m residual of the RTP data in an attempt to separate sources from different depths (Jacobsen, 1987). The source depths should correspond to half of the upward continuation level. For this residual, that would be about 250m-1000m depth.

Magnetic data-processing results images (continued)

► Standard filtering — Medium-scale residual

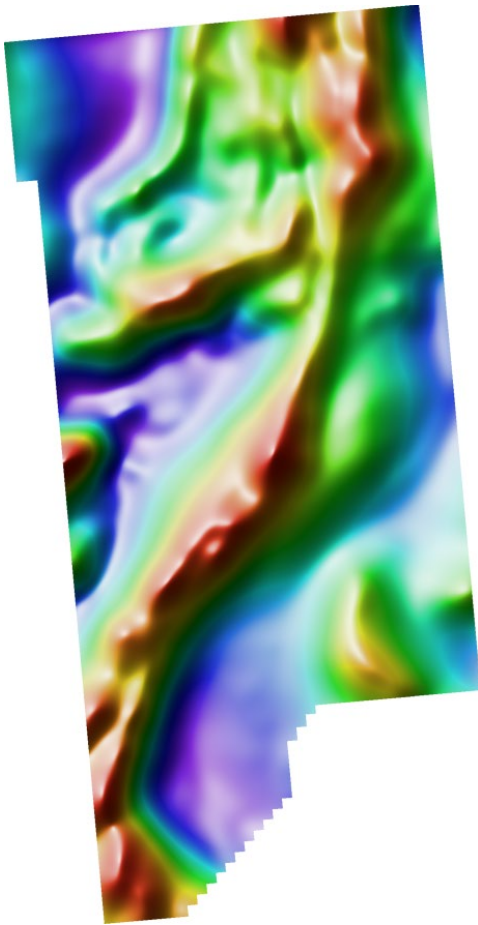


NS_RMI_RTP_res2000_5000_HSI_NW

Figure 12: Differential upward continuation was applied to calculate the 2000m-5000m residual of the RTP data in an attempt to separate sources from different depths (Jacobsen, 1987). The source depths should correspond to half of the upward continuation level. For this residual, that would be 1000m-2500m depth.

Magnetic data-processing results images (continued)

► Standard filtering — Large-scale residual

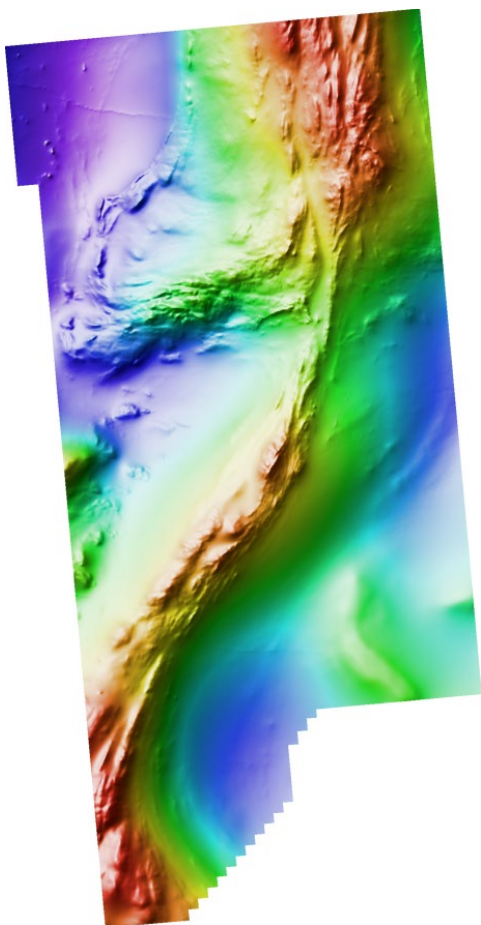


NS_RMI_RTP_res5000_10000_HSI_NW

Figure 13: Differential upward continuation was applied to calculate the 5000m-10000m residual of the RTP data in an attempt to separate sources from different depths (Jacobsen, 1987). The source depths should correspond to half of the upward continuation level. For this residual, that would be 2500m-5000m depth.

Magnetic data-processing results images (continued)

► Standard filtering — Pseudogravity

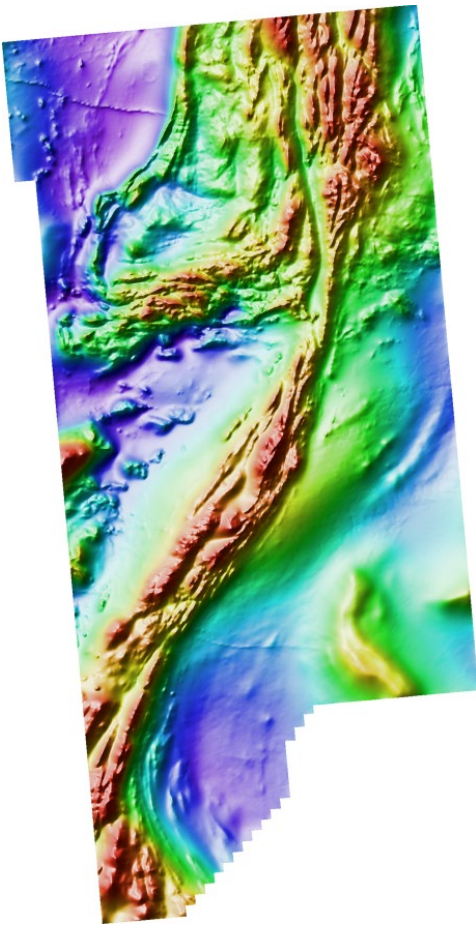


NS_RMI_RTP_PGgrav_HSI_NW

Figure 14: Pseudogravity is generated by calculating the vertical integral of reduced-to-the-pole magnetic data and then using Poisson's relation (correlation between magnetic potential and gravitational potential) to scale the result. This generates a grid that is the expected gravity field if density were distributed in the same way as magnetic susceptibility in the project area. This is not a true gravity grid because it is highly unlikely that susceptibility and density are perfectly correlated. This filter enhances long-wavelength features and is good for highlighting large-scale features.

Magnetic data-processing results images (continued)

► Standard filtering — Pseudogravity residual

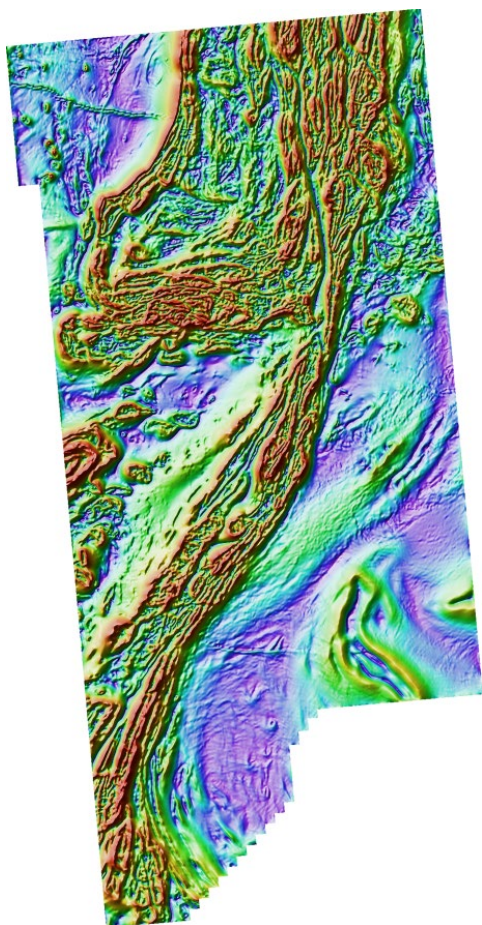


NS_RMI_RTP_PGravRes_HSI_NW

Figure 15: Differential upward continuation was applied to the pseudogravity grid to generate a 0-2000m residual. This removes the longest wavelength features to allow intermediate-scale features to be seen.

Magnetic data-processing results images (continued)

► Standard filtering — HGM of pseudogravity residual



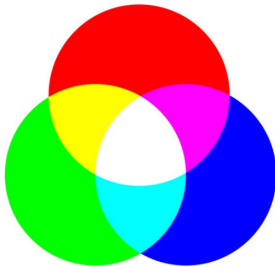
NS_RMI_RTP_PGravResHGM_HSI_NW

Figure 16: The horizontal gradient was calculated from the pseudogravity residual as described in the caption for **Figure 5**. The results highlight the edges of intermediate-scale features. However, this filter is affected by magnetization direction and remanent magnetization.

Magnetic data-processing results images (continued)

► Standard filtering images — Using ternary images

RGB



For RGB images:

Green + blue = cyan

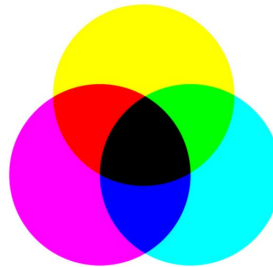
Red + blue = magenta

Red + green = yellow

Red + green + blue = white

Low in red + green + blue = black

CMYK



For CMY images:

Magenta + yellow = red

Cyan + yellow = green

Cyan + magenta = blue

Cyan + magenta + yellow = black

Low in red + green + blue = white

Figure 17: The information above shows how to interpret the colors in the RGB and CMY ternary images appearing in the next few figures, which are:

(i) Ternary of directional derivatives — This image encapsulates information about how steeply the gradient is changing in 3 orthogonal directions, namely the X and Y directions (within the plane of the image), and the Z direction (perpendicular to the plane of the image). All of this gradient information combines to help the observer intuitively identify the various major geological domains residing throughout the area of interest, and how these domains relate to each other.

(ii) Ternary of 1VD, tilt angle, and HGM — This image helps the observer intuitively understand where major structural features are situated, where breaks in the continuity of the magnetic 'fabric' occur, and how the textural character of the magnetic data changes from one locale to the next.

(iii) Ternary of residuals — Again, this image helps the observer intuitively understand where major structural features are situated, where breaks in the continuity of the magnetic 'fabric' occur, and how the textural character of the magnetic data changes from one locale to the next. However, features seen are generally coarser than those appearing in the ternary combining 1VD, tilt and HGM.

(iv) Ternary of RTP, VIAS, and analytic signal — This image helps the observer intuitively understand which subareas may be most affected by remanence (red locales in the CMY image).

(v) Ternary of pseudogravity results — This image combines three pseudogravity-related grids and produces an image that may assist the observer with intuitively grasping the geological affinity of features in the data.

Magnetic data-processing results images (continued)

► Standard filtering — Ternary of directional derivatives

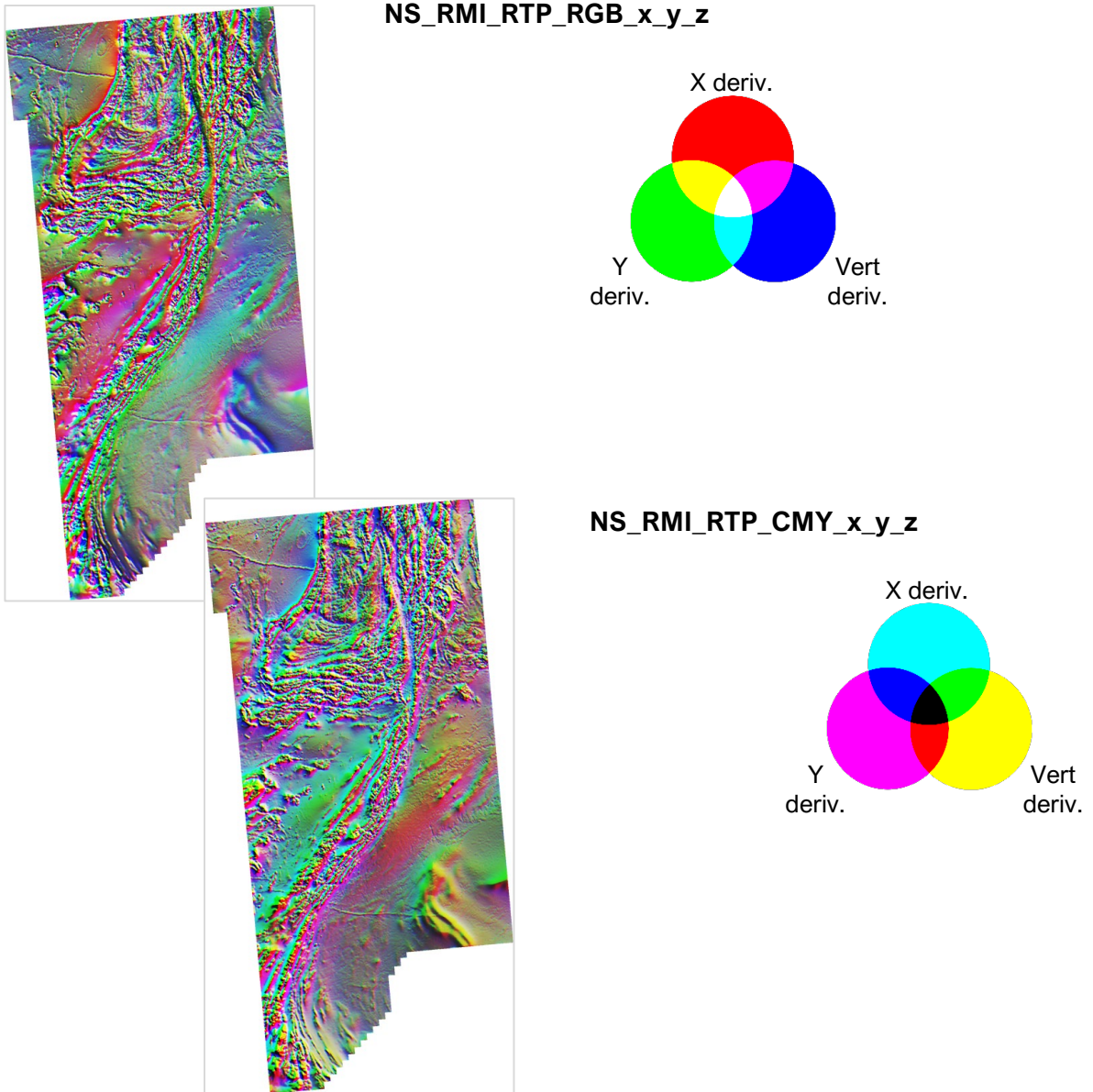
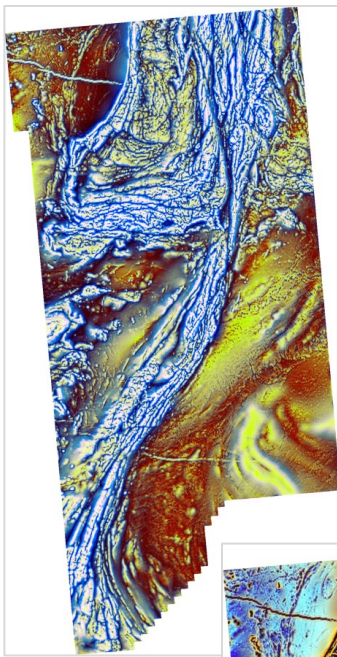


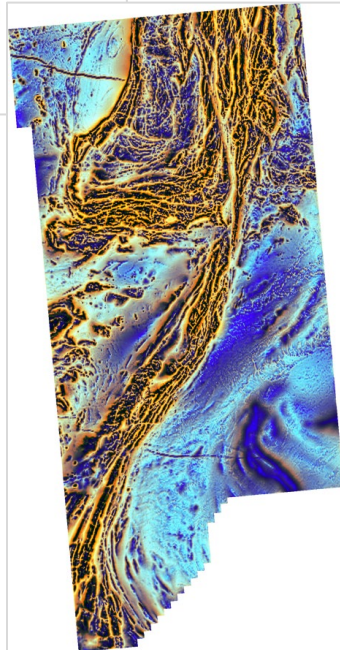
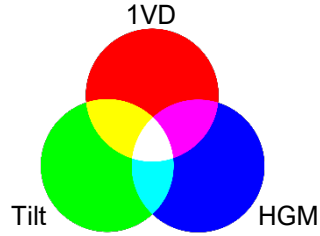
Figure 18: RGB and CMY ternary images co-displaying the X-gradient (R/C channels), Y-gradient (G/M channels), and Z-gradient (i.e., vertical derivative) (B/Y channels).

Magnetic data-processing results images (continued)

► Standard filtering — Ternary of 1VD, tilt, HGM



NS_RMI_RTP_RGB_1vd_tilt_hgm



NS_RMI_RTP_CMY_1vd_tilt_hgm

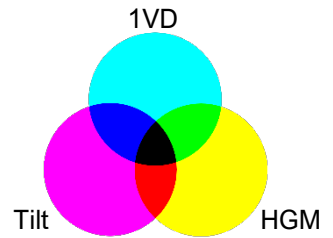
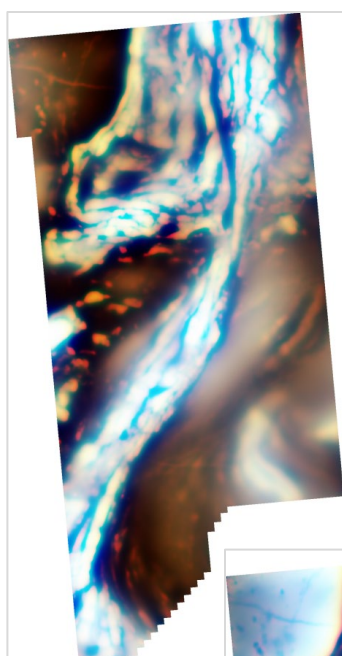


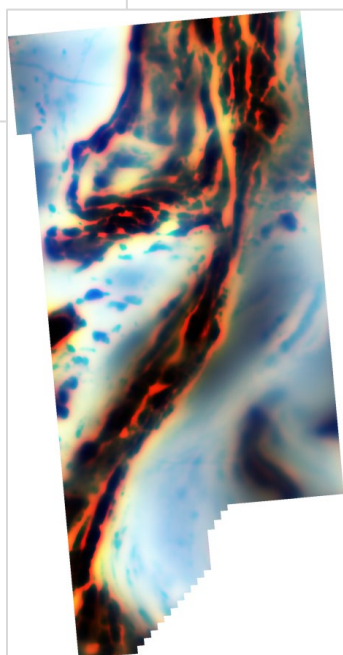
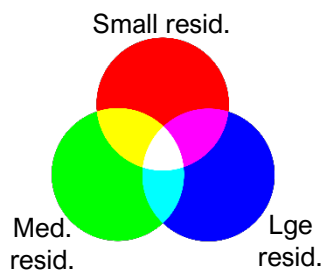
Figure 19: RGB and CMY ternary images co-displaying the vertical derivative (R/C channels), tilt angle (G/M channels), and HGM (B/Y channels).

Magnetic data-processing results images (continued)

► Standard filtering — Ternary of residuals



NS_RMI_RTP_RGB_SmRes_MedRes_LgRes



NS_RMI_RTP_CMY_SmRes_MedRes_LgRes

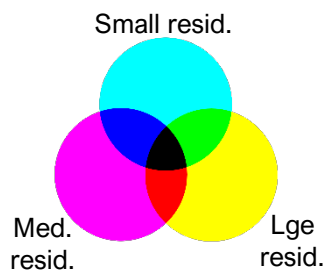
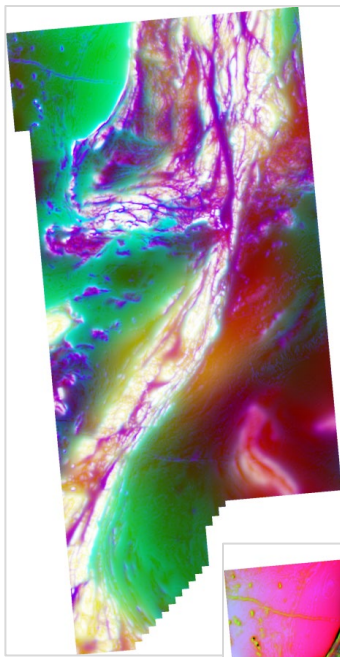


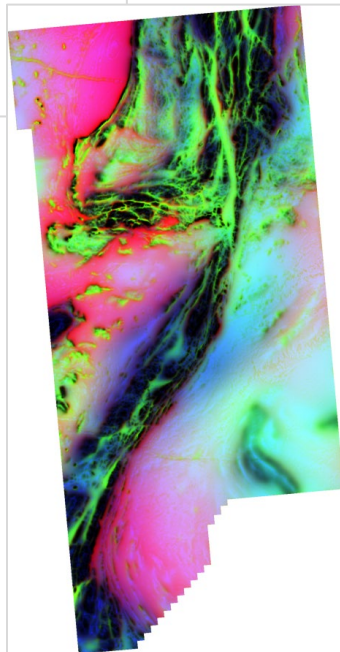
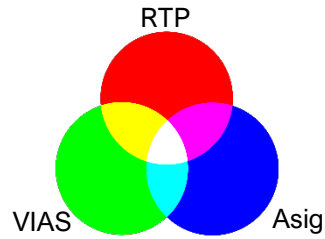
Figure 20: RGB and CMY ternary images co-displaying the small-scale (R/C channels), medium-scale (G/M channels), and large-scale residuals (B/Y channels).

Magnetic data-processing results images (continued)

► Standard filtering — Ternary of RTP, VIAS, Asig



NS_RMI_RTP_RGB_RTP_vias_asig



NS_RMI_RTP_CMY_RTP_vias_asig

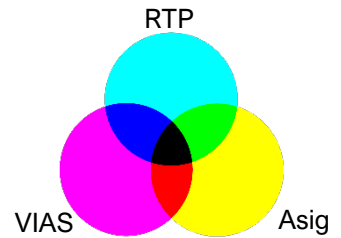
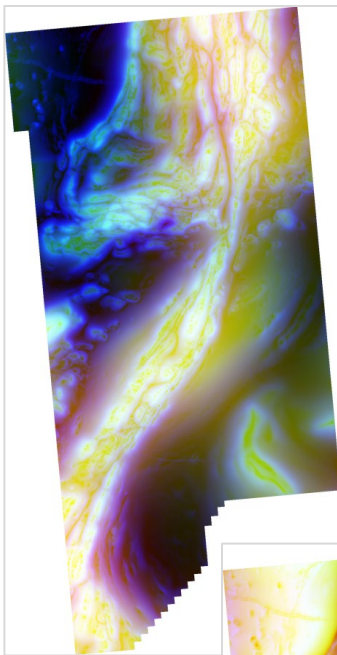


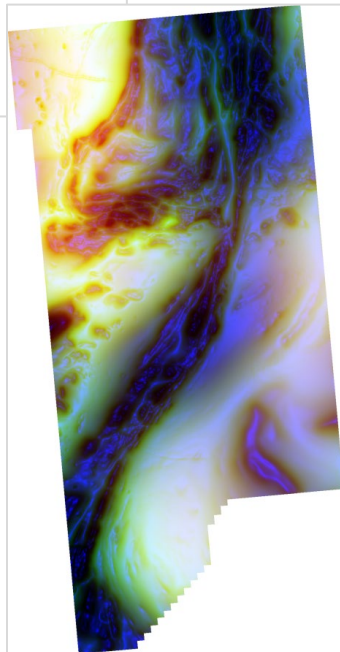
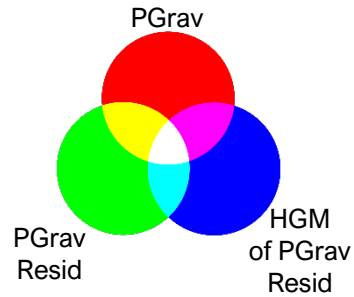
Figure 21: RGB and CMY ternary images co-displaying the RTP (R/C channels), VIAS (G/M channels), and analytic signal (B/Y channels).

Magnetic data-processing results images (continued)

► Standard filtering — Ternary of pseudogravity results



NS_RMI_RTP_RGB_PG Grav_
PG Grav Resid_PG Grav Res HGM



NS_RMI_RTP_CMY_PG Grav_
PG Grav Resid_PG Grav Res HGM

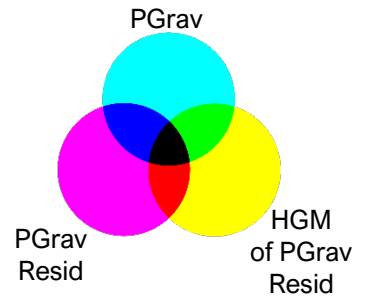
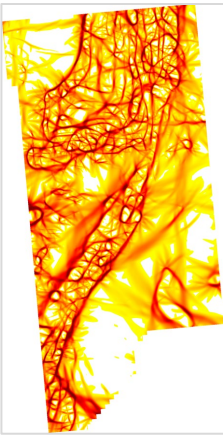


Figure 22: RGB and CMY ternary images co-displaying pseudograv (R/C channels), pseudograv residual (G/M channels), and HGM of pseudograv residual (B/Y channels).

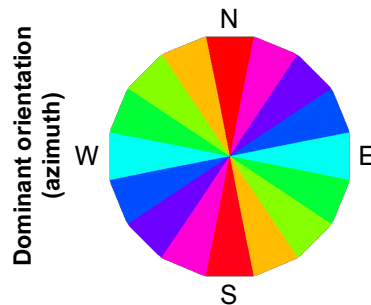
Magnetic data-processing results images (continued)

► Total structure detection — Analysis of RTP

Figure 23: Representative image** showing 800m structure detection results for the RTP data. TOP: Total structure detected. MIDDLE: Map of thresholded structural orientations. BOTTOM: Total structure in vectorized form (black lines with displayed thickness varying according to median value) over the project area's RTP image. The dominant fabric is north to NE-trending. NW and ENE-trending cross structures are the most common.



NS_RMI_RTP_Struct800_Total



NS_RMI_RTP_Struct800_OriDom_Th



NS_RMI_RTP_Struct800_Total_Vec

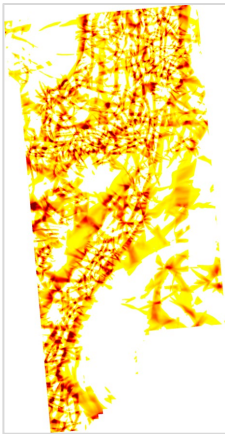
NS_RMI_RTP_HSI_NW

** Further scales of results also delivered.

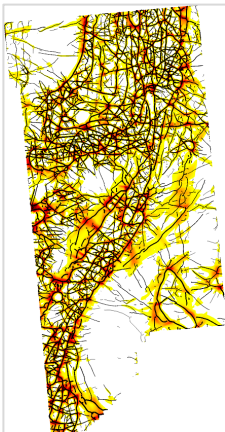
Magnetic data-processing results images (continued)

► Total structure detection — Analysis of RTP

Figure 24: Representative image** showing 800m structure detection results for the RTP data. TOP: Total structure intersections detected. MIDDLE: Intersections co-displayed with same-scale structures (line color and thickness varies according to structure's median value). BOTTOM: Intersections co-displayed with strong intersections (black-lined polygons) over gray RTP.

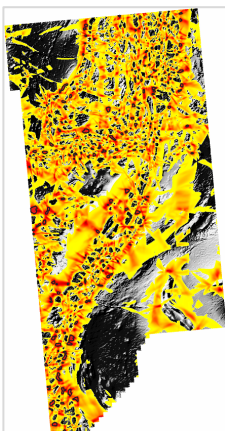


NS_RMI_RTP_Struct800_Int



NS_RMI_RTP_Struct800_Int

NS_RMI_RTP_Struct800_Total_Vec



NS_RMI_RTP_Struct800_Int

NS_RMI_RTP_Struct800_Int_HTh_Vec

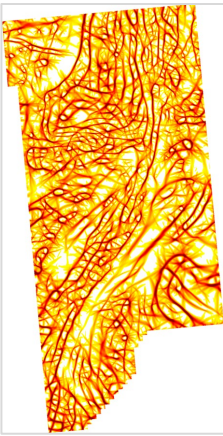
NS_RMI_RTP_HSI_NW (grayscale)

** Further scales of results also delivered.

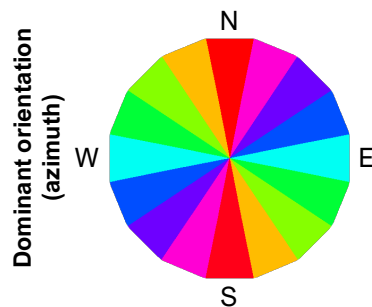
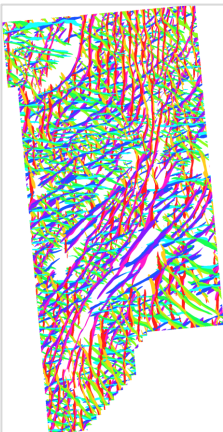
Magnetic data-processing results images (continued)

► Total structure detection — Analysis of AGC

Figure 25: Representative image** showing 800m structure detection results for the RTP's AGC. TOP: Total structure detected. MIDDLE: Map of thresholded structural orientations. BOTTOM: Total structure in vectorized form (black lines with displayed thickness varying according to median value) over the project area's RTP image. The AGC does a better job of highlighting detailed features and highlighting features in quiet parts of the dataset.



NS_RMI_RTP_AGC30_Struct800_Total



NS_RMI_RTP_AGC30_Struct800_OriDom_Th



NS_RMI_RTP_AGC30_Struct800_Total_Vec

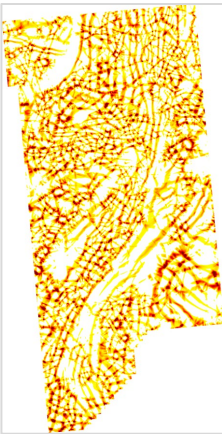
NS_RMI_RTP_HSI_NW

** Further scales of results also delivered.

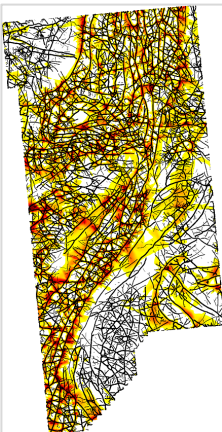
Magnetic data-processing results images (continued)

► Total structure detection — Analysis of AGC

Figure 26: Representative image** showing 800m structure detection results for the RTP's AGC. TOP: Total structure intersections detected. MIDDLE: Intersections co-displayed with same-scale structures (line color and thickness varies according to structure's median value). BOTTOM: Intersections co-displayed with strong intersections (black-lined polygons) over gray RPT.

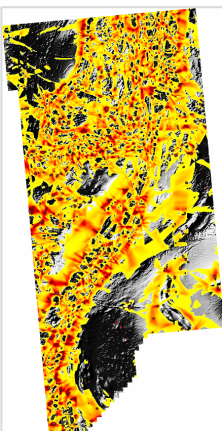


NS_RMI_RTP_AGC30_Struct800_Int



NS_RMI_RTP_AGC30_Struct800_Int

NS_RMI_RTP_AGC30_Struct800_Total_Vec



NS_RMI_RTP_AGC30_Struct800_Int

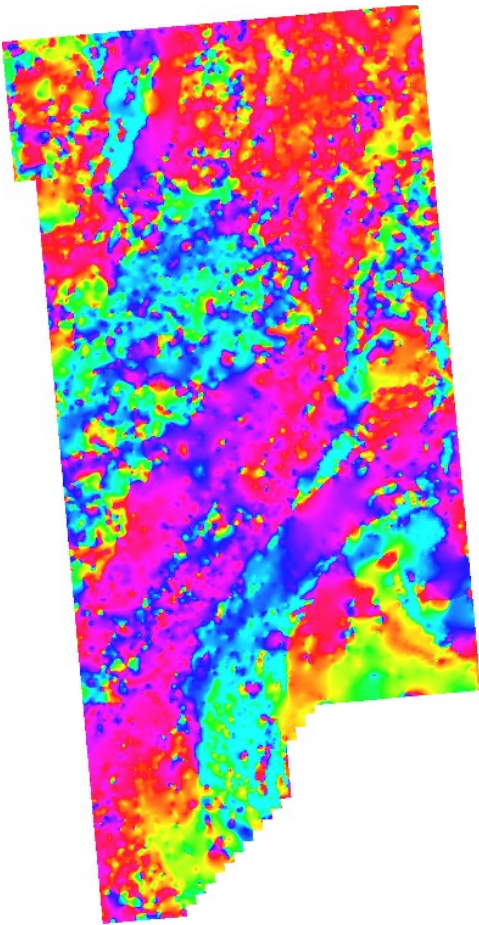
NS_RMI_RTP_AGC30_Struct800_Int_HTh_Vec

NS_RMI_RTP_HSI_NW (grayscale)

** Further scales of results also delivered.

Magnetic data-processing results images

► Fabric orientation derived from RTP magnetic data



NS_RMI_RTP_Fabric_Orientation

Figure 27: Fabric orientation derived from the RTP magnetic data. In quiet areas, this product will reflect the orientation of long-wavelength features. The fabric derived from the AGC (**Figure 30**) will do a better job of highlighting stratigraphic orientations in these areas.

Magnetic data-processing results images (continued)

► Parallel/cross structure — RTP



Figure 28: Representative image** showing 800m belt-parallel structure detection results for the RTP data. TOP: Parallel structures detected. MIDDLE: The same results in vectorized form (displayed line thickness varies according to structure's median value). BOTTOM: Vectorized results co-displayed with the RTP image. These relatively large-scale fabric-parallel features may represent belt-parallel shear zones.

NS_RMI_RTP_Struct800_Para



NS_RMI_RTP_Struct800_Para_Vec



NS_RMI_RTP_Struct800_Para_Vec

NS_RMI_RTP_HSI_NW

** Further scales of results also delivered.

Magnetic data-processing results images (continued)

▶ Parallel/cross structure — RTP

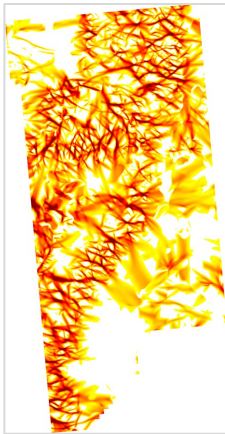
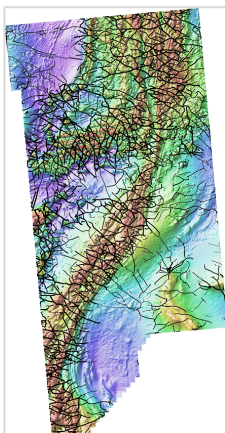


Figure 29: Representative image** showing 800m belt-crossing structure detection results for the RTP data. TOP: Cross structures detected. MIDDLE: The same results in vectorized form (displayed line thickness varies according to structure's median value). BOTTOM: Vectorized results co-displayed with the RTP image. Fabric-crossing features can indicate areas where fluid flow would be focused.

NS_RMI_RTP_Struct800_Cross



NS_RMI_RTP_Struct800_Cross_Vec



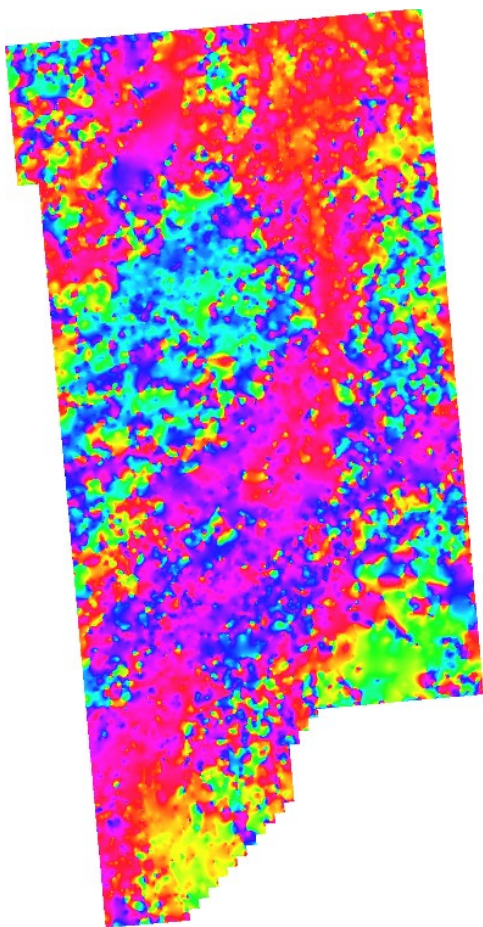
NS_RMI_RTP_Struct800_Cross_Vec

NS_RMI_RTP_HSI_NW

** Further scales of results also delivered.

Magnetic data-processing results images

► Fabric orientation derived from AGC of the RTP magnetic data



NS_RMI_RTP_AGC30_Fabric_Orientation

Figure 30: Fabric orientation derived from the AGC of the RTP magnetic data. This product is more affected by high-frequency features and subtle features than the fabric derived from the RTP magnetic data. This orientation map should work better to highlight stratigraphic orientations in quiet parts of the dataset.

Magnetic data-processing results images (continued)

▶ Parallel/cross structure — AGC



Figure 31: Representative image** showing 800m belt-parallel structure detection results for the RTP's AGC. TOP: Parallel structures detected. MIDDLE: The same results in vectorized form (displayed line thickness varies according to structure's median value). BOTTOM: Vectorized results co-displayed with the RTP image. The features extracted from the AGC are generally more detailed than those from the RTP. Many stratigraphic contacts are likely being highlighted by the AGC fabric-parallel results.

NS_RMI_RTP_AGC30_Struct800_Para



NS_RMI_RTP_AGC30_Struct800_Para_Vec



NS_RMI_RTP_AGC30_Struct800_Para_Vec

NS_RMI_RTP_HSI_NW

** Further scales of results also delivered.

Magnetic data-processing results images (continued)

▶ Parallel/cross structure — AGC

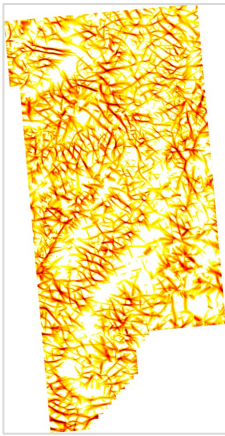
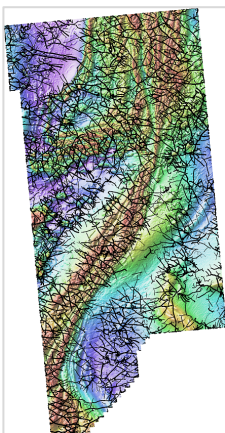


Figure 32: Representative image** showing 800m belt-crossing structure detection results for the RTP's AGC. TOP: Cross structures detected. MIDDLE: The same results in vectorized form (displayed line thickness varies according to structure's median value). BOTTOM: Vectorized results co-displayed with the RTP image. The AGC cross features sometimes appear to be highlighting smaller features that are less significant than those highlighted by the RTP cross structures.

NS_RMI_RTP_AGC30_Struct800_Cross



NS_RMI_RTP_AGC30_Struct800_Cross_Vec



NS_RMI_RTP_AGC30_Struct800_Cross_Vec

NS_RMI_RTP_HSI_NW

** Further scales of results also delivered.

Magnetic data-processing results images (continued)

► Radial symmetry analysis — RTP

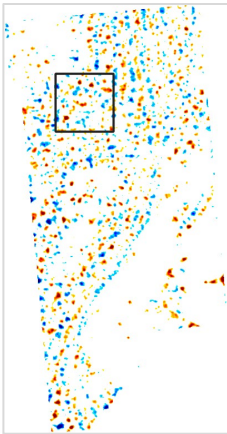
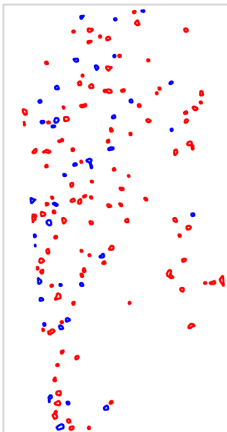


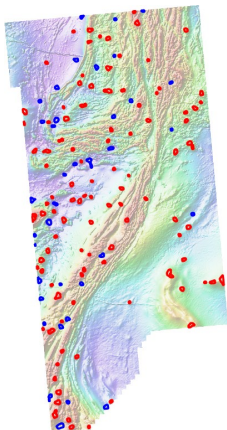
Figure 33: Representative image** showing 1000m magnitude-independent radial symmetry results for the RTP data. TOP: Radially symmetric features detected (both positive and negative anomalies). The area inside the black square is shown in detail in **Figure 34**. MIDDLE: Vectorized polygons representing strong anomalies obtained via thresholding. BOTTOM: Polygons co-displayed with the RTP image. Radially symmetric features are more common in the west than in the east. This is likely due to less deformation in the west.

**NS_RMI_RTP_res250_400_RSym1000_
mi_Highs_and_Lows**



**NS_RMI_RTP_res250_400_RSym1000_
mi_HTh_Vec_Highs**

**NS_RMI_RTP_res250_400_RSym1000_
mi_HTh_Vec_Lows**



**NS_RMI_RTP_res250_400_RSym1000_
mi_HTh_Vec_Highs**

**NS_RMI_RTP_res250_400_RSym1000_
mi_HTh_Vec_Lows**

NS_RMI_RTP_HSI_NW

** Further scales of results also delivered.

Magnetic data-processing results images (continued)

► Radial symmetry analysis — RTP

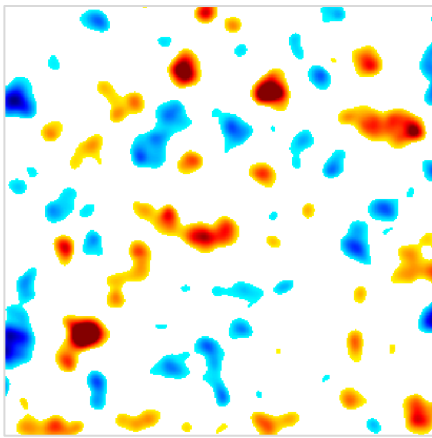
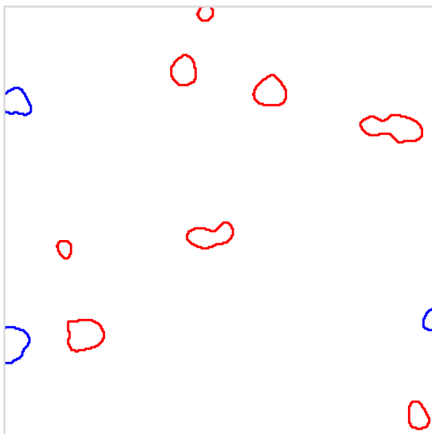


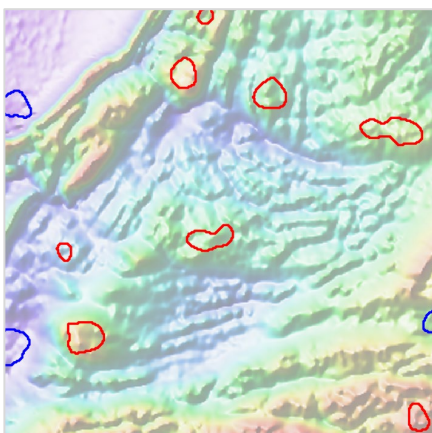
Figure 34: View of the area indicated by the black square in **Figure 33** showing 1000m magnitude-independent radial symmetry results for the RTP data. TOP: Radially symmetric features detected (both positive and negative anomalies). MIDDLE: Vectorized polygons representing strong anomalies obtained via thresholding. BOTTOM: Polygons co-displayed with the RTP image. The vectorization highlights the stronger anomalies in the radial symmetry image. These areas are more likely to be possible intrusions.

NS_RMI_RTP_res250_400_RSym1000_mi_Highs_and_Lows



NS_RMI_RTP_res250_400_RSym1000_mi_HTh_Vec_Highs

NS_RMI_RTP_res250_400_RSym1000_mi_HTh_Vec_Lows



NS_RMI_RTP_res250_400_RSym1000_mi_HTh_Vec_Highs

NS_RMI_RTP_res250_400_RSym1000_mi_HTh_Vec_Lows

RMI_RTP_HSI_NW

**** Further scales of results also delivered.**

Appendix 1: Structure detection algorithm

The goal in developing structure detection was to move towards automated interpretation of potential field data that would be most similar to an interpretation by a person. The structure detection is a phase congruency algorithm based on oriented exponential filters (**Kovesi, 1999**).

The structure detection filter is a feature detection algorithm used to highlight ridges, valleys or edges in gridded data. The results are significantly different from other feature detection routines.

Perhaps the biggest difference is that the results are a measure of symmetry or asymmetry, irrespective of amplitude. This is because the analysis is completed using the local phase rather than the signal amplitude.

This means that features in areas of low contrast are highlighted just as well as those in areas of high contrast, as long as the frequencies are present. High values in the structure grid indicate that the structure is close to a step edge. A small step change will have a higher value than a higher amplitude change that is more gradual.

The method is also multi-scale by design. For structures to be highlighted, they must be present at more than one scale. This eliminates more-minor edges that may be present over a narrow frequency range.

The use of exponential filters to determine the scale allows for some inference as to the depth of the structures detected when the filter is applied to potential field data. The wavelength in the filename is the shallowest upward continuation level used and the approximate depth should range between 0.5 and 1 times this wavelength.

This depth estimate is based on **Jacobsen (1987)**. This method is not perfect at separating sources from different depths. It is possible to generate long-wavelength features from shallow sources as evidenced by the fact that there are long wavelength features present in radiometric data, which do not have a significant depth component. However, the method should provide a good first pass estimate of which features extend to depth and which are only surficial. It is possible for deep tapping structures to be missed if there is not a significant property contrast across them.

Appendix 1: Structure detection algorithm (continued)

The structure detection filter produces orientation grids that show the orientation of the strongest edge at a given location. When these orientation grids have been thresholded to remove low amplitude features, it's easier to see the prominent structural orientations.

References

Kovesi, P., 1999, Image Features From Phase Congruency. *Videre: A Journal of Computer Vision Research*, v. 1, no. 3.

Jacobsen, B.H., 1987, A case for upward continuation as a standard separation filter for potential-field maps. *Geophysics*, v.52, no. 8, pp. 1138-1148.

Appendix 2: Radial symmetry algorithm

The goal in developing the radial symmetry filter is a move towards automated interpretation of potential field and topographic data that would be most similar to an interpretation by a person.

The filter highlights round features (as opposed to linear features) in the data. This allows us to locate areas that have a higher likelihood of being intrusive bodies or discrete alteration zones.

We have developed several radial symmetry filters. The filter that was used for this project is a gradient-based filter that looks for points where the grid slopes away in all directions. Detected locations are magnetic highs that are discrete bodies. Discrete magnetic lows are areas where the grid slopes toward the location from all directions. This algorithm is based on **Loy and Zelinsky (2002)**.

The filter can be used in a magnitude independent (MI) or magnitude dependent (MD) mode. The MI measure is a strict measure of radial symmetry, making it a direct measure of how round an anomaly is, irrespective of the magnitude of the gradients involved there. The MD measure is the MI measure scaled according to the magnitude of the gradients in the grid.

The filter looks for features with a radius between a base radius and two times that radius. It will not locate features that are significantly smaller than the range used. The filter will highlight the center of some features that are larger than the radius range.

References

Loy G., Zelinsky A., 2002, A Fast Radial Symmetry Transform for Detecting Points of Interest. In: Heyden A., Sparr G., Nielsen M., Johansen P. (eds) Computer Vision — ECCV 2002. ECCV 2002. Lecture Notes in Computer Science, vol 2350. Springer, Berlin, Heidelberg